# Identification and characterization of retinoid X receptors (RXR) in Atlantic cod (*Gadus morhua*) and their response to organic tin exposure


Master thesis in environmental toxicology

By Anders Vandeskog Borge

Department of Biological Sciences

Faculty of Mathematics and Natural Sciences

University of Bergen

September 2021

## Acknowledgements

This study has been funded by the Research Council of Norway and has been part of the iCod 2.0 project (project no. 244564) and dCod 1.0. project (project no. 248840)

First and foremost, I wish to thank my supervisors Odd André Karlsen and Anders Goksøyr for allowing me to do my master thesis in environmental toxicology. Thank you both for your engagement, excitement and taking time to answer which ever question I might have, whether it would be related to the experimental process or writing process. I would like to further extend my gratitude towards Odd André who first introduced me to the field of toxicology during my bachelor's degree. The way you were always available whether it was the day before Christmas or on the phone during the weekends, is something I truly appreciate.

Next, I wish to thank Rhîan Gaenor Jacobsen for getting me safely through the lab. Your patience with me and your ability to encourage me to try again if/when things went wrong, is something I am truly grateful for. Further, I cannot thank you enough for checking in on me and continuing to help while you were away. I hope some of the laughs you got from my mistakes can be some form of repayment for the help you provided.

I would also like to thank fellow students and friends for the support and for dragging me away from the lab/desk sometimes. To my family, even though you might not understand what I am doing, your constant support and hours of listening to my pessimism is well and truly appreciated.

Bergen, September 2021
Anders Vandeskog Borge

# Disposition

## List of abbreviations

| Full name | Abbreviation |
|---|---|
| 9-cis-retinoic acid | 9-cis-RA |
| Activation function 1 & 2 | AF-1, AF-2 |
| All-trans retinoid acid | ATRA |
| Base pair | bp |
| Complementary deoxyribonucleic acid | cDNA |
| Cytochrome P450 | CYP |
| *Danio rerio* retinoid x receptor | drRXR |
| Deoxynucleotides | dNTP |
| Deoxyribonucleic acid | DNA |
| Dichlorodiphenyltrichloroethane | DDT |
| Dimethyl sulfoxide | DMSO |
| DL-dithiothreitol | DTT |
| DNA-binding domain | DBD |
| Dulbeccos modified eagle's medium | DMEM |
| Ethylene glycol-bis(2-aminoethylether)-N,N,N′,N′-tertacetic acid | EGTA |
| Ethylenediaminetetraacetic acid disodium salt hydrate | EDTA |
| Farnesoid X receptor | FXR |
| Fentin chloride | FC |
| Fentin hydroxide | FH |
| Fetal bovine serum | FBS |
| *Gadus morhua* retinoid X receptor | gmRXR |
| Guanine-cytosine | GC |
| Half maximal effective concentration | $EC_{50}$ |
| Kilo Daltons | kDa |
| Kilobase | Kb |
| Ligand-binding domain | LBD |
| Liver X receptor | LXR |
| Maximum efficacy | $E_{max}$ |
| Melting temperature | Tm |
| Multiple sequence alignment | MSA |
| Nuclear receptor | NR |

| | |
|---|---|
| Over night | o/n |
| Organic tin compound | OTC |
| Ortho-2-nitrophenyl-B-D-galactopyranoside | ONPG |
| Ortho-nitrophenol | ONP |
| Perfluorooctanesulfonic acid | PFOS |
| Peroxiosome proliferator activated receptor | PPAR |
| Persistent organic pollutant | POP |
| Phosphate-buffered saline | PBS |
| Polychlorinated biphenyl | PCB |
| Polychlorinated dibenzo-p-dioxin | PCDD |
| Polychlorinated dibenzofuran | PCDF |
| Polycyclic aromatic hydrocarbon | PAH |
| Polymerase chain reaction | PCR |
| Polyvinyl chloride | PVC |
| Pregnane X receptor | PXR |
| Quantitative polymerase chain reaction | qPCR |
| Retinoic acid receptor | RAR |
| Retinoid responsive transcription factor | REF |
| Retinoid X receptor | RXR |
| Revolutions per minute | RPM |
| *Sebastiscus marmoratus* retinoid x receptor | smRXR |
| Shrimp alkaline phosphatase | SAP |
| Sodium-dodecyl-sulfate | SDS |
| Standard error of mean | SEM |
| Teleost-specific whole genome duplication | TS-WGD |
| Tributyltin chloride | TBT |
| Trimethyltin chloride | TMTC |
| Tripropyltin chloride | TPT |
| Ultraspiracle protein | USP |
| Upstream activation sequence | UAS |
| Vitamin D receptor | VDR |
| Whole genome duplication | WGD |

## Abstract

The retinoid X receptor (RXR) is a ligand-activated transcription factor and a member of the nuclear receptor (NR) superfamily. RXR consists of three major isotypes, i.e., RXRα, RXRβ and RXRγ, and several isoforms. This diversity makes RXR to be directly and indirectly involved in a vast array of cellular signaling pathways, mediating cellular responses as both a homo- and heterodimeric transcription factor. Depending on RXR isotype/isoform, ligand, and associated NR partner proteins, RXR regulates physiological processes such as embryogenesis, organogenesis, lipid metabolism and homeostasis. Along with endogenous ligands (9-cis-retinoic acid), some environmental pollutants have been observed to disrupt RXR signaling and gene regulation. Organic tin compounds (OTCs) are a subgroup of environmental pollutants that are particularly prominent and potent in marine environments, when compared to terrestrial, which previously have been observed to act in an endocrine disruptive manner through binding to RXR. The identification and characterization of RXR isoforms in ecologically and economically important marine species, such as Atlantic cod (*Gadus morhua*), along with the potential RXR-disruptive properties of environmental pollutants, including OTCs, have not yet been carried out. Thus, this study was performed to uncover and characterize the primary structures of the RXR isoforms encoded in the Atlantic cod genome (gmRXRs), analyze their tissue specific expression profiles, and assess the potential of endogenous (9-cis-RA) and exogenous (i.e., tributyltin, tripropyltin, triphenyltin and trimethyltin) ligands to induce the transcriptional activation of gmRXR proteins. Through genome mining and phylogenetic analysis, four RXR isoforms were identified in the Atlantic cod genome; gmRXRα, gmRXRβ1, gmRXRβ2 and gmRXRγ. cDNA derived from juvenile Atlantic cod tissues was used to assess the tissue specific expression of the gmRXR isoforms. Based on the expression profiles, gmRXRβ1 and gmRXRγ were cloned from Atlantic cod liver and used in establishing luciferase reporter gene assays. gmRXRγ was transactivated by both 9-cis-RA and most of OTCs tested. In contrast, gmRXRβ1 was not activated during by 9-cis-RA or by OTC exposure. Based on expression- and ligand activation profiles, gmRXRγ and gmRXRβ1 are suggested to act as important regulatory NRs in Atlantic cod. However, our study suggests that gmRXRβ1 act as an obligate non-permissive heterodimer, while gmRXRγ retains functionality as both a homo- and heterodimer. Importantly, the observed potential of OTCs to transactivate the Atlantic cod RXRγ, along with the proposed physiological importance of RXR in Atlantic cod, could further indicate that OTC exposure may cause adverse effects in this species and potentially in other marine cold-water teleosts.

# 1 Introduction

## 1.1 *Perspective*

As a result of the continuous industrialization and globalization over the last two centuries, anthropogenic pollutants have been emerging at an alarming rate in areas previously perceived to be unscathed. Offshore oil drilling, refineries, municipal discharges, mining and commercial travel and shipping are to name a few of the major perpetrators of land, water and air pollution. Common for many pollutants are their ability to persist in the environment by resisting physical and chemical degradation, allowing accumulation in biota and long-time exposures of organisms. Marine ecosystems are especially vulnerable to these compounds as they are being exposed to both legacy pollutants as well as acting as a sink for runoffs associated with terrestrial agriculture, industrial- and consumer waste. The potential adverse effects caused by pollutant exposure are many, with compounds possessing endocrine disrupting properties especially highlighted. Even at low concentrations (μM and nM ranges) these compounds can interfere with synthesis, transportation, secretion, elimination and general function of hormones and the endocrine system (Lauretta et al., 2019). The adverse effects reported of such pollutants include disruption of reproduction, reduced growth, and altered behavior, which may negatively affect individuals or even whole ecosystems. Increasing our knowledge of the physicochemical properties and adverse effects of environmental pollutants may give rise to preventive and prohibiting actions, in hopes to minimize their destructive potential.

## 1.2 *Environmental pollutants*

The term environmental pollution commonly refers to the influx of harmful anthropogenic chemicals into an environment at rates higher than that of storage, dispersion or decomposition (Scott & Sloman, 2004). Depending on the pollutant itself and their interaction with the environment, these compounds can be found residing in air, water and soil (Ukaogo et al., 2020). The physicochemical properties of these environmental pollutants may vary greatly, however, some properties seem to be recurring. Especially troublesome are their ability to persist in environments and organisms through degradational resilience and potential for bioaccumulation and biomagnification (Windsor et al., 2020). Bioaccumulation occurs when the rate of absorption exceeds the rate of elimination in an organism, usually resulting in storage and accumulation in fatty tissue due to their lipophilic nature (Yarsan & Yipel, 2013). Biomagnification is the increase in pollutant concentrations in organisms at higher trophic

levels, as predators higher in the food chain are exposed to increased levels of accumulated pollutants through prey (Yarsan & Yipel, 2013). This allows pollutants to be readily available to exert their toxicological effects potentially at high concentrations. Examples of groups of environmental pollutants include metals (e.g., Pb, As, Hg, Cd, Sn), polycyclic aromatic hydrocarbons (PAH), dioxins, polychlorinated biphenyls (PCBs), brominated diphenyl ethers (flame retardants), perfluorinated compounds, pesticides (e.g., organotin, organochlorine, organophosphate and neonicotinoid compounds), phthalates, and micro/nano-plastics (Griffith et al., 2015).

Persistent organic pollutants (POPs) are an important and commonly highlighted fraction when discussing environmental pollutants. POPs are usually referring to highly toxic compounds able to cause both acute and adverse health effects even at low concentrations (Mortimer, 2013). Moreover, POPs are known to resist chemical and physical degradation and can bioaccumulate and biomagnify in lipid rich biota (Windsor et al., 2020). Another important property shared by many POPs, are their ability to volatilize from soil and water, entering the atmosphere where they are carried over great distances before re-depositing (Ashraf, 2017). This becomes a cyclical phenomenon and is proposed as the mechanism in which POPs end up in remote environments far from where they were released (K. C. Jones & de Voogt, 1999). Due to the ability of long transportation and the highly toxic potential of POPs, the Stockholm convention of 2001 proposed a priority list of twelve POPs called the “dirty dozen”. The goal was to reduce and/or eliminate their production and use. These POPs were recognized to cause adverse effects in humans and ecosystems, and included pesticides, industrial chemicals and by-products, such as aldrin, chlordane, dichlorodiphenyltrichloroethane (DDT), dieldrin, endrin, heptachlor, hexachlorbenzene (HCB), mirex, toxaphene, polychlorinated biphenyls (PCB), polychlorinated dibenzo-p-dioxins (PCDD) and polychlorinated dibenzofurans (PCDF) (Tokuç, 2013). Although only twelve compounds were initially added, groups like PCB contain 209 individual congeners. Later, nine POPs were added to the Stockholm convention (denoted as the “nasty nine”) including among others hexabromobiphenyl, chlordecone, lindane and perfluorooctanesulfonic acid (PFOS) (Palanisami & Naidu, 2010). However, although the production of many chemicals has significantly decreased, the prolonged half-life of POPs in the environment makes these compounds still present in hotspots and remote areas alike.

## 1.3 *Organic tin compounds (OTCs)*

Organic tin compounds (OTCs) constitute the most widely used organometallic chemicals, and are characterized by their tin (Sn) atom bound to organic substituents (e.g., propyl, phenyl, methyl, butyl) (Hoch, 2001). OTCs are found in industrial commodities including pesticides such as fungicides, biocides, molluscicides, anti-fouling agents and polyvinyl chloride (PVC) stabilizers (Haschek et al., 2010). Some OTCs can also be found in surface disinfectants, curing agents, ballistic additives and even rocket fuel (Okoro et al., 2014). Of the 800 or so known OTCs, all but methyltin stem from an anthropogenic origin. From its first commercial use as an PVC stabilizer in the 1940s, OTC production increased by a tenfold from 1950 (~5000 tons) to 1992 (~50 000 tons) (Hoch, 2001). Although many OTCs are banned from commercial use today, the large-scale use of these compounds throughout the 20$^{th}$ century and early 2000s has given rise to ubiquitous contamination of marine environments (Ho et al., 2016). Although not yet classified as a POP, many of the most prominent members of the OTC family share the functional properties with their POP counterparts.

Historically, tributyltin (TBT) and triphenyltin (fentin) have been some of the most used OTCs. Along with tripropyltin (TPT), TBT and fentin are two of the most toxic OTCs with properties making them resistant to natural degradation (Haschek et al., 2010). These OTCs are presumably more toxic in marine environments compared to terrestrial, and due to the extensive use as antifouling biocides for ships, TBT and fentin are ubiquitously distributed in aquatic ecosystems (Doherty & Irwin, 2011). At the surface and in the water column, the half-life of these compounds ranges from 10-100 days, whereas TBT and fentin deposited in sediments allow for a drastic increase in half-life ranging from 1-4 years (Cruz et al., 2015). TBT and fentin, along with other OTCs, are also able to bioaccumulate and biomagnify in both vertebrates and invertebrates (Doherty & Irwin, 2011). TBT and fentin have been associated with endocrine disruption in marine and terrestrial organisms, especially prominent is the phenomenon of imposex found in gastropods. Organotin induced imposex have been observed in over 150 species of gastropods at low concentrations (ng/L), resulting in reproductive abnormalities (Pellizzato et al., 2004). These abnormalities involve a superimposition of male features in female organisms, e.g. a penis or *vas deferens*, which can lead to infertility and premature death able to affect entire populations (Pellizzato et al., 2004). Interestingly, recent studies indicate the involvement of a nuclear receptor (NR), i.e. the retinoid X receptor (RXR), in developing imposex through OTC-mediated disruption of RXR signaling (Huang et al., 2020). Giulianelli et al., (2020) reported that expression of gastropod RXR was significantly

different between OTC exposed and non-OTC exposed gastropods, providing further evidence of OTC role in imposex development through inducing RXR disruption (Giulianelli et al., 2020). Furthermore, RXR is reported to regulate aromatase activity through transcriptional regulation of CYP19 in *Danio rerio*. It is reported that OTC binding to *D. rerio* RXR disrupts RXR signaling causing disruption of CYP19 synthesis resulting in aromatase inhibition, causing masculinization of female *D. rerio* individuals (Cheshenko et al., 2008). In contrast, OTCs are observed to markedly enhance the rate of estradiol biosynthesis and increase aromatase activity in human carcinoma cells (Nakanishi et al., 2005). Some papers state that an aromatase-like inhibition is also found during gastropod imposex development. However, as the CYP19 aromatase enzymes believed to be involved in vertebrate masculinization and decreased/increased aromatase activation, are not present in gastropods (Fodor et al., 2020). Thus, resent studies disregard the hypothesis of OTC induced aromatase-like inhibition in gastropod imposex, concluding that the RXR target genes during OTC-induced signaling disruption is yet to be elucidated (Fodor et al., 2020; He et al 2021). Nevertheless, the evidence of OTC-induced sexual differentiation through RXR disruption in marine organisms is strong, however, the processes and factors triggering changes in CYP19 activity, or other enzymes, is not clear. Continuing, prolonged exposure of OTCs is observed to result in cytotoxicity, hepatotoxicity and neurotoxicity through perturbation of calcium homeostasis and depression of aminopyrine demethylase in organisms ranging from bacteria to mammals (Hagger et al., 2005; Cruz et al., 2015).

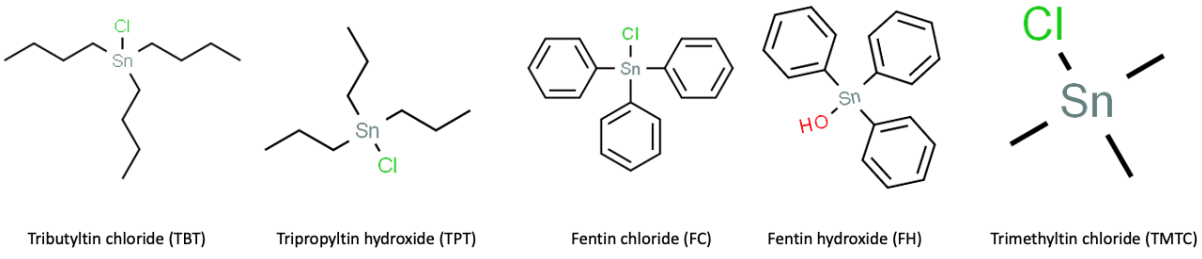


**Figure 1. Organic tin compounds.** The chemical structure and names of five prominent OTCs found in marine environments. These compounds were used in this study to assess transactivation of gmRXR by OTC exposure.

## 1.4 *Nuclear receptors*

Nuclear receptors (NRs) are an evolutionary related superfamily of mostly ligand-activated transcription factors. All NRs are structurally similar proteins and share five functional domains, including an N-terminal DNA binding domain (DBD), a hinge region, and a ligand binding domain (LBD) (Jin & Li, 2010). Although nuclear receptors share structural similarities, variations in the LBD and DBD allow NRs to regulate a vast amount of different cellular processes in order to preserve normal cellular physiology. These processes include development, reproduction, metabolism, cell proliferation, immune response, and enzymatic activity (Porter et al., 2019). Due to the diversity of NRs and their widespread cellular involvement, irregularities in their expression and function as a result of internal and external stressors have long been associated with a magnitude of diseases. The suspected involvement of NRs in cancer, cardiovascular diseases, and type II diabetes as a result of endocrine disrupting xenobiotics, has resulted in continuous research and development of NR targeted drugs (Sladek, 2003). Further, the ability of environmental pollutants to disrupt NR function is of great importance for our understanding of how continuous exposure to pollution might manifest as negative adverse health effects on single organisms, populations and even whole environments.

In order to exert their roles as transcription factors, nuclear receptors bind mostly small lipophilic ligands (e.g., steroids, hormones, retinoids and phospholipids) and/or form dimeric partners (Porter et al., 2019). Unlike most intercellular signaling molecules, which act via surface receptors, NR ligands are able to cross the cell membrane and interact directly with the nuclear receptors within the cells (Miller & Lappin, 2021). Once bound to a NR, the ligand mediates conformational changes to the nuclear receptor into an active conformation. Depending on the NR and the structural alterations caused by the ligand-binding, the nuclear receptor will either bind (as homodimers, heterodimers or tetramers) or release themselves from specific response elements in DNA upstream of their target genes (Penvose et al., 2019). If the response to ligand binding causes release from DNA, or inhibition to bind to DNA, the ligand is said to have an antagonistic effect. Promotion of binding to DNA and mediating transcription of target genes as a result of ligand-binding is called agonism (Lagarde et al., 2016). As a result of their sequence similarity, as well as ligand- and DNA binding characteristics, NRs are commonly grouped into nine major subfamilies: NR0, NR1, NR2, NR3, NR4, NR5, NR6, NR7 and NR8 (Weikum et al., 2018). Perhaps the most notable of these subfamilies, are NR1 and NR2. NR1 is the largest subfamily and contains several NRs regulated by a variety of

liphophilic ligands. The NRs of the NR1 subfamily include thyroid hormone receptor (TR), retinoic acid receptor (RAR), peroxiosome proliferator activated receptors (PPAR), and others (Fig 2). NR2 is the second largest subfamily, this subfamily is often highlighted due to the inclusion of RXR, which is known to form heterodimeric relations with many NR1 NRs (Penvose et al., 2019), and in turn directly and indirectly regulate signaling and function of these partner NRs.

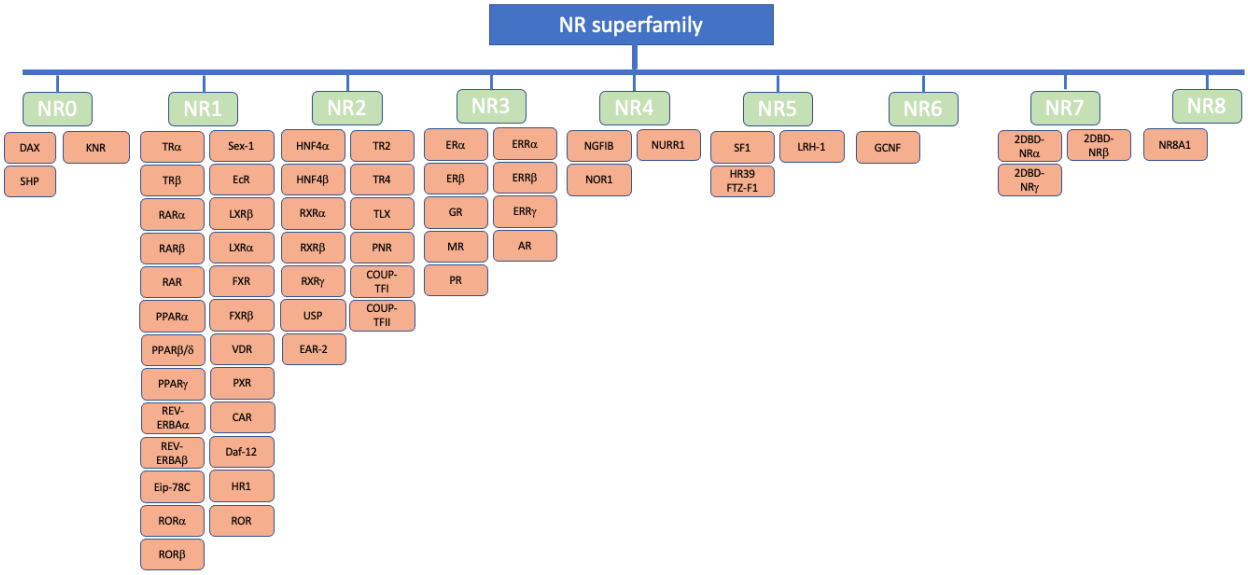


**Figure 2. The NR superfamily**. A schematic overview of the nine different NR subfamilies (NR0-NR8) and the individual NRs belonging to each subfamily.

## 1.5 *Retinoid X receptor*

### 1.5.1 *Isoforms, dimeric interactions and functional roles*

The retinoid X receptor (RXR) is a subfamily II (NR2B) NR and unique in its ability to heterodimerize with a vast array of NRs in most metazoan life (Moraes et al., 2007). RXR consists of three distinct isotypes (α, β and γ) each encoded by separate genes located on different chromosomes. Due to genome duplication events, multiple isoforms of the three isotypes exist (α1, α2, β1, β2, γ1, γ2, δ and ε) (Mukha et al., 2021). The many isotypes and isoforms of RXR make this NR able to associate, heterodimerize and activate a plethora of other NRs, including peroxisome proliferator-activated receptor (PPAR), retinoic acid receptors (RARs), pregnane X receptor (PXR), liver X receptor (LXR) and farnesoid X receptor (FXR) (Szanto et al., 2004). In these functional dimers, RXR acts both in a non-permissive and a permissive manner (Aranda & Pascual, 2001). As a non-permissive partner, RXR form heterodimers with NRs like vitamin D receptor (VDR) and RAR. Here, RXR ligands alone are

incapable of initiating transcriptional activation, and ligand binding to RXR is precluded. Once the partner NR has activated the heterodimer, ligand binding to RXR can occur to enhance the transcriptional response in an additive or synergistic fashion (Evans & Mangelsdorf, 2014). In contrast, RXR:PPAR and RXR:FXR are permissive partners where ligand binding to one of the two NRs is sufficient to transcriptionally activate the heterodimeric-complex. Synergistic activation is possible when both RXR and partner NR is bound by a ligand (Castillo et al., 2004).

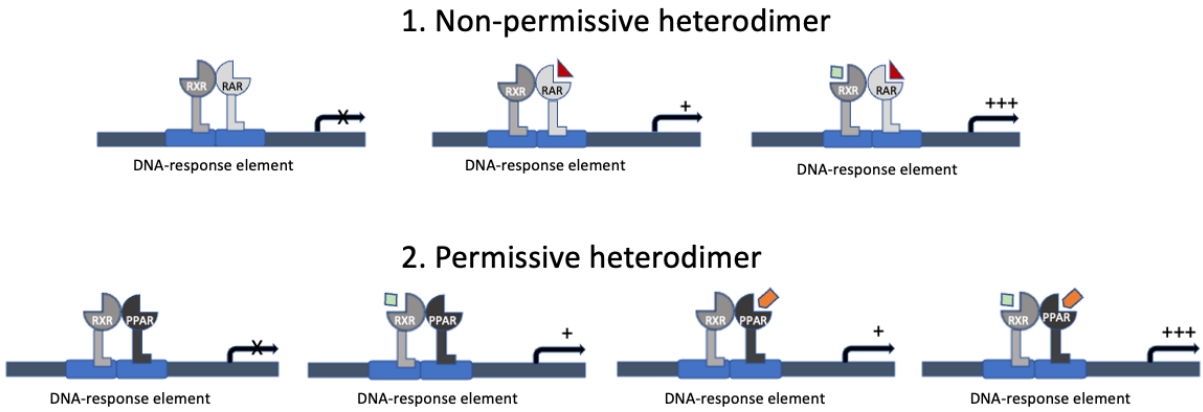


**Figure 3. RXR as a non-permissive and permissive heterodimer.** Figure shows RXR as a non-permissive heterodimer (1) and permissive heterodimer (2) bound to DNA response elements (blue). (1) Non-permissive heterodimer of RXR and RAR and (2) permissive heterodimer between RXR and PPAR. "X" indicates no transcriptional activation, "+" indicates transcriptional activation of target gene, and "+++" indicates synergistical transcriptional activation of target gene.

As a homodimer, RXR isoforms have been observed to activate transcription of non-native target genes such as genes normally targeted by PPAR (IJpenberg et al., 2004). Although RXR possess the ability to activate transcription as a homodimer has been documented, the physical mechanisms and the distinct pathways, including target genes, remain poorly understood. RXRs ability to heterodimerize, and thus activate numerous partner NRs, alongside its ability to function in an homodimeric fashion makes it directly and indirectly involved in numerous crucial cellular signaling pathways (Evans & Mangelsdorf, 2014). These pathways act as regulatory mechanisms in several processes, including lipid metabolism, cell differentiation, homeostasis, apoptosis and developmental processes such as organogenesis and embryogenesis (Dawson & Xia, 2012). However, RXRs ability to both homo- and heterodimerize and exert its role in signaling pathways, depends not solely on homo- and heterodimeric interactions but also the presence of a ligand along multiple co-factors. In fact, the absence of ligands and co-factors results in a homo-tetrameric configuration in which RXR remains unactive (Gampe et al., 2000).

### 1.5.2 *RXR protein structure*

Small differences in the primary structures of RXRα, RXRβ and RXRγ manifests as their ability to associate with different ligands and dimeric partners and thus be involved in different cellular pathways and processes. As with most NRs, all RXR isoforms exhibit a modular structure with regions of distinct functional domains. These domains are the non-conserved N-terminal domain (A/B), a highly conserved DBD (C), a non-conserved hinge region (D), a moderately conserved LBD (E) and a highly varied C-terminal (F) (Dawson & Xia, 2012). The specific functions of the different domains are outlined below.

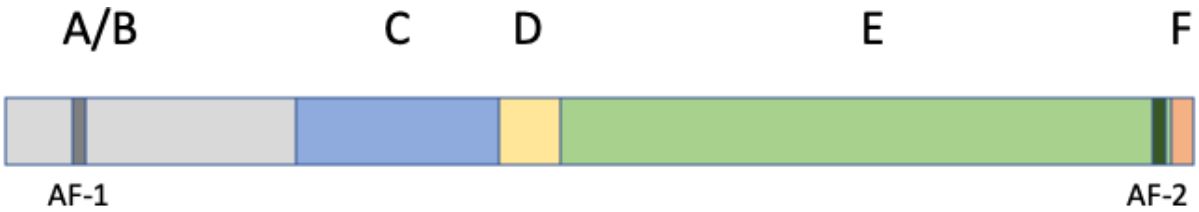


**Figure 4.** Illustration of the five functional domains of RXR, including activation function 1 and 2 (AF-1 and AF-2). A/B= N-terminal domain, C= DNA binding domain, D= hinge region, E= ligand binding domain and F= C-terminal.

- The N-terminal domain, or activation function 1 (AF1), acts in a promoter-specific manner through ligand independent interactions with several co-regulators. This site is further associated with post-translational modifications to repress or increase the rate of transcription (Dowhan & Muscat, 1996).
- The DBD is the domain that is most conserved in all the isoforms. The DBD contains two subdomains consisting of an amphipathic helix and a peptide loop. The amphipathic helix in the first domain interacts with the major groove through a DNA-reading helix, making base specific interactions. The second subdomain interact with the DNA backbone through non-specific interactions. The peptide loop in the second subdomain is also responsible for dimerization as it contains the distal box (D-box). Together the two subdomains create the DNA-binding zinc finger motif that recognizes and binds specific DNA-sequences (response elements) at a high affinity in a monomeric or dimeric fashion (Dawson & Xia, 2012).
- The hinge region functions as a flexible link between the DBD and the LBD. This region is the generally shortest in length and most commonly the least conserved part, but it may contain a nuclear localization signal and is a region where post translational modification may occur (Weikum et al., 2018).

- The LBD is moderately conserved, however, changes to this amino acid sequence manifests as the major differences in practical functionality between the receptor isoforms. The LBD is a highly complex multifunctional allosteric signaling domain, where binding of both ligand and co-factors, as well as hetero- and homodimeric mediation and interaction with other proteins, such as heatshock proteins, occurs (Egea et al., 2000). The binding of ligand and/or co-factors results in conformational changes of the LBD, increasing or inhibiting RXRs rate of transcription as well as formation of partner protein complexes. The LBD consists of 12 alpha-helices (H1-H12), and in between H5 and H6 a small single beta-turn. The structure of the LBD is commonly referred to as an antiparallel helical sandwich, which creates a hydrophobic cavity at the base of the LBD termed the ligand binding pocket. As the name entails, this is where ligands are accommodated and bound to the LBD. The activation function 2 (AF2) is responsible for dynamic changes upon ligand binding, as ligand binding facilitate oriental change forcing AF2 to interact with new co-regulator proteins (Dawson & Xia, 2012).
- The C-terminal domain contains the highest amounts of variability in amino acid sequence. Due to the high sequence variability, little is known about its functional role in RXR and other NRs in general.

### 1.5.3 *Transcriptional activation of RXR*

Upon ligand binding RXR undergoes major conformational changes in the helices and loops of the LBD. The LBD of RXR exists in two forms: “apo” or “holo” (Egea et al., 2000). The apo form is the configuration of the LBD where all helices are present due to the absence of a bound ligand. When bound by a ligand, the LBD retains a holo form where a structural reconfiguration occurs through unwinding of H2, permitting a tilt of H3 where a surface structure between H3, H4 and H12 forms. This surface structure unmasks recognition sites called NR box motifs allowing co-factor binding, as well as altering the homo- and heterodimeric interfaces (Dawson & Xia, 2012). The structural reconfiguration of the LBD can therefore potentially result in three distinct alterations to the receptor function. First, changed state of multimerization due to alterations to the self-associative activity; second, altered degree of co-activator or co-repressor binding by conformational changes; finally, altered interface structure resulting in increased/decreased homo- or heterodimeric stability (Ahuja et al., 2003).

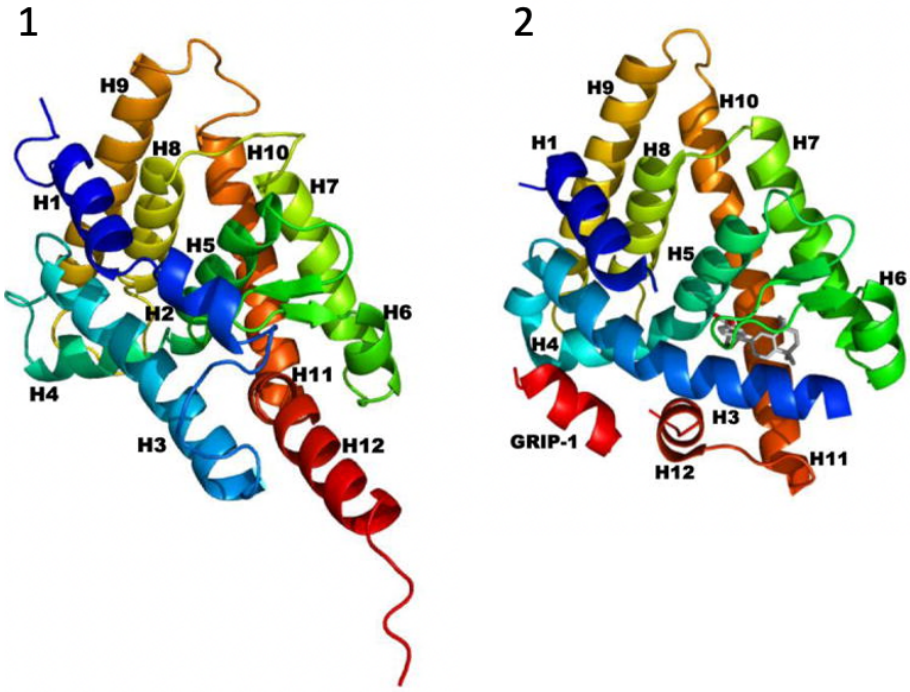


**Figure 5. Apo- and holo-configuration of RXRα LBD with helices (H1-H12).** (1) Unligated Human RXRα-LBD retaining its un-active apo-configuration. (2) Human RXRα-LBD bound by agonist ligand allowing an holo-configuration and subsequent transcriptional activation. Crystal structures obtained from on Protein Data Bank (PDB), crystal structure 1LBD (apo) and 1MVC (holo), with modifications by (Dawson & Xia, 2012).

### 1.5.4 *RXR endogenous ligands*

The matter of RXRs natural endogenous ligand(s) is perhaps one of the most controversial and enigmatic aspects of RXR research. Vitamin A studies in the late 1980s and early 1990s observed RXR as a novel retinoid responsive transcription factor (Levin et al., 1992). Subsequent research proposed 9-cis-retinoic acid (9-cis-RA) as a likely natural ligand for RXR due to its high affinity binding. Both organic and synthetic 9-cis-RA are vitamin A derivates containing a carboxylate group and a long aliphatic chain (Tsuji et al., 2015). This retinoid is involved in numerous physiological pathways as a non-steroidal hormone, enforcing their pleiotropic effects through signal transduction of RXR and retinoic acid receptor (RAR) (Kane, 2012). Unlike RAR, which bind 9-cis-RA among other retinoic acids such as all-trans-RA (ATRA), RXR is known to exclusively bind 9-cis-RA with high affinity (Tate et al., 1994). In linages such as vertebrates, annelids and mollusks, this canonical high affinity 9-cis-RA binding to RXR has been confirmed (Fonseca et al., 2020). Interestingly, in cephalochordates this binding is maintained albeit at a much lower affinity, whilst in *Daphnia magna,* 9-cis-RA binding does not always yield transcriptional activation (Fonseca et al., 2020). The difficulties in detecting and validating endogenous 9-cis-RA in embryos and developing tissues are what mainly fuels the debate regarding its status as a bona fide endogenous RXR ligand (Wolf, 2006).

Thus, in recent times, other compounds have been proposed as potential endogenous ligands. Some of the common examples are docosahexaenoic acid, lithocholic acid, and phytanic acid, all capable of binding to- and activating RXR at high affinity and efficiency (Szanto et al., 2004). However, since high affinity binding of 9-cis-RA to RXR is found conserved throughout evolution, 9-cis-RA is commonly used as a ligand in RXR research.

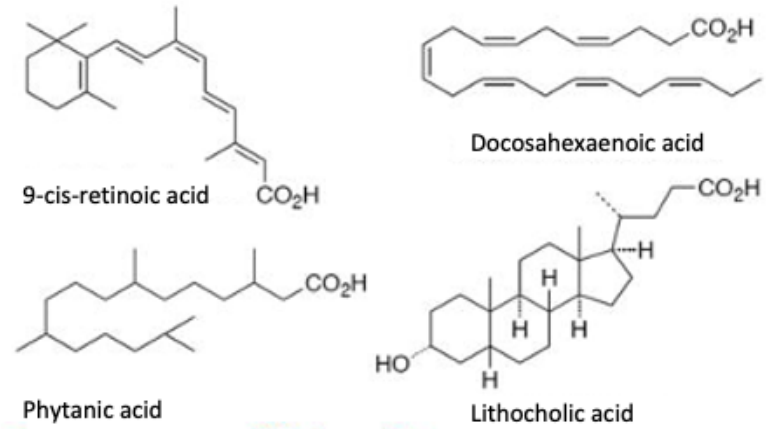


**Figure 6.** Endogenous ligands capable of inducing RXR-mediated transcription through receptor binding.

### 1.5.5 *Organic tin compounds as exogenous RXR ligands*

With the discovery of OTCs innate ability to deregulate and disrupt endocrine pathways at low concentrations, OTCs such as TBT was later observed to activate RXR:PPAR heterodimers (le Maire et al., 2009; Hagger et al., 2005). The result of the heterodimeric activation was promotion of adipocyte differentiation and disruption of aromatase transcription in human carcinoma cell lines (i.e. JAr, JEG-3 and BeWo) (Nakanishi et al., 2005). Thus, RXR and PPAR became dominant nuclear receptors in uncovering the mechanism of action of OTCs as an exogenous ligand. Interestingly, OTCs do not resemble 9-cis-RA or other retinoids chemically or physically, as OTCs lack a functional polar group (Hiromori et al., 2015). Although RXR and PPAR form a permissive heterodimer, le Maire *et al.,* (2009) suggested that the lack of appropriate cysteine groups in PPAR-LBD deterred OTCs from binding. It was further suggested that the lack of a polar group in OTCs caused the compound to interact with different amino acids in the LBD compared to 9-cis-RA, in fact, OTCs seemingly interact with only a small subset of the LBD amino acid residues in RXR. Particularly important for RXR-OTC interactions, is a highly conserved cysteine-residue located on the C-terminal. Upon OTC binding, the ligands will form weak van der Waals contacts between themselves and the LBD. Here, OTCs alkyl groups further positions the innate tin (Sn) atom, in the core of OTCs, according to the C-residue. From here, the Sn atom is bound covalently to the C-residue of the

RXR-LBD, with the C-residue acting as anchoring point and stabilator during binding. Active OTCs, such as TBT, TPT, FC and FH, are shown to mediate RXR disruption through such interactions with the C-residue. In contrast, OTCs with fewer and/or too short/long alkyl groups (i.e., triethyltin or trioctyltin) results in too few contact points to align the Sn-atom with the C-residue, leading to RXR´s inability to accommodate OTC binding (le Maire et al., 2009).

### 1.6 *Atlantic cod (Gadus morhua)*

Atlantic cod is a common teleost widely distributed across the North Atlantic Ocean, spanning form the north-eastern coast of North America to the Barents Sea in Northern Europe. Atlantic cod is often divided into coastal- and oceanic cod based on their migratory behavior and genomic divergence (Berg et al., 2016). The costal cod populations are known to remain within relatively small geographic locations along shallow coastal waters (0-500 meters) and fjords. They are commonly found in the benthopelagic zone but do reside closer to the surface (pelagic) during spawning. In contrast, the oceanic cod is pelagic and known to migrate over large distances. The oceanic cod population of the North-east Arctic migrates from the Barents Sea along the Norwegian coast down to Møre during spawning season (Wennevik et al., 2008).

**Figure 7. Atlantic cod distribution.** Illustration of the global distribution of Atlantic cod, with populations spanning the Atlantic Ocean from the North-east of North America to the Baltic Sea. Illustration based on Aquamaps (2015), modified by Madsen (2016).

For Norway, export of commercially captured Atlantic cod has been, and continues to be, important for economic growth. In 2019, the Norwegian export of fresh, dried and salted Atlantic cod was estimated to provide over 7 billion NOK in revenue. However, this was the result of 330 thousand tons of Atlantic cod being captured during the same year (SSB, 2020). In the late 90s to the early 2000s, several Atlantic cod populations collapsed due to overfishing in areas around Canada and the North Sea (Stokstad, 2021). Today the repercussions are still present as many of these populations are yet to recover. However, capture quotas have allowed many of these recovering populations to slowly experience a steady incline (Garrod, 2011). Although there is a general positive trend in Atlantic cod populations, it is still a threatened species where many theorize that additional stress from environmental pollutants and climate change will disrupt spawning season and inhibit the populations to fully recover (Link et al., 2009).

Both coastal- and oceanic cod are pivotal in maintaining a stable ecosystem, as they act as the major piscivore predators in their ecosystems, along being important prey for other species such as minke whales (*Balaenoptera acutorostrata)* and harp seals (*Pagophilus groenlandicus)* (Haug et al., 2017). Due to the ecological and economical importance of Atlantic cod, it has since the 1980s been used in environmental monitoring studies as a bioindicator species (Søfteland et al., 2010). A focal point of these studies is to better understand the effects environmental pollutants have on Atlantic cod and marine teleost´s. The publishing of the whole Atlantic cod genome by Star et al. 2011, facilitated the opportunity to obtain quantitative response data to pollutant exposure in Atlantic cod on a genomic scale. Such data may provide an important insight to how Atlantic cod, and marine wildlife in general, responds to the increasing pressures of manmade chemicals.

### 1.6.1 *RXR in Atlantic cod*

Although RXR isoforms from model organisms such as *D. rerio* are relatively well described, little is known about the structural or functional characteristics of RXR in other teleost species, such as Atlantic cod. However, in contrast to most mammalian species that possess only one isoform of RXRα, RXRβ and RXRγ, teleost RXR constitutes numerous RXR isoforms, including two RXRα, two RXRβ and two RXRγ variants, along with an RXRε and an RXRδ that are only observed in some teleost fish. The vast array of different RXR isoforms present in teleost species are believed to be the result of teleost specific whole genome (TS-WGD) events, or tandem duplication events of RXR encoding genes. This has allowed teleost specific RXR isoforms to arise with new functional properties compared to mammalian orthologs, through neo- and subfunctionalization events. Eide et al. published in 2018 a genome mining study where all members of the NR superfamily were identified in Atlantic cod genome, demonstrating the presence of four RXR isoforms. Interestingly, this paper showcased the loss of PXR in Atlantic cod, and most other species in the *Gadiformes* order. The PXR-RXR heterodimer is believed to play an important role in mediating and controlling the xenobiotic response in vertebrates through binding of several NR response elements, including the CYP3A4 promoter (Delfosse et al., 2021)(Aranda & Pascual, 2001). Thus, the absence of PXR raise several interesting questions from an evolutionary and toxicological perspective, regarding the xenobiotic response mechanisms and the potential alteration of RXR function in Atlantic cod. Particularly interesting is the mechanisms in which OTC may affect RXR function. As described in 1.3, RXR in *D. rerio* is strongly linked to OTC induced masculinization through aromatase inhibition of CYP19 enzymes. OTCs in other teleost species such as *Salmo salar* and *Acanthopagrus schleigelii*, have further been observed to mediate RXR disruption resulting in fluctuating gonadal and neural aromatase activity (Cheshenko et al., 2008). Thus, it is suggested that OTCs induces RXR disruption in several teleost species. However, as of today, the primary structure, ligand activation, tissue specific expression, and xenobiotic activation of gmRXR are yet to be characterized and is vital to the understanding of RXRs role as a NR in Atlantic cod.

## 1.7 *Aim of the study*

RXR has not previously been characterized on a molecular level in Atlantic cod. The present study therefore aims to uncover and characterize the primary structures and phylogeny of the gmRXR isoforms and analyze their tissue specific expression profiles. The tissue specific expression profile will provide insight into possible gmRXR function and based on liver expression profiles, the isoforms most prominently expressed here will further be cloned and integrated into a luciferase-based reporter gene assay. Through the luciferase reporter gene assay, the efficacies and potencies of 9-cis-RA and OTCs (TBT, TPT, FC, FH and TMTC) in transactivating gmRXRs will be assessed *in vitro*. The natural endogenous ligand for RXR is still debated, however, 9-cis-RA is widely regarded as a viable candidate. Therefore, the ability of 9-cis-RA to induce transactivation of RXR in Atlantic cod is assessed to investigate its proposed role as an endogenous RXR ligand. Further, OTCs are a group of highly toxic pollutants, reported to be potent agonists for RXR in other species. However, the effects of OTCs on RXR in marine cold-water teleosts are scarce, and no data exists on OTC-mediated transactivation in Atlantic cod. Although the abundance of OTCs in environments is declining, the hormone disruptive properties of OTCs through RXR disruption are reported to be significantly more potent in marine environments compared to terrestrial environments. Therefore, this study aims to assess the possibility for these compounds to induce activation of Atlantic cod RXR at low concentrations (nM-μM) and investigate the potential adverse effects OTC induced RXR activation may cause. The four major objectives for this study are listed below.

I. Perform bioinformatical analyses of DNA- and protein sequences of Atlantic cod RXR isoforms, including phylogeny and annotation of important functional domains and sequence features such as the DBD, LBD and ligand binding residues.
II. Analyze the tissue specific expression profiles of RXR in Atlantic cod using a comprehensive library of tissue samples.
III. Establish an *in vitro* reporter gene assay for assessing ligand-binding and transcriptional activation of RXR isoforms.
IV. Examine possible transcriptional activation of RXR isoforms induced by the endogenous ligand 9-cis-RA and a selected set of different OTCs.

# 2 Materials

## 2.1 *Chemicals and reagents*

**Table 1. List of chemicals and reagents used**

| Name | Chemical formula | Supplier |
|---|---|---|
| 10X loading buffer | - | TaKaRA |
| 2-Log DNA ladder | - | New England |
| 2-β-Mercaptoethanol | $HSCH_2CH_2OH$ | Aldrich |
| 2-nitrofenyl-β-D- galactopyranoside | $C_{12}H_{15}NO_8$ | Sigma-Aldrich |
| 3-(4.5-Dimethyliazol-2-yl)-2.5-Diphenyltetrazoliumbromide | $C_{25}H_{20}BrN_3O_2S$ | Merck |
| 5-Carboxyfluorescein diacetate, Acetoxymethyl ester | $C_{28}H_{20}O_1$ | Thermo Fisher Scientific |
| Acetic acid | $CH_3COOH$ | Sigma-Aldrich |
| Acrylamide-Bis | | Bio-Rad |
| Adenosin 5´trifosfat disodium salt hydrate | $C_3H_5NO$ | Sigma-Aldrich |
| Agar-agar | - | Merck |
| Agarose | - | Sigma-Aldrich |
| Ammonium persulfate | $(NH_4)_2S_2O_8$ | Sigma-Aldrich |
| Ampicillin sodium salt | $C_{16}H_{18}N_3NaO_4S$ | Sigma-Aldrich |
| Betain | $C_5H_{11}NO_2$ | Sigma-Aldrich |
| Boric acid | $H_3BO_3$ | Merck |
| Bovine serum albumin | - | Sigma-Aldrich |
| Co-enzyme A | - | Thermo Fisher |
| CHAPS | $C_{32}H_{58}N_2O_7S$ | Thermo Fisher |
| Dimethyl sulfoxide | $C_2H_6OS$ | Sigma-Aldrich |
| Disodiumhydrogenphosphate | $Na_2HPO_4$ | Sigma-Aldrich |
| DL-Dithiothreitol | $HSCH_2CH(OH)CH(OH)CH_2SH$ | Sigma-Aldrich |
| D-luciferin sodium salt | $C_{11}H_8N_2O_3S_2$ | Biosynth |
| Dulbecco´s modified Eagle's medium (phenol red) | - | Sigma-Aldrich |
| Dulbecco´s modified Eagle's medium (w/o phenol red) | - | Sigma-Aldrich |
| Erythrosin-B | $C_{20}H_8I_4O_5$ | Sigma-Aldrich |
| Ethanol | $C_2H_5OH$ | Sigma-Aldrich |
| Ethidium bromide | $C_{21}H_{20}BrN_3$ | Sigma-Aldrich |
| Ethylene glycol-bis(β-aminoethyl ether)-N´,N´,N´,N´-tetraacetic acid | $C_{14}H_{24}N_2O_{10}$ | Sigma-Aldrich |
| Ethylenediaminetetraacetic acid | $C_{10}H_{16}N_2O$ | Sigma-Aldrich |
| Fetal bovine serum | - | Sigma-Aldrich |
| Galactose | - | Sigma-Aldrich |
| Gel Red | - | Biotium |
| Glycerol | $C_3H_8O_3$ | Sigma-Aldrich |
| Isopropanol | $C_3H_8O$ | Kemetyl |
| L-glutamine | $C_5H_{10}N_2O_3$ | Sigma-Aldrich |
| L-α-Phosphatidylchlorine | $C_{44}H_{88}NO_8P$ | Sigma-Aldrich |
| Magnesium carbonate hydroxide pentahydrate | $(MgCO_3)_4 \bullet Mg(OH)_2 \bullet 5H_2O$ | Sigma-Aldrich |

| | | |
|---|---|---|
| Magnesium chloride hexahydrate | $Mg(CL_2) \bullet 6H_2O$ | Sigma-Aldrich |
| Magnesium sulfate heptahydrate | $H_{14}MgO_{11}S$ | Sigma-Aldrich |
| Methanol | $CH_3OH$ | Sigma-Aldrich |
| Monosodium phosphate | $NaH_2PO4$ | Sigma-Aldrich |
| OPTI-MEM | - | Gibco |
| Polysorbate 20 | $C_{58}H_{114}O_{26}$ | Thermo Fisher |
| Rezasurin sodium salt | $C_{12}H_6NNaO_4$ | Sigma-Aldrich |
| Penicillin-Streptomycin | - | Sigma-Aldrich |
| Phosphate-buffered saline | $Cl_2H_3K_2Na_3O_8P_2$ | Sigma-Aldrich |
| Phenylmethylsulfonyl fluoride | $C_7H_7FO_2S$ | Sigma-Aldrich |
| Potassium chloride | KCl | Sigma-Aldrich |
| Sodium chloride | NaCl | Merck |
| Sodium dodecyl sulfate | $NaC_{12}H_{25}SO_4$ | Merck |
| Sodium pyruvate | $C_3H_3NaO_3$ | Sigma-Aldrich |
| Trans IT-LT1 | - | Mirus Bio LLC |
| Tricine | $C_6H_{13}NO_5$ | Sigma-Aldrich |
| Tris-hydrochloric acid | HCL | Sigma-Aldrich |
| Triton | - | Sigma-Aldrich |
| Trypsine-EDTA | - | Sigma-Aldrich |
| Yeast extract | - | Sigma-Aldrich |

## 2.2 *Primers (Oligonucleotides)*

**Table 2. All forward (fwd) and reverse (rev) primers used**

| ID | Name | Sequence 5´→3´ |
|---|---|---|
| MT1984 | RXRγ fwd (qPCR) | CAGAGATGTACACGGACAGCA |
| MT1985 | RXRγ rev (qPCR) | TCTAGGGGCAGCTCAGAGAA |
| MT2002 | RXRβ1 fwd (qPCR) | AGGTCTATGCATCACTGGAAGC |
| MT2003 | RXRβ1 rev (qPCR) | CAGATGCTCCAAGCACTTCA |
| MT2022 | RXRβ2 fwd (qPCR) | TTCCCTGGAGTCCTACTGCAAGC |
| MT2023 | RXRβ2 rev (qPCR) | TCCAGGCACTTCAGACCAAT |
| MT1990 | RXRα fwd (qPCR) | CAACAAGGACTGCATCATCG |
| MT1991 | RXRα rev (qPCR) | GAACGGCTGCGTGTAACAACA |
| MT74 | β-Act fwd | GAGAAGATCTGGCATCACACCTTC |
| MT75 | β-Act rev | GGTCTCGTGGATACCGCAAGATTC |
| MT41 | T3 fwd | ATTAACCCTCACTAAAGGGA |
| MT43 | T7 rev | TAATACGACTCACTATAGGG |
| MT2024 | RXRβ1 fwd | ggaaccGAATTCAAGGCTCTTGCGGTGCAGGA |
| MT2025 | RXRβ1 rev | cgagtcGCTAGCCTAAGATAACTGGTGGGGCGCTTCAAG |
| MT2034 | RXRγ fwd | gcagcaGAATTCAAGAGAGAAGCGGTGCAGGA |
| MT2035 | RXRγ rev | ttgccgGCTAGCTCATGTGATCTGGTGGGGAGCC |
| MT1077 | PCMX fwd | TGCCGTCACAGATAGATTGG |
| MT1279 | PCMX rev | AATCTCTGTAGGTAGTTTGTCCA |
| MT1200 | Arp fwd | TGATCCTCCACGACGATGAG |
| MT1999 | Arp rev | CAGGGCCTTGGCGAAGA |

## 2.3 *Enzymes*

**Table 3. Overview of different enzymes used**

| Name | Supplier |
|---|---|
| AmpliTaq Gold DNA polymerase | Thermo Fisher Scientifics |
| Big dye terminator v3.1 | Applied Biosystems |
| DreamTaq green DNA-polymerase | Life Technologies |
| EcoRI- Restriction enzyme | Takara |
| NheI- Restriction enzyme | Takara |
| Phusion Hot Start II DNA polymerase | Thermo Fisher Scientifics |
| RNase | New England Biolabs |
| RNaseOUT | Invitrogen |
| Superscript III reverse transcriptase | Invitrogen |
| Shrimp alkaline phosphatase (SAP) | Affymetric |

## 2.4 *Plasmids*

**Table 4. List of plasmids used**

| Name | Use |
|---|---|
| pCMX-GAL4-DBD | Construction of pCMX-GAL4-RXRβ1/γ |
| pCMX-GAL4-RXRβ1 | Luciferase reporter gene assay |
| pCMX-GAL4-RXRγ | Luciferase reporter gene assay |
| pSC-B | Blunt cloning vector |
| pSC-B-RXRβ1 | Construction of pCMX-GAL4-RXRβ1/γ |
| pSC-B-RXRγ | Construction of pCMX-GAL4-RXRβ1/γ |
| mh(100)x4tk luc | Luciferase reporter gene assay |
| pCMV-β-Gal | Luciferase reporter gene assay |

## 2.5 *Eukaryotic and prokaryotic cell lines*

**Table 5. Different cell lines used in thesis and their domain**

| Name | Domain | Supplier |
|---|---|---|
| COS-7 | Eukaryote | (Gluzman, 1981) |
| StrataClone Solo Pack Competent Cells | Prokaryote | Agilent |
| StrataClone “Mix&Go” Competent Cells | Prokaryote | Agilent |

## 2.6 *Growth medium*

**Table 6. Lysogeny Broth (LB) growth medium**

| Component | LB-agar | LB-medium |
|---|---|---|
| Tryptone | 10 g/L | 10 g/L |
| NaCl | 10 g/L | 10 g/L |
| Yeast extract | 5 g/L | 5 g/L |
| Agar-agar | 15 g/L | - |
| Ampicillin | 100 mg/L | 100 mg/L |
| dd$H_2O$ | - | - |

**Table 7. Freezing medium and cultivation medium for COS-7-cell line**

| Component | Concentration |
|---|---|
| Dulbecco's modified Eagle´s medium | 1 X |
| Fetal bovine serum | 10% |
| L-glutamine | 4 mM |
| Sodium pyruvate | 1 mM |
| Penicillin-Streptomycin | 1 U/mL |
| DMSO | 5% |

## 2.7 *Buffers and solutions*

### 2.7.1 *Agarose gel*

**Table 8. TBE buffer**

| Component | Concentration |
|---|---|
| Tris | 0.45 M |
| Boric acid | 0.45 M |
| EDTA | 0.01 M |
| $ddH_2O$ | - |

**Table 9. Agarose gel**

| Component | Concentration |
|---|---|
| TBE-buffer | 0.5 X |
| Agarose | 0.7-2% |
| GelRed | 0.0002% |

### 2.7.2 *Western blot assay*

**Table 10. Components and volumes for running and stacking gel for one 12% SDS-page**

| Component | 12% Running Gel | 12% Stacking gel |
|---|---|---|
| $ddH_2O$ | 2.48 mL | 2.27 mL |
| 30% Acrylamide-Bis | 3.0 mL | 0.65 mL |
| 1.5M Tris pH8.8 | 1.9 mL | - |
| 0.5M Tris pH6.8 | - | 1.0 mL |
| 20% SDS | 37.5µL | 20.0 µL |
| 10% APS | 75µL | 40.0 µL |
| TEMED | 3µL | 4 µL |

**Table 11. 5X sample buffer**

| Component | Concentration |
|---|---|
| Tris HCl pH6.8 | 250 mM |
| SDS | 10% |
| Glycerol | 30% |
| 2-β-mercaptoethanol | 5% |
| Bromophenolblue | 0.02% |

**Table 12. Lysis buffer for protein preparation**

| Component | Concentration |
|---|---|
| 5X Sample buffer | 2X |
| 10X PBS pH 7.4 | 1X |
| Protease inhibitor | 1X |
| $ddH_2O$ | - |

**Table 13. 1X Running buffer**

| Component | Concentration |
|---|---|
| Tris base | 25 mM |
| Glycine | 192 mM |
| SDS | 0.1% |

**Table 14. 10X Tris buffer saline (pH 7.5)**

| Component | Concentration |
|---|---|
| Tris base | 24 g |
| NaCl | 88 g |
| $MQH_2O$ | 900 ml |
| 32-N-HCL | Adjust pH |

**Table 15. 0.05% TBS-Tween**

| Component | Concentration |
|---|---|
| 10X TBS | 0.5 X |
| Tween 20 | 0.05% |
| $MQH_2O$ | - |

**Table 16. 10X Tris-glycine (TG) buffer**

| Component | Concentration |
|---|---|
| Tris base | 30.3 g |
| Glycine | 14.4 g |
| $MQH_2O$ | - |

**Table 17. 1X Transfer buffer (TB)**

| Component | Concentration |
|---|---|
| 10X TG buffer | 1X |
| Methanol | 2X |
| $ddH_2O$ | - |

**Table 18. Blocking solution with 7% milk**

| Component | Concentration |
|---|---|
| Powder milk | 3.5 g |
| TBS-tween | 50 mL |

### 2.7.3 *Luciferase assay*

**Table 19. 1X Cell lysis buffer**

| Component | Concentration |
|---|---|
| Tris pH7.8 | 25 mM |
| Glycerol | 15% |
| CHAPS | 2% |
| L-α-Phosphatidylcholine | 1% |
| BSA | 1% |

**Table 20. Cell lysis reagent solution**

| Component | Concentration |
|---|---|
| Cell lysis buffer | 1X |
| EGTA | 4 mM |
| $MgCl_2$ | 8 mM |
| PMSF | 0.4 mM |
| DTT | 1 mM |

**Table 21. 4X Luciferase base buffer (4X pH 7.8)**

| Component | Concentration |
|---|---|
| Tricine | 80 mM |
| $(MgCO_3)_4 \bullet Mg(OH)_2 \bullet 5H_2O$ | 4.28 mM |
| $Na_2EDTA$ | 0.4 mM |
| $MgCl_2$ | 10.68 mM |
| - | - |

**Table 22. Luciferase reaction solution**

| Component | Concentration |
|---|---|
| Luciferase buffer | 1X |
| ATP | 0.5 mM |
| DTT | 5 mM |
| Coenzyme A | 0.2 mM |
| D-luciferin | 0.5 mM |

**Table 23. β-galactosidase buffer (10X)**

| Component | Concentration |
|---|---|
| $Na_2HPO_4$ | 60 mM |
| $NaH_2PO4$ | 40 mM |
| KCl | 10 mM |
| $MgSO4\bullet 7H_2O$ | 1 mM |

**Table 24. β-galactosidase reaction solution**

| Component | Concentration |
|---|---|
| β-gal buffer | 1X |
| β-mercaptoethanol | 4 mM |
| ONPG | 8 mM |

### 2.7.4 *Cell viability and cytotoxicity assay*

**Table 25. L-15/ex A**

| Component | Conc. |
|---|---|
| NaCL | 80 g |
| KCl | 4 g |
| $MgSO4\bullet 7H_2O$ | 2 g |
| $MgCl_2\bullet 6H_2O$ | 2 g |
| $ddH_2O$ | 600 mL |

**Table 26. L-15/ex B**

| Component | Conc. |
|---|---|
| $CaCL_2$ | 1.4 g |
| $ddH_2O$ | 100 mL |
| - | - |
| - | - |

**Table 27. L-15/ex C**

| Component | Conc. |
|---|---|
| $Na_2HPO_4$ | 1.9 g |
| $KH_2PO4$ | 0.6 g |
| $ddH_2O$ | 300 mL |
| - | - |
| - | - |

**Table 28. Cell viability solution**

| Component | Concentration |
|---|---|
| L-15/ex A | 34 mL |
| L-15/ex B | 6 mL |
| L-15/ex C | 17 mL |
| Galactose | 0.8 mg/mL |
| Pyruvate | 0.5 mg/mL |
| $ddH_2O$ | 500 mL |
| Resazurin | 0.03 mg/mL |
| CFDA-AM | 0.00 1mg/mL |

## 2.8 *Antibodies*

**Table 29. Primary and secondary antibodies used in western blot assay**

| Name | Supplier |
|---|---|
| Anti-GAL4-DBD mouse monoclonal | Santa Cruz |
| Horseradish peroxidase linked antibody sheep Anti-mouse IgG, polyclonal | GE Healthcare |
| Anti β-actin monoclonal | Abcam |

## 2.9 *Commercial kits*

**Table 30. Overview of different commercial kits and their application**

| Name | Supplier | Application |
|---|---|---|
| NucleoBond Xtra Midi/Mini plasmid purification kit | Macherey-Nagel | Plasmid purification |
| NucleoSpin Plasmid EasyPure kit | Thermo Scientific | Protein expression verification in COS-7 cells |
| SuperSignal West Pico Chemiluminescent Substrate | Thermo Scientific | Protein expression verification in COS-7 cells |
| NucleoSpin Gel and PCR clean-up | Macherey-Nagel | Agarose gel extraction |
| SuperScript Reverse Transcriptases | Bio-Rad | cDNA synthesis |
| BigDye Terminator v4.1 cylce sequencing kit | Thermo Scientific | Sanger sequencing |
| LightCycler 480 SyBR green I mastermix | Roche | qPCR amplification |
| StrataClone Blunt PCR cloning kit | Agilent | Blunt cloning into pSC-B |
| T4 DNA-ligase kit | Takara | Digest ligation of RXR and pCMX |
| TaKaRa Ex Taq | Takara | PCR amplification |

2.10 *Ligands for luciferase assay*

**Table 31. Ligands used for luciferase assay with 9-cis-RA and different organotins**

| Name | Supplier | CAS number |
|---|---|---|
| 9-cis-retinoic acid | Sigma-Aldrich | 5300-03-8 |
| Tributyltin chloride | Sigma-Aldrich | 1461-22-9 |
| Tripropyltin chloride | Sigma-Aldrich | 76-87-9 |
| Fentin chloride | Sigma-Aldrich | 639-58-7 |
| Fentin hydroxide | Supleco | 76-87-9 |
| Trimethyltin chloride | Sigma-Aldrich | 1066-45-1 |

2.11 *Instruments*

**Table 32. Overview of instruments and their application**

| Name | Supplier | Application |
|---|---|---|
| Buerker hemocytometer | Marienfield | Cell counting |
| C1000™ Thermal Cycler | Bio-Rad | qPCR amplification |
| ChemiDoc™ XRS+system | | Agarose gel picture |
| Heraeus pico 21 | Thermo Scientific | Centrifugation |
| DM IL inverted microscope | Leica | Cell count and confluency determination |
| EnSpire™ 2300 Multilabel Reader | PerkinElmer | |
| GD100 | Grant | Heat-shocking in water bath |
| Heraeus multifuge X3R | Thermo scientific | Centrifugation |
| HS 501 Digital | IKA®-Werle | Shaker |
| MilliQ A10 advantage | Merck | $MQH_2O$ dispenser |
| MP220 | Bergman | pH-meter |
| Nanodrop 1000 | Thermo Scientific | Concentration of RNA, DNA and cDNA |
| PowerPac™ HC | Bio-Rad | Electric power to electrophoresis |
| Multitron Standard shaking incubator | Infors HT | Cell cultivation incubation |
| Ultraspec 10 cell density meter | Amersham Biosciences | Culture density |
| UV-transiluminator | UVP | Agarose gel extraction |
| Thermomixer compact | Eppendorf | Heat-block |
| Panasonic mco-170aicuv-pe | Lab-tec | Incubation of CO7 with $CO_2$ |
| Termaks incubator | Termaks | Incubator for transfected colonies |
| CleanAir EuroFlow Class II biosafety cabinet | Baker | Sterilized workspace for handling COS-7 cells |

## 2.12 *Software*

**Table 33. Overview of software and online tools and their application**

| Name | Provider | Application |
|---|---|---|
| Clustal Omega | EMBL-EBI | Multiple sequence alignment |
| Muscle | EMBL-EBI | Multiple sequence alignment |
| EMBOSS Needle | EMBL-EBI | Pairwise sequence alignment |
| MegaX v.10.2.6 | Tamura et al. 2015 | Phylogenetic analysis |
| Ensembl | EMBL-EBI | Genome browser |
| Blast | NCBI | Protein and DNA homology searches |
| Genome Data Viewer | NCBI | Chromosome location tool |
| Protein Data Bank | PBD | Protein crystalline structures |
| ExPASy | SIB | DNA to protein conversion |
| Excel 2020 | Microsoft | Processing data and statistics |
| Jalview 2.11.1.4 | Waterhouse et al. 2009 | Visualization of sequence alignments |
| GraphPad 9 | Graphpad software | Figures and statistics |
| Primer3 v.0.4.0 | Howard Hughes Medical Institute | Primer design |
| SnapGene 5.3 | Biotech | Primer design and cloning simulations |
| PowerPoint 2020 | Microsoft | Figure preparation |
| UniProt | EMBL-EBI and PIR | Genome browser |
| Wormweb 4.0 | Nikhil Bhatla | Intron-exon illustrator |
| Word 2020 | Microsoft | Thesis writing |

# 3 Methods

## 3.1 *Experimental outline*

Throughout this thesis several bioinformatical- and molecular methods were applied. Figure 8 represents an experimental outline containing the most significant steps.

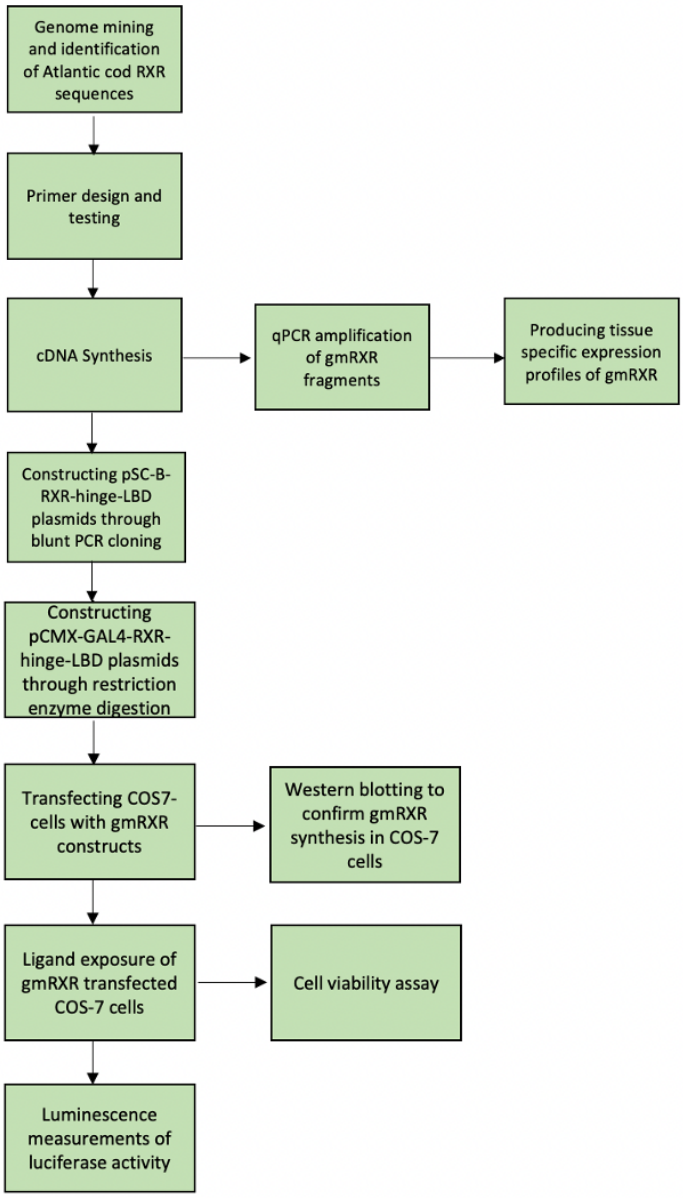


**Figure 8. Experimental outline and important methods used.** gmRXR-encoding gene sequences were revealed through genome mining. cDNA was prepared from various tissues and qPCR was used to obtain tissue-specific expression profiles of gmRXR isoforms in Atlantic cod. gmRXRβ1 and RXRγ were cloned from liver tissue and inserted into the pSC-B-RXR-hinge-LBD, and subsequently pCMX-GAL4-RXR-hinge-LBD. Sanger sequencing was used to verify incorporation of gmRXRβ1/γ into the plasmids. gmRXRβ1/γ transfected COS-7 cells were further utilized to verify synthesis of gmRXR fusion proteins, measure OTCs and 9-cis-RA mediated activation of RXR in a luciferase reporter gene assay and to determine the cytotoxicity of test compounds.

## 3.2 *Bioinformatical analyses*

### 3.2.1 *Locating gmRXR isoforms in the Atlantic cod genome*

Well-annotated RXRα, RXRβ1, RXRβ2 and RXRγ sequences from various species were obtained from UniProt, including *Homo sapiens*, *D. reiro*, *S. salar* and *Rattus norvegicus*. Protein Blast ® (NCBI) searches against the Atlantic cod genome (taxonomy identification 8049) using these RXRs as queries were used to identify and locate the Atlantic cod isoforms (gmRXR). Protein Blast ® output provides percentage identity and query cover, along other information, allowing selection of predicted gmRXR sequences. Predicted gmRXRα, gmRXRβ1, gmRXRβ2 and gmRXRγ were identified from these Blast searches. Genome Data Viewer (NCBI) was used to find the chromosomal location of the genes encoding the different isoforms.

The DNA sequences encoding the putative RXR proteins were extracted from GenBank ® (NCBI) by using the accession number attached to the Blast-obtained hits. Expasy (SIB) translate tool was used to translate the DNA sequences into amino acid sequences.

### 3.2.2 *Multiple sequence alignment and phylogenetic analysis*

Multiple sequence alignments (MSA) were produced in Clustal Omega (EMBL-EBI) by using RXR protein sequences from Atlantic cod and a diverse set of other organisms. Jalview 2.11.1.4 was used to visualize the alignment.

A phylogenetic analysis was performed to categorize the different gmRXR isoform sequences into their specific isoforms. A comprehensive MSA including the predicted gmRXR proteins and RXR sequences obtained from variety of other species was generated in Clustal Omega (EMBL-EBI). Phylogenetic analysis provides different outputs representing the evolutionary history between subjects. In this study a phylogenetic tree was produced to visualize the evolutionary relationship of different RXR isoforms from different species, subsequently categorizing them based on sequence homology. MEGAX (PSU) was used to produce a maximum likelihood tree, which allowed categorization of the gmRXR isoform as gmRXRα, gmRXRβ1, gmRXRβ2 and gmRXRγ.

### 3.2.3 *Annotation of DBD, hinge and LBD*

RXR protein sequences from *H. sapiens* and *D. rerio* containing well-annotated DBD, hinge-region and LBD, were obtained from UniProt. A MSA was then produced with Clustal Omega using the annotated domain sequences and the gmRXR sequences. From the MSA, the DBD, hinge-region, and LBD were identified and defined in the gmRXR isoforms.

### 3.2.4 *Exon-intron mapping*

To map the exon-intron boarders in the gmRXR-encoding genes, the Ensembl (EMBL-EBI) genome browser was used. The gene ID of the different gmRXR isoforms were used as search inputs. Ensembl provides a vast array of sequence information including intron and exon sequences. WormWeb v.4. was used to illustrate the exon-intron boarders.

## 3.3 *Complementary DNA synthesis*

Complementary DNA (cDNA) was synthesized by the reverse transcriptase enzyme using RNA as template and the cDNA synthesis protocol provided by iScript™. The RNA templates consisted of elven different tissue samples from three individual juvenile female Atlantic cod (denoted as TB3, TB4 and TB5), obtained from preexisting RNA tissue bank in our laboratory. The tissue samples were from ovary, muscle, head kidney, skin, spleen, heart, stomach, liver, brain, gill, and eye. The iScript™ cDNA synthesis kit includes a reverse transcriptase, a reaction mix, and a RNase-inhibitor. The reaction mix include components such as dNTPs, primers, and a buffer. Of the primers in the reaction mix, there are two types: oligio(dT)-primer and random hexamer. Oligio(dT)-primers are rich in thymine acting as hybridization probes that bind and hybridize poly-A tales in mRNA. The random hexamer consists of six random oligonucleotides able to bind mRNA on different locations. The reaction mix, reverse transcriptase and $MQH_2O$ was first mixed without template and incubated at 70°C for 5 min and then left on ice. The RNA was then added, and the mix was centrifuged, before polymerase chain reaction (PCR) was performed. Synthesized cDNA was stored at -20°C.

**Table 34. Protocol followed for cDNA synthesis with qScript Kit**

| Reagents | Volume | Concentration |
|---|---|---|
| RNA template | - | 1 μg |
| qScript Reaction Mix (5x) | 4 μL | 1X |
| qScript Reverse Transcriptase | 1 μL | 1X |
| $MQH_2O$ | To 20 μL | - |

**Table 35. PCR-program**

| Temperature | Time | Cycles |
|---|---|---|
| 25°C | 5 min | |
| 46°C | 30 min | 1 |
| 96°C | 1 min | |

### 3.4 *Polymerase chain reaction*

Polymerase chain reaction (PCR) is a method in which a vast amount of specific, and unspecific, DNA sequences can be produced from a primary pool by using single stranded DNA primers. The PCR protocol used was a three step PCR where cyclical events of denaturation, annealing and elongation occurs to produce DNA copies. During denaturation, the DNA is normally heated to 95°C, where the double helix is broken into two separate strands. During annealing, temperatures are lowered to the optimal temperature in which primers most efficiently bind to 5′-DNA and 3′-DNA. Elongation is the final step where temperatures are increased to 72°C as it is the optimal temperature for DNA-polymerase binding and activation. The DNA-polymerase synthesize new strands, allowing double helixes to form and the number of DNA helices are now doubled. This is cycle is repeated until the desired amount of DNA is produced, typically 20-40 cycles.

### 3.5 *DNA-electrophoresis*

Agarose gen electrophoresis was used to analyze amplified DNA (PCR products). Electrophoresis uses agarose gels to separate differently sized DNA strands based on size-dependent migration through an electric field. Due to DNAs negative charge, it will migrate towards a positive electrode, with smaller molecules able to migrate longer distances through the porous agarose gel.

Agarose and 0,5 X TBE buffer was mixed and heated to produce 0.5-2% agarose gel, as desired. 0,5 µL or 0,7 µL GelRed was added to 30 ml or 50 ml agarose gels, respectively, before agarose was left to polymerize. GelRed, is a fluorescent nucleic acid dye used to stain DNA. Once set, 0,5 X TBE buffer was added on top of the gel. The PCR product mixed with 10X loadingbuffer was then loaded into wells in the agarose gel. 10 X loadingbuffer was used to ensure samples descending to the bottom of the wells. A 2-log DNA ladder was used as a size marker. The gel was running at 80-100V for 30-45 min and visualized with a ChemiDoc XRS+ (Bio-Rad) instrument.

### 3.6 *Gel extraction of DNA*

Gel extraction of DNA was done using NucleoSpin® Gel and PCR Cleain-up (Macherey-Nagel). To extract DNA from an agarose gel and further purify the product, the gel was first placed at a UV-table which allowed visualization of the DNA bands. The desired DNA band(s) were then cut out using a scalpel, transferred to an Eppendorf tube, mixed with a guanidium chloride-based buffer and heated at 50°C until gel was dissolved. The DNA was then transferred to a column containing a silicon membrane allowing DNA to bind the membrane, where it was washed and centrifuged. DNA was eluted using a Tris-HCL buffer. A Nanodrop1000 instrument was used to measure the concentrations of DNA achieved from the extraction.

### 3.7 *Quantitative polymerase chain reaction (qPCR) assay*

Quantitative polymerase chain reaction (qPCR), or real-time polymerase chain reaction (RT-PCR) as it is also called, is based on the same principles as PCR. However, qPCR uses in addition a fluorescent agent allowing quantification and detection of DNA amplified in each cycle.

#### 3.7.1 *Primer design*

To amplify gmRXR transcripts, a specific primer pair of forward (5′) and reverse (3′) primers were designed for RXRα, RXRβ1, RXRβ2 and RXRγ. To ensure optimal and specific binding to cDNA template the primers consisted of 18-30 nucleotides, a GC (guanine-cytosine) content of 40-60%, and a melting temperature (Tm) no less than 4°C between the primer pairs. The primers were designed in Primer3web version 4.1.0. Primers were tested through PCR amplification and visualized on a 2% agarose gel.

**Table 36. Primer sequences used for qPCR assay.**

| Primers | Sequence 5´→3´ |
|---|---|
| RXRα (MT1990+MT1991) | CAACAAGGACTGCATCATCG<br>GAACGGCTGCGTGTAACAACA |
| RXRβ1 (MT2002+MT2003) | AGGTCTATGCATCACTGGAAGC<br>CAGATGCTCCAAGCACTTCA |
| RXRβ2 (MT2022+MT2023) | TTCCCTGGAGTCCTACTGCAAGC<br>TCCAGGCACTTCAGACCAAT |
| RXRγ (MT1984+MT 1985) | CAGAGATGTACACGGACAGCA<br>TCTAGGGGCAGCTCAGAGAA |
| β-actin (MT74+MT75) | GAGAAGATCTGGCATCACACCTTC<br>GGTCTCGTGGATACCGCAAGATTC |

**Table 37. Reagents for PCR used to test primers**

| Reagents | Volume | Concentration |
|---|---|---|
| Lightcycler ® SyBR green master mix | 10 µL | 1X |
| Template (cDNA) | - | - |
| Primer (F+R) | 1 µL | 0,5 µM |
| $MQH_2O$ | To 20 µL | - |

**Table 38. PCR program**

| Temperature | Time | Cycles |
|---|---|---|
| 95°C | 5 min | - |
| 95°C<br>55°C<br>72°C | 10 sec<br>20 sec<br>30 sec | 40 |
| 72°C | 5 min | - |
| 12°C | - | - |

### 3.7.2 *qPCR protocol*

LightCycler®480 SYBR Green I Master (Rocher) was used as a fluorescent agent. In a 96-well plate, 5 µL of the different tissue templates (cDNA) was mixed with 15 µL reaction mix and added to each well. The reaction mix consisted of 0,5 µM total forward and reverse primers and 10 µL master mix. To fit everything in one 96-well plate, tissue samples derived from individuals TB4 and TB5 were added to the 96-well plate in triplicates (i.e., TB4 in wells A1-D5 and TB5 in wells E5-H9) and TB3 in duplicates (wells A10-H12). A plastic seal was added, before centrifuging the plate at 500 rpm for 3 minutes. The plate was then transferred to the C1000™ Thermal Cycler using the program found in Table 39. To ensure purity and specificity of primers used in qPCR a melting curve analysis was performed. A melting curve obtained with a specific primer pair will consist of only one peak, while non-specific primer pairs will consist of two or more peaks due to differences in the Tm of the products the primers have produced. In this study, tissue specific expression of the Atlantic cod RXR isoforms was examined. A no template qPCR reaction was performed and used as a negative control. Further, the housekeeping gene β-actin was used to later normalize the tissue specific expression across samples.

**Table 39. qPCR program**

| Step | Temperature | Time | Cycles |
|---|---|---|---|
| Denaturation | 95°C | 5 min | 1 |
| Denaturation | 95°C | 10 sec | |
| Annealing | 55°C | 20 sec | 40 |
| Elongation | 72°C | 30 sec | |
| Melting curve | 95°C | 10 sec | - |
| | 65°C | 5 sec | - |
| | 95°C | - | - |

### 3.7.3 *Efficiency of primer pairs*

A standard curve was produced to determine the efficiency of the primer pairs. Gel-extracted PCR products from initial primer testing was used as templates. The DNA was diluted 1/10 with a subsequent 2-fold serial dilution. Reaction mix was added, and qPCR was done using the same protocol as described in Table 38. From the standard curve, the amplification-efficiency (E) for each primer were verified to be withing the desired 90-110% range (E-value between 1,9-2,1).

### 3.7.4 *Analyzing qPCR data*

To calculate normalized tissue expression of *gmrxr* isoforms in Atlantic cod tissue, the ΔCq method (Livak & Schmittgen) was used (Formula 1). This method uses differences in Cq-values between reference genes and target genes for each sample. Cq-values are defined as the number of cycles needed for fluorescent signal to exceed background fluorescence. Normalized tissue expression was calculated in Microsoft Excel and visualized using GraphPad Prism 9.

**Formula 1. Normalizing tissue specific expressions of gmRXR in in Atlantic cod tissues**

$$Ratio\ (\Delta\mathrm{Cq}) = 2^{Cq(ref)-Cq(target)}$$

## 3.8 *Blunt cloning and pCMX-GAL4-RXR construction*

### 3.8.1 *Primer design*

Individually designed primes were used for incorporation of gmRXRβ1- and gmRXRγ-hinge-LBD sequences into a pSC-B vector (Methods 3.8.2-3.8.4), and subsequently when constructing the pCMX-GAL4-RXRβ1/γ-hinge-LBD (Methods 3.8.6-3.8.8). The primers designed and used in cloning followed the same criteria as those of the qPCR in order to achieve optimal template binding. These primers were 18-30 nucleotides long, a GC content between 40-60% and no less than 4°C Tm difference between the primer pair. The forward primer was placed at the N-terminal of the hinge-region with the reverse primer at the far C-terminal of the LBD. SnapGene 5.3 software was used for primer design where secondary structure prediction and *in silico* cloning simulation was performed.

Another feature of the cloning primers is the introduction of recognition sequences for restriction enzymes with an additional random 6bp tail. Restriction enzymes are endonucleases that can recognize and cut specific DNA sequences. To construct the pCMX-GAL4-RXR-hinge-LBD plasmids, restriction enzymes was used to cut and ligate the gmRXR hinge-LBD sequences into pCMX-GAL4 plasmids. In the primers used, EcoRI and NheI recognition sequences were introduced in the forward and reverse primers respectively. Primers was tested using PCR and a 0,7% agarose gel.

**Table 40. Primers designed and used for producing gmRXR-hinge-LBD fragments**

| Primer | Sequence 5′→3′ |
|---|---|
| gmRXRβ1 fwd | ggaaccGAATTCAAGGCTCTTGCGGTGCAGGA |
| gmRXRβ1 rev | cgagtcGCTAGCCTAAGATAACTGGTGGGGCGCTTCAAG |
| gmRXRγ fwd | gcagcaGAATTCAAGAGAGAAGCGGTGCAGGA |
| gmRXRγ rev | ttgccgGCTAGCTCATGTGATCTGGTGGGGAGCC |

**Table 41. Reagents for PCR used to test cloning primers**

| Reagents | Volumes | Concentrations |
|---|---|---|
| 5X Phusion HF buffer | 10 µL | 1X |
| dNTP | 4 µL | 200 µM |
| Template | - | - |
| Phusion hotstart polymerase | 0,5 µL | 1U |
| Primer (F+R) | 2,5 µL | 10 µM |
| $MQH_2O$ | To 50 µL | - |

**Table 42. PCR program**

| Temperature | Time | Cycles |
|---|---|---|
| 98°C | 30 sec | - |
| 98°C | 10 sec | |
| 67°C | 30 sec | 40 |
| 72°C | 30 sec | |
| 72°C | 5 min | - |
| 4°C | - | - |

### 3.8.2 *Blunt PCR cloning and transformation of Escherichia coli*

Blunt cloning was a procedure used to clone gmRXR-PCR-products into pSC-B vectors. The StrataClone Blunt PCR cloning kit (Agilent) was used. Purified PCR products extracted from agarose gel were added to cloning buffer and vector mix from supplier. The lysis mix was incubated at RT°C for 5 min and then put on ice.

The cells used were provided by StrataClone and are competent *E. coli* cells submerged in a saline solution to increase absorption of extracellular DNA, e.g., PCR product. By adding PCR product to cell mix on ice, DNA binding to cells is promoted and subsequent heating causes a change in membrane fluidity allowing bound DNA to be absorbed completely by the cells.

The Strataclone *E. coli* cells were stored at -80°C and thawed on ice before 1 µL ligation mix was added to the cells. The ligation mix consisted of 3 µL blunt cloning buffer, 2 µL extracted PCR product and 1 µL blunt vector mix. The cell-mix was incubated on ice for 20 min, and 3

mL of LB-medium was pre-warmed in a water bath at 42°C. After incubation, the cell-mix was heatshocked by submerging in the 42°C water bath for 45 sec, before being incubated on ice for 2 min directly after. 250 µL of the prewarmed LB-medium was added to the cell-mix and centrifuged at 250 rpms for 1,5h. 40 µL 2% X-gal was smeared out on duplicate agar-plates. 5 µL cell-mix+50 µL LB-medium was added to half the duplicate plates and 100 µL cell-mix to the other. A sterilized glass rod was used carefully to evenly distribute the content on the agar plates. The plates were then incubated at 37°C until enough transformed *E. coli* colonies had been produced.

**Table 43. Reagents for blunt cloning and screening of PCR product**

| Reagents | Volume |
|---|---|
| StrataClone competent E. coli | - |
| StrataClone blunt cloning buffer | 3 µL |
| Gel/PCR product | 2 µL |
| Strataclone blunt vector mix | 1 µL |
| LB-medium | - |
| 2% X-gal | 40 µL |

### 3.8.3 *Blue-White screening*

Blue-White screening is a method used to efficiently differentiate between transformed and non-transformed bacterial colonies. In this study 2% X-gal was used as screening agent. In colonies formed by non-recombinant cells X-gal is hydrolyzed by β-galactosidase to form 5-bromo-4c-chloro-indoxyl which dimerizes to produce a blue pigment (5,5′-dibromo-4′4-dichloro-indigo). In recombinant cells, the plasmid (pSC-B) is manipulated to disrupts α-complementation leading to no functional β-galactosidase synthesis. This causes recombinant colonies to have a pale appearance and can be isolated and purified through miniprep.

### 3.8.4 *Colony PCR*

This method is used to assess transformed bacteria to verify the existence of a desired introduced genetic construct. Here, a portion of the construct is amplified using PCR. In this study it was used to verify the insertion of a product into the pSC-B and pCMX-GAL4-DBD plasmids. Colonies grown on agar plates are used as templates where the desired colonies are

poked using a pipette tip and mixed with 5 µL $MQH_2O$. 1 µL of colony+$MQH_2O$ was then added to a master-mix and amplification was done with PCR. Agarose gel electrophoresis with a 0,7% agarose gel was used to confirm the presence of an inserted DNA fragment.

**Table 44. Colony PCR reagents used for both pSC-B-RXR and pCMX-GAL4-RXR**

| Reagents | Volumes | Concentrations |
|---|---|---|
| 10X DreamTaq Green Buffer | 1 µL | 1X |
| dNTP | 0,8 µL | 200 µM |
| Primer (F+R) | 0,5 µL | 10 µM |
| Template | - | - |
| DreamTaq DNA polymerase | 0,05 µL | 1,25U |
| $MQH_2O$ | To 10 µL | - |

**Table 45. Primers used for colony PCR of pSC-B and pCMX-GAL4 plasmids**

| Primer | Sequence 5′→ 3′ |
|---|---|
| pSC-B MT41 (F) | ATTAACCCTCACTAAAGGGA |
| pSC-B MT42 (R) | TAATACGACTCACTATAGGG |
| pCMX-GAL4 MT1077 (F) | TGCCGTCACAGATAGATTGG |
| pCMX-GAL4 MT 1279 (R) | AATCTCTGTAGGTAGTTTGTCCA |

**Table 46. Colony PCR program for both pSC-B-RXR and pCMX-GAL4-RXR**

| Temperature | Time | Cycles |
|---|---|---|
| 95°C | 3 min | - |
| 95°C<br>55°C<br>72°C | 30 sec<br>30 sec<br>1 min | 30 |
| 72°C | 5 min | - |
| 4°C | - | - |

### 3.8.5 *Plasmid purification*

Two methods of purifying plasmid DNA were used during construction and sequencing of plasmids vectors, including miniprep and midiprep. Both methods include growing cells in LB-medium with added antibiotics (ampicillin), centrifugation, and addition of a resuspension buffer. The cells are further lysed and added a neutralization buffer where chromosomal DNA and other cellular components are liberated, and plasmid DNA can retain a supercoiled conformation. Liberated cellular components are precipitated through centrifugation and plasmid DNA is isolated and added to a silica-based membrane allowing the DNA to bind. Further, a washing step containing ethanol-based buffer is used to remove impurities from the membrane. Finally, a slightly alkaline elution buffer (AE-buffer) is used to free purified DNA from the membrane. Midiprep has an additional cleaning step in which DNA is precipitated with isopropanol, centrifuged, washed with ethanol and then dried. A Nanodrop1000 instrument was used to measure concentrations of plasmid DNA.

Miniprep was used to purify plasmid-DNA used in construction and sequencing of pSC-B-RXR and pCMX-GAL4-RXR-hinge-LBD plasmids. Cells containing plasmids were added to 3 mL of LB-medium containing ampicillin (0,1 mg/mL) and incubated on a shaker at 250 rpm for 24h at 37°C. NucleoSpin ® kit (Macherey-Nagel) was used and the protocol from the manufacturer was followed, where final purified DNA was eluted in 50 µL AE-buffer.

Midiprep was used for purification of the pCMX-GAL4-RXR-hinge-LBD plasmids, the luciferase reporter plasmid and the β-galactosidase normalization plasmid, which all are used in the luciferase reporter gene assays. Cells containing the desired plasmids were added to 200 mL LB-medium containing ampicillin (0,1 mg/mL) and placed in a 37°C incubator at 250 rpm for ~24h. Ultraspec 10 Cell Density meter (Amersham Biosciences) was used to measure cell density. Optical density volume (ODV)=200 was calculated, and the midiprep purification was further performed using instructions from the Plasmid DNA purification NucleoBond ® PC100 kit (Macherey-Nagel).

### 3.8.6 *Restriction enzyme double digestion*

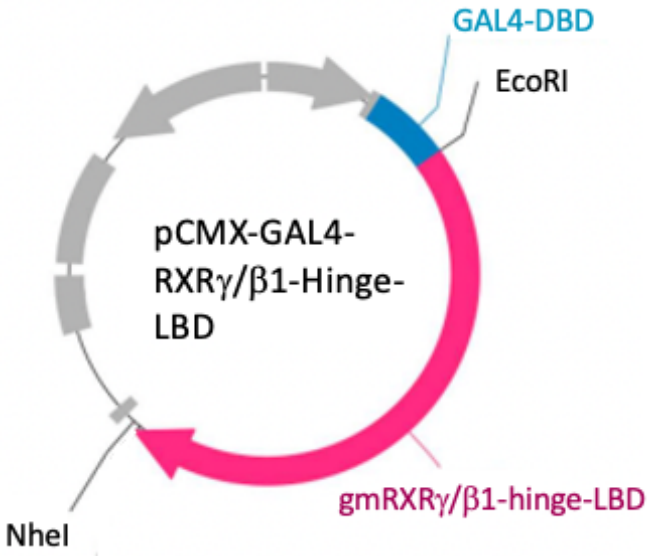


**Figure 9.** Simplified visualization of pCMX-GAL4-RXRβ1/γ-hinge-LBD plasmids with restriction enzyme recognition sites used in digestion reactions.

To allow incorporation of the gmRXR-sequences into the pCMX-GAL4-DBD, both a pCMX-GAL4-DBD plasmid and the pSC-B-RXRβ1/γ were digested using two restriction enzymes (EcoRI and NheI). Recognition sequences for the restriction enzymes are preexisting in pCMX-GAL4-DBD plasmid and introduced to gmRXR through the primers designed. The digestion reaction was incubated at 37°C for 3h. A dephosphorylation agent (SAP) was added 45 min before incubation end to dephosphorylate the plasmid. SAP removes the 5´-phosphate group created during the digestion reaction to inhibit relegation of linearized pCMX-GAL4-DBD. Dephosphorylation reactions was ended by adding the digest mix to a 65°C heating block for 15 min. 10 X loading buffer was added to the digest and an agarose gel were used to locate the digested pCMX-GAL4-DBD and gmRXR. Using a UV-table, the corresponding bands were cut out and cleaned using the gel-extraction/PCR-cleanup kit

**Table 47. Reagents for double digest with restriction enzymes**

| Reagent | Volume | Concentration |
|---|---|---|
| EcoRI | 1 µL | 0,375 U/µL |
| NheI | 1 µL | 0,375 U/µL |
| 10X Buffer M | 4 µL | 1X |
| Template (pCMX or RXR) | 1 µL | 10µg/40 µL (pCMX) or 2µg/40 µL (RXR) |
| $MQH_2O$ | 33 µL | - |
| SAP | 1,3 µL | 1U |

### 3.8.7 *Ligation*

To construct the pCMX-GAL4-RXR-hinge-LBD plasmids after restriction enzyme digestion, the products extracted from gel (digested plasmid and gmRXR) was ligated. The ligation reaction uses the enzyme T4 DNA-ligase, which promotes production of phosphodiester bonds between phosphate and hydroxyl groups in DNA. A ligation reaction mix consisting of pCMX-GAL4-digest, gmRXR-digest, T4-ligase, 10 X T4 DNA-ligase buffer and $MQH_2O$ was produced and incubated at 4°C for ~15h. Reaction was terminated through a 15 min incubation in a heating block at 65°C. Formula 2 was used to calculate the mass of inserted DNA needed for the ligation reaction, where a 3:1 molarity ratio was used of inserted gmRXR fragment compared to pCMX-GAL4-digest.

**Formula 2. Calculating the molecular mass of DNA for pCMX-GAL4 insertion**.

$$Mass(ng) = molar\ insertion * mass\ of\ vector\ (pCMX - GAL4) * ratio\ of\ insertion\ and\ vector\ length$$

**Table 48. Reagents for ligation protocol**

| Reagent | Volume | Concentration/amount |
|---|---|---|
| Digested RXR | - | - |
| Digested pCMX-GAL4 | - | 25 ng |
| 10X T4 DNA ligase buffer | 1 µL | 1X |
| T4 ligase | 1 µL | 17,5 U/µL |
| $MQH_2O$ | To 10 µL | |

### 3.8.8 *Transformation of plasmid construct*

To transform the plasmid constructs into *E. coli* cells, StrataClone competent cell Mix&Go was used. The cells were stored in -80°C and thawed on ice. 2 µL of ligation product was then added to cells and mixed carefully in. 5 µL cell mix and 15 µL LB-medium was then added to one agar plate, and 20 µL cell mix to another (no LB-medium). Both were evenly distributed by using a sterilized glass rod and incubated for 24-30h at 37°C. Colony PCR and agarose gel electrophoresis was then used to confirm transformants containing the pCMX-GAL4-RXR-hinge-LBD plasmids. Plasmids was then purified using midiprep (method 3.7.8).

### 3.8.9 *Sanger sequencing*

Sequencing of pCMX-GAL4-RXR-hinge-LBD constructs were performed at the Department of Biological Sciences (UiB). Preparation of the sequencing reaction was done in accordance with the BigDye v3.1 protocol provided by UiB. The reaction setup and thermal cycle program is found in Tables 49 and 51, with template being the pCMX-GAL4-RXR-hinge-LBD plasmids. After PCR reaction is completed, 10 µL $MQH_2O$ is added to the product and sent for sequencing. Sanger sequencing is limited to 900bp where the primers used allowed sequencing of whole RXR insertion. Sequencing data was analyzed in SnapGene v5.3, where sequence output was aligned with predicted RXR sequences obtained from the cod genome.

**Table 49. Sanger sequencing preparation reagents using BigDye v3.1 protocol**

| Reagents | Volume | Concentration |
|---|---|---|
| Big Dye | 8,5 µL | 1U |
| 5X Sequencing buffer | 8,5 µL | 1X |
| Template | - | - |
| Primer (F+R) | 8,5 µL | 3,2 µM |
| $MQH_2O$ | To 80 µL | - |

**Table 50. Primers used**

| Primers | Sequence 5′→ 3′ |
|---|---|
| MT1077 (F) | TGCCGTCACAGATAGATTGG |
| MT 1279 (R) | AATCTCTGTAGGTAGTTTGTCCA |

**Table 51. PCR program**

| Temperature | Time | Cycles |
|---|---|---|
| 96°C | 5 min | - |
| 96°C<br>50°C<br>60°C | 10 sec<br>5 sec<br>4 min | 25 |
| 4°C | - | - |

## 3.9 *Western blot assay*

### 3.9.1 *Sodium-dodecyl-sulfate (SDS) polyacrylamide gel electrophoresis (PAGE)*

SDS-PAGE electrophoresis is a method to separate proteins according to their molecular size. The proteins are first denaturated at 95°C, mixed with a sample buffer containing β-mercaptoethanol and SDS. β-mercaptoethanol acts as a reducing agent breaking disulfide bonds, while the anionic detergent SDS, promotes denaturation and coating of the peptides, producing a negatively charged polypeptide chain. The negative charge allows migration through a polyacrylamide gel for separation of differently sized proteins.

### 3.9.2 *Preparation of cell lysates*

COS-7 cells were seeded (Method 3.10.1) in 96-well plates and incubated for 18-24h. The following day, medium was discarded, and new medium added before COS-7 cells were transfected with the pCMX-GAL4-RXR plasmids (Methods 3.10.11). On day three, medium was once more discarded, and wells were washed with 100 µL 1 X PBS. 20 µL lysis reagent (Table 12) was then added to each well and incubated on ice on a shaker for 5min. The lysate was removed from the wells and transferred to a -80°C freezer for storage.

### 3.9.3 *Total protein staining*

A 1 mm thick polyacrylamide gel was casted and used for separation and visualization of total protein content. The gel was composed of a stacking gel and a separation gel that were transferred to an electrophoresis chamber after polymerization. The electrophoresis chamber was filled with appropriate volumes of 1 X TGS buffer. For protein molecular weight marker, 5 µL Precision Plus Protein ™ Prestained Protein Standards was used. 20 µL cell lysate was added to four wells. The gel was run at 200V for 45-60 min. To visualize the protein content, the gel was placed in a container and further on a shaker at RT°C and stained with InstantBlue ™ Coomassie Protein Stain (Expedeon) over night. Excess Coomassie was poured off and the gel was rinsed with ddH2O. A ChemiDoc XRS+ (Bio-Rad) instrument was used to photograph the stained gel.

### 3.9.4 *Western blotting*

Western blotting is a process also known as protein immunoblotting, in which specific proteins separated by SDS-PAGE can be detected through use of anti-bodies. In this study, Western blotting was used to verify the expression and synthesis of GAL4-RXR-hinge-LBD fusion proteins in transfected COS-7 cells. Mini Trans-Blot Electrophoretic Transfer Cell was used for western blotting. To prepare the western blot "sandwich", a PVDF-membrane (9*6cm) was submerged in methanol for 20 sec and then washed with dd$H_2O$. The membrane along the other sandwich components (two sponges and two filter papers) were submerged in transfer buffer for 15 minutes. The sandwich was then assembled in a specialized holder in the following order: sponge→ paper →membrane →gel →paper →sponge. The holder containing the sandwich was then placed in the electrophoresis chamber filled with transfer buffer and containing two cooling units. The blotting was run at 100V for 50 min-1hour. The membrane was transferred to a container and blocked with 7% dry-milk in TBS-tween (TBS-T) and placed on a shaker at 4°C overnight. The TBS-T+7% dry-milk was then poured off and the membrane was washed with TBS-T. Primary antibodies (mouse anti-Gal4-DBD) were diluted 1:500 in TBS-T and incubated at RT°C on a shaker for 1h. Excess/unbound primary antibody+TBS-T was poured of and the membrane was rinsed with TBS-T. Secondary antibodies (sheep anti-mouse IgG) was diluted 1:2000 in TBS-T and added to the membrane, placed on a shaker, and incubated for 1h at RT°C. Excess/unbound secondary antibody+TBS-T was poured of and washed with TBS-T. SuperSignal™ West Femto Maximum Sensitivity Substrate kit was used to visualize the GAL4-RXR-hinge-LBD fusion proteins. 3 mL solution was prepared, poured on the

membrane, and incubated at RT°C for 5 min. Protein bands were visualized with ChemiDoc XRS+ (Bio-Rad).

β-actin was used as loading control as it is ubiquitously expressed in all eucaryotic cells. The same membrane from the western blot with the mouse anti-GAL4-DBD antibody, was used here. The membrane was washed in TBS-T, and primary mouse anti-β-actin antibody was diluted 1:1000 and poured over the membrane where it was incubated for 1h at RT°C on a shaker. Primary antibody+TBS-T was poured off and the membrane washed with TBS-T on a shaker for 10 min three times. Secondary antibody (Sheep-anti-mouse) was diluted 1:2000 and poured over membrane and incubated at RT on a shaker for 1h. The membrane was subsequently washed with TBS-T on a shaker for 10 min three times. SuperSignal ™ West Femto Maximum Sensitivity Substrate kit was added (3 mL), and the protein bands were visualized in ChemiDoc XRS+ (Bio-Rad).

### 3.10 *Luciferase reporter gene assay*

Luciferase reporter gene assays were used to measure ligand-induced activation of gmRXR. Here, COS-7 cells were transfected with a reporter-plasmid ((MH100)x4tkluc)) containing the luciferase reporter gene, a β-galactosidase-encoding normalization plasmid, and the pCMX-GAL4-RXR-hinge-LBD receptor plasmid. Upstream activation sequences (GAL4-UAS) in the reporter-plasmid promotor region, regulates the transcription of the luciferase gene. Through binding of ligand, the translated reporter receptor (GAL4-RXR-hinge-LBD) will undergo confirmational changes allowing the reporter receptor to bind GAL4. The complex then binds to an upstream activation sequence (UAS), in turn promoting transcription and production of luciferase enzymes. The transcription and subsequent translation allow measurement of luciferase enzymatic activity, producing oxyluciferin and light (550nm-570nm) through interaction with luciferin substrates. The amount light produced from this reaction is quantified in a luminometer and correlates to the level of gmRXR activation. β-galactosidase is used to normalize the transfection efficiency of COS-7 cells. β-galactosidase produces ONP and galactose through hydrolysis of the substrate ONPG. ONP absorbs light at 420nm and levels of ONP can be quantified and correlated to β-galactosidase activity. An overview of the luciferase reporter gene assay used in this study is found in Figure 10.

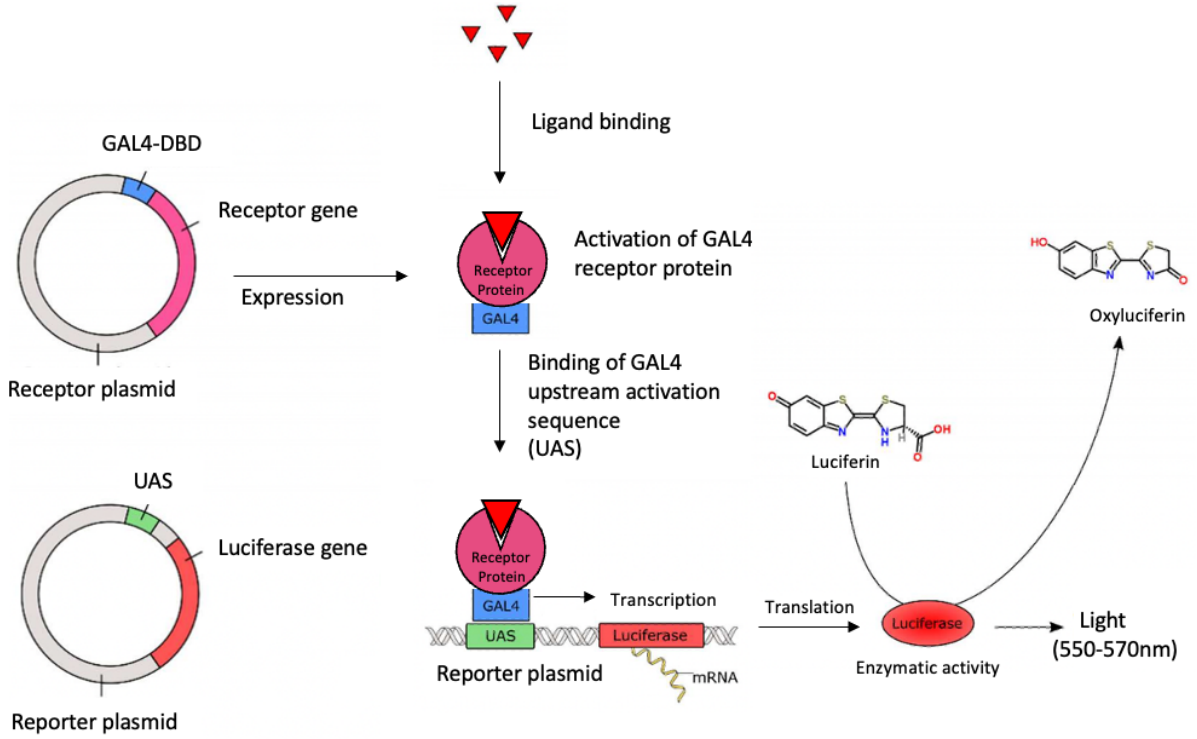


**Figure 10. Overview of the GAL4-UAS based luciferase reporter gene assay.** Receptor plasmids and reporter plasmids are transfected into cells, where the receptor-gene are constitutively expressed and translated into protein. When bound by ligand, the receptor protein goes through a conformational change and associates with GAL4-DBD which further binds UAS in the reporter plasmid. Luciferase is subsequently synthesized, and the enzyme catalyze the conversion of luciferin into oxyluciferin and light (550nm-570nm). The figure is modified from Madsen (2016).

### 3.10.1 *Cultivation of COS-7 cells*

COS-7 cells were stored in a freezing medium submerged in liquid nitrogen. A vile of COS-7 cells was removed from storage and quickly thawed before 10 mL of growth medium (DMEM-10%FBS) was added and the COS-7-cells+medium was centrifuged for 5 min at 500 rpm (RT). Excess medium was removed before resuspending cells in fresh medium. Cells where then seeded in 10 cm petri dishes and incubated at 37°C with 5% $CO_2$ until confluency of 70-90%. At this confluency medium was removed from dishes and cells were washed in 1X PBS twice. 1.5 mL of Trypsine-EDTA (0,05% trypsin, 0,02% EDTA) was added to the Petridis and incubated for 45 sec, allowing cells to release. Trypsin-EDTA was removed by pipetting, and cells were resuspended in growth medium and transferred to new Petri dishes diluted 1:20. Petri dishes were placed in an incubator at 37°C with 5% $CO_2$.

### 3.10.2 *Seeding COS-7 cells in 96-well plates*

When the COS-7 cells reached a confluency of 70-90%, determined through light microscopy (Leica DM IL inverted microscope), cells were washed, trypsinated and resuspended as described above. 50 µL of resuspended cell+medium was mixed with 50µL erythrosin-B and the cell density was determined with a hemocytometer (Marienfield) and light microscopy. Cells were seeded in 96-well plates at a cell density of 5000 cells per well with a total volume of 100 µL using growth medium. Cells were incubated at 37°C with 5% $CO_2$ for 18-24h.

### 3.10.3 *Transfection*

A transfection mix consisting of Opti-MEM I, TransIT-LT1, plasmid mix was prepared and incubated at RT for 30min. The plasmid mix contained (MH100)x4 tk luc, pCMV β-Gal and pCMX-GAL4-RXRβ1/γ-hinge-LBD with a ratio of 10:1 of (MH100)x4 tk luc and pCMV β-Gal compared to pCMX-GAL4-RXRβ1/γ-hinge-LBD. The transfection mix was added to the growth medium. Old medium was discarded from the 96-well plate and 101 µL transfection mix+growth medium was added to each cell and incubated at 37°C with 5% $CO_2$ for 24h.

**Table 52. Amount of plasmid added to each well**

| Plasmid | Amount |
|---|---|
| (MH100)x4 tk luc | 47.62 ng |
| pCMV-β-Gal | 47.62 ng |
| pCMX-GAL4-RXRβ1/γ--hinge-LBD | 4.76 ng |

**Table 53. Reagents for transfection of COS-7**

| Reagents | Volume per well |
|---|---|
| Opti-MEM I | 9 µL |
| TransIT-LT1 | 0,3 µL |
| Plasmid-mix | 0,1 µL |
| DMEM-10% FBS | 92 µL |

### 3.10.4 *Ligand exposure*

Transfected COS-7 cells were exposed to ligands dissolved in DMSO at a dilution factor of 5 in phenol-red free growth medium (DMEM-10% FBS w/o phenol red). A deep 96-well plate was used for the dilution series with concentrations of ligand declining from well A to G. Well H was used as a no-ligand control containing only growth medium and DMSO. The dilution series was made in a 2 X concentration. Growth medium from 96-well plate was discarded and 100 µL 2 X dilution mix was added to their designated wells. 100 µL phenol-red free growth medium was mixed in the wells containing 2 X dilution mix, giving a final 1 X concentration of ligand. Final DMSO concentration was between 0.2-0.5%. Cells were incubated and exposed for 24h at 37°C with 5% $CO_2$.

**Table 54. Serial diluted exposure ligands with dilution factor 5 (µM)**

| Well | 9-cis-retinoic acid | Tributyltin chloride | Fentin chloride | Fentin hydroxide | Tripropyltin chloride | Trimethyltin chloride |
|---|---|---|---|---|---|---|
| A | 20.0 | 0.5 | 0.5 | 0.5 | 0.5 | 0.5 |
| B | 4.0 | 0.1 | 0.1 | 0.1 | 0.1 | 0.1 |
| C | 0.8 | 0.02 | 0.02 | 0.02 | 0.02 | 0.02 |
| D | 0.16 | 0.004 | 0.004 | 0.004 | 0.004 | 0.004 |
| E | 0.032 | 0.0008 | 0.0008 | 0.0008 | 0.0008 | 0.0008 |
| F | 0.006 | 0.00016 | 0.00016 | 0.00016 | 0.00016 | 0.00016 |
| G | 0.001 | 0.00003 | 0.00003 | 0.00003 | 0.00003 | 0.00003 |

### 3.10.5 *Lysis and enzymatic measurements*

After 24h of exposure, the medium was discarded, and 125 µL lysis reagent solution was added to each well of the 96-well plate. The plate was put on a shaker at RT°C and incubated for 30 min. The lysis buffer disrupts membrane integrity and inhibits protease activity, allowing the release of luciferase and β-galactosidase. 50 µL of lysate was transferred to a clear 96-well plate and a white luminescence 96-well plate for β-galactosidase and luciferase activity measurements respectively. 100 µL of β-galactosidase reaction solution was added to each well of the clear plate and incubated for 20 min or until a yellow color had formed. Enspire 2300 plate reader (PerkinElmer) was used to measure absorption at 420nm. 100 µL of luciferase reaction solution was added to the white plate and immediately placed in the Enspire 2300 plate reader (PerkinElmer) for luminescence measurement. Luciferase activity was divided on

corresponding β-galactosidase activity to adjust for variability in transfection efficiency. A non-linear regression curve was produced in GraphPad Prism 9 to visualize dose-response activation profiles induced by the different ligands.

### 3.11 *Cell viability assay*

A cell viability assay was used to assess the potential cytotoxic effect of the ligands used in the luciferase reporter gene assay. Here, a combination of resazurin and CFDA-AM was used as an indication of decreased metabolic activity and cell-membrane integrity respectively. A 96-well plate was seeded, including wells without cells. The empty wells were used to account for background signals. gmRXR transfected COS-7 cells were exposed to the three highest concentrations of ligand from the luciferase reporter gene assay and incubated at 37°C with 5% CO2 for 24h. 0.5 µL Triton X-100 was used as a positive control for reduced cell viability. Medium was then removed, and cells were washed with 1 X PBS before 100 µL of a rezasurin/CFDA-AM mixture was added to each well. The cells were incubated at 37°C with 5% CO2 for 2h. Fluorescence signals were then measured using the Enspire 2300 plate reader (PerkinElmer) and 530/590nm (excitation/emission) for rezasurin and 485/530nm for CFDA-AM. GraphPad Prims 9 was used for visualizing changes in metabolic activity and membrane integrity.

# 4 Results

## 4.1 *Bioinformatics*

### 4.1.1 *Genome mining and phylogenetic analysis of the Atlantic cod RXR-isoforms*

Manually annotated RXR sequences from teleost and mammalian species, including species *D. rerio, S. salar* and *H. sapiens*, were used for homology searches in the Atlantic cod genome using the BLAST (NCBI) algorithm. Four predicted RXR encoding genes were identified (GeneID: LOC115532083, LOC115545518, LOC115535425 and LOC115555583). The deduced amino acid sequences from these genes were obtained and a phylogenetic analysis was performed to confirm the identification of these genes as gmRXR isoforms and investigate their evolutionary relationship. Hence, an MSA was constructed by using a vast array of RXR protein sequences, including the gmRXR isoforms from Atlantic cod and RXR sequences obtained from mammals (*H. sapiens*, *Mus musculus*, etc.) and teleost (*D. rerio*, *S. salar*, *Esox lucius*, etc.), including two other species from the *Gadiformes* order (*Melanonus gracilis* and *Melanogrammus aeglefinus*). From the MSA a maximum likelihood tree was produced, placing the different RXR isoforms based on their phylogenetic relations (Fig 11). The gmRXR proteins were found to be closely related to other well characterized RXRα, RXRβ or RXRγ isoforms, and were subsequently categorized accordingly. From this analysis, the four predicted Atlantic cod RXR isoforms were identified as gmRXRα (LOC115532083), gmRXRβ1 (LOC115545518), gmRXRβ2 (LOC115535425) and gmRXRγ (LOC115555583). The gmRXR isoforms were observed to primarily be closely related to species from the *Gadiformes* order, and further reflecting a close phylogenetic relationship to other teleost fishes, with mammalian RXRs being the most distantly related from an evolutionary perspective. Furthermore, the RXR-encoding genes were all located on different chromosomes, with gmRXRα located on chromosome 19, gmRXRβ1 on chromosome 6, gmRXRβ2 on chromosome 22 and gmRXRγ on chromosome 12 (Fig 12). The gmRXR isoforms also varied slightly in length and the gene sequences revealed that *gmrxrα*, *gmrxrβ*, *gmrxrβ2* and *gmrxrγ* constituted of an open reading frame of 1515bp, 1323bp, 1400bp, and 1398bp, respectively. From the protein sequences, the molecular weight of the predicted gmRXR isoforms were calculated. Due to an elongated N-terminal tail gmRXRα, which was not observed conserved in the other isoforms, this isoform was by far the largest at 63kDa (584 amino acids). gmRXRβ2 and gmRXRγ were found to be similar in size at approx. 52kDa (472 amino acids and 466 amino acids respectively), and gmRXRβ1 were the smallest protein at 49kDa (441 amino acids).

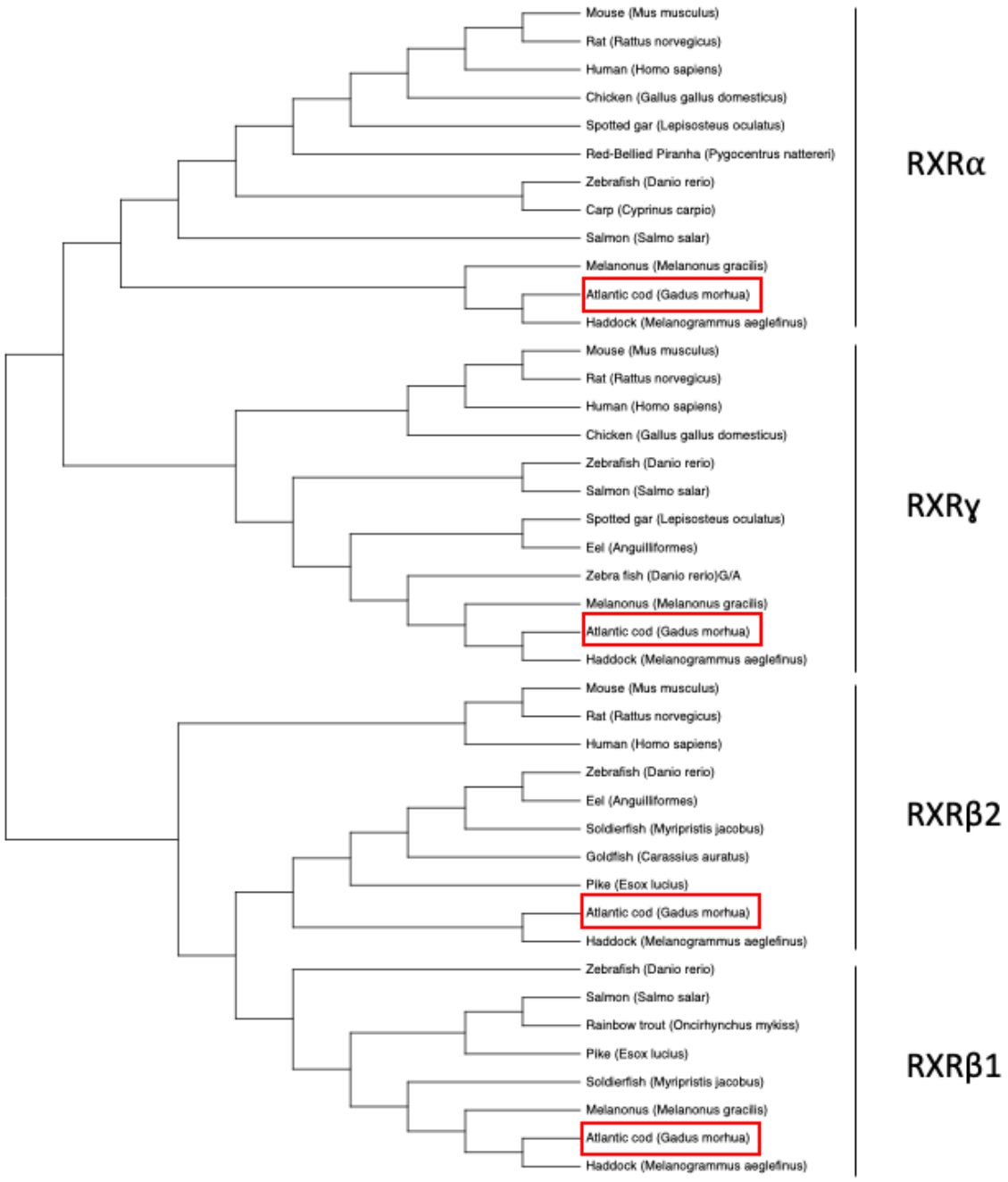


**Figure 11. Phylogenetic tree analysis of RXR.** The phylogenetic tree is a maximum likelihood tree illustrating evolutionary relationship between the gmRXR-isoforms (boxed in red) and RXR-isoforms obtained from different species, as indicated. The clusters containing sequences belonging to either the RXRα, RXRβ1, RXRβ2 or RXRγ isoforms are indicated to the right. Phylogenetic analysis was performed in MEGAX, including construction of the MSA using the Muscle algorithm.

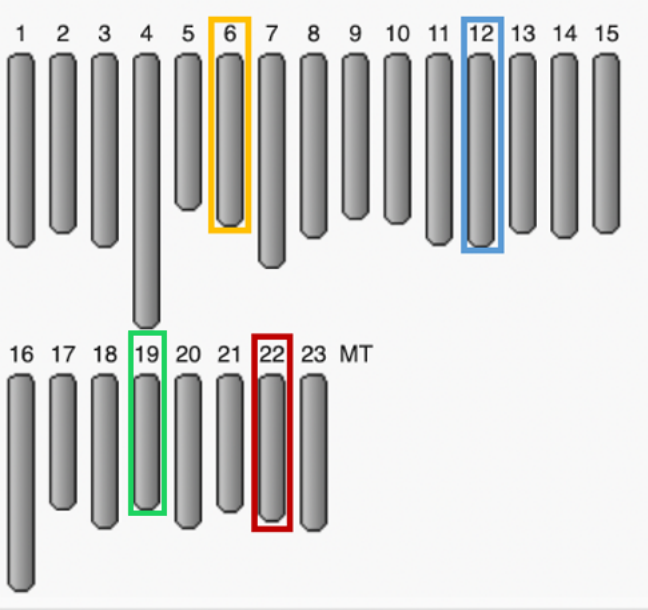


**Figure 12. Chromosomal location of RXR-isoforms in Atlantic cod**. The 23 chromosome pairs of Atlantic cod are illustrated in grey with their chromosomal numbers indicated above. The genes encoding gmRXRα (green), gmRXRβ1 (orange), gmRXRβ2 (red) and gmRXRγ (blue) are all located on distinct chromosomes, as indicated.

### 4.1.2 *gmRXR intron-exon mapping*

Exon and intron sequences from the *gmrxr* isoforms were derived from Ensembl. Cross-referencing the predicted Ensembl exon sequences with the deduced protein sequences, verified that the exons belonged to the predicted gmRXR isoforms. From the genomic sequences, the number of exons, exon-intron borders and intron/exon sequence lengths were obtained (Fig 13). From this, *gmrxrα*, *gmrxrβ*, *gmrxrβ2* and *gmrxrγ* were demonstrated to consists of 11, 11, 12, and 10 exons, respectively. The intronic sequences of gmRXRα were observed to be considerably longer compared to those of gmRXRβ1, gmRXRβ2 and gmRXRγ.

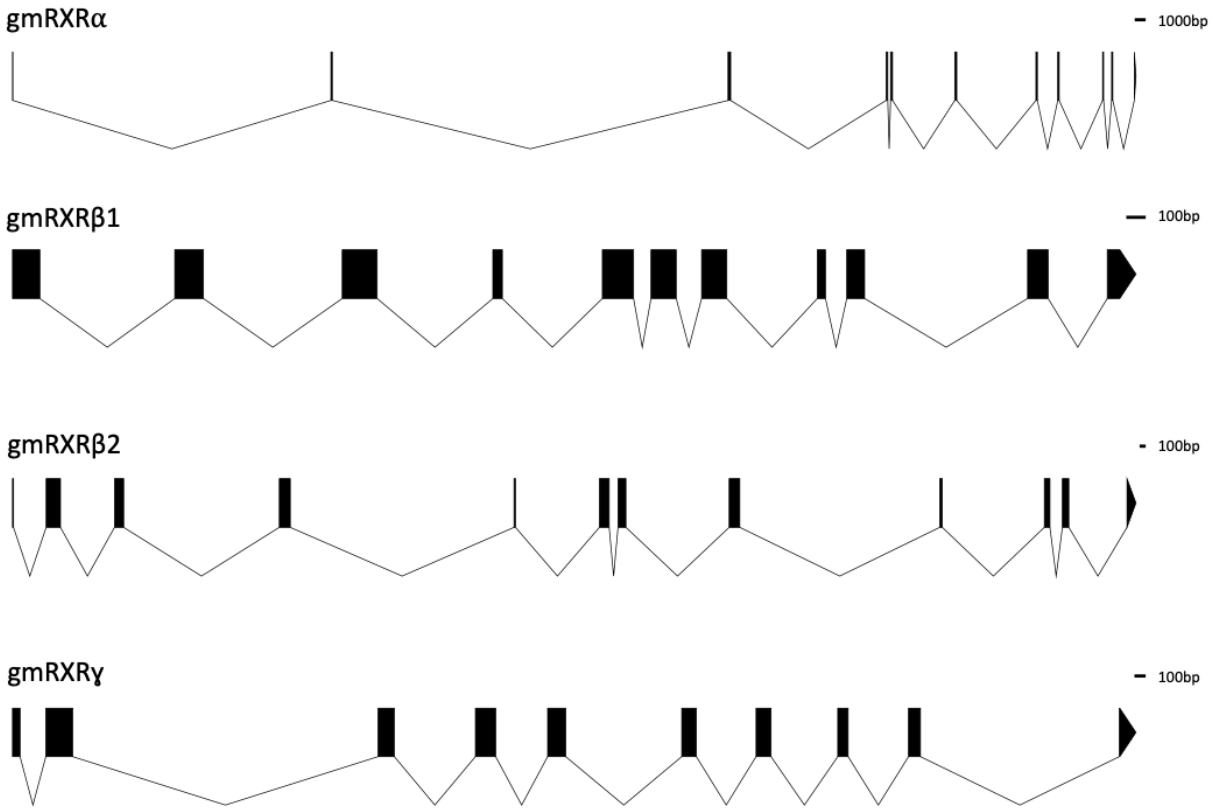


**Figure 13. Illustration of intron-exon borders for the *gmrxr*-isoforms.** Black boxes represent exons and connecting lines represent introns. *gmrxrα* intron sequences are substantially longer compared to the other isoforms; the scale is 1000bp for *gmrxrα, while gmrxrβ1, gmrxrβ2 and gmrxrγ* are scaled with 100bp, as indicated with bars. Illustration was prepared using WormWeb GraphicMaker.

### 4.1.3 *Identifying the DBD, hinge and LBD of gmRXR isoforms*

Well characterized RXR sequences from *D. rerio* and *H. sapiens* were aligned with the protein sequences of the gmRXR isoforms for identifying the DBD, the hinge-region, and the LBD. From this MSA produced the DBD, hinge-region and LBD was located and annotated in the gmRXR proteins as shown in figure 14. In accordance with other nuclear receptors, the DBDs of the gmRXR isoforms was highly conserved when compared to one another (91.2%), while the hinge was poorly conserved and the LBD moderately conserved (63.38%). For the DBD, three subdomains important in DNA binding were located, including the T-, P-, and D-box. Further, 11 α-helices (H1, H3-H12) were also predicted and profiled in the gmRXR-LBDs based on previous studies of *D. rerio* RXR and *H. sapiens* RXR (Tsuji et al., 2015; Billas et al., 2001). When comparing the domain sequences of gmRXR to corresponding *D. rerio* sequences, high level of conservation was observed. The DBDs sequence percentage similarity exceeded 80% for all isoforms, while the LBDs where moderately conserved at approx. 56%.

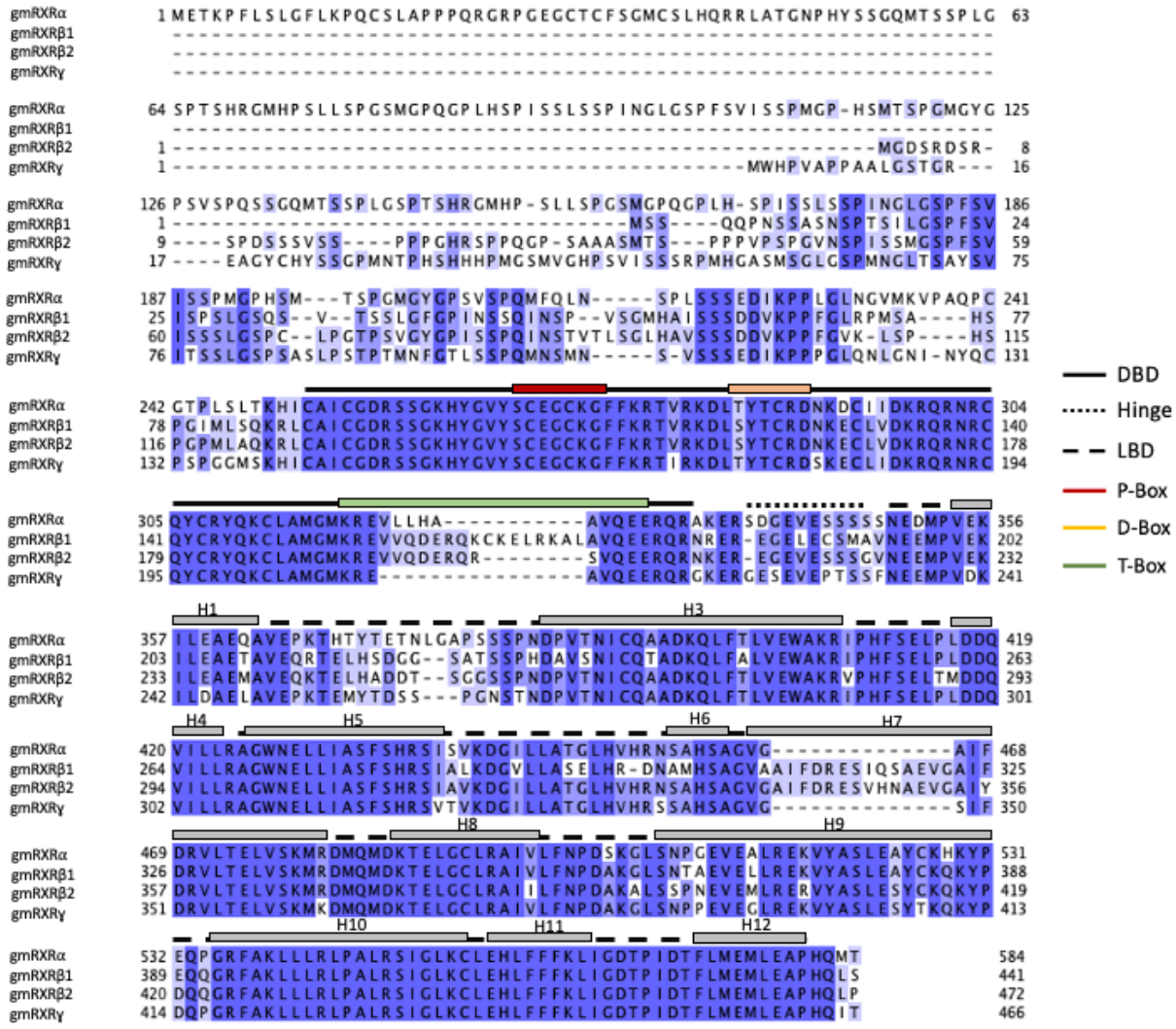


**Figure 14. Multiple sequence alignment of the gmRXR-isoforms.** gmRXRα, gmRXRβ1, gmRXRβ2 and gmRXRγ were aligned in Clustal Omega and visualized in JalView. Blue colored residues amino acid sequence percentage identity. Included in the alignment is the annotation of the DBD, the hinge-region, the LBD (including helices 1 and 3-12), P-box (red), D-box (orange) and T-box (green), annotated based on Tsuji *et al.,* (2015) and Billas *et al.,* (2001).

## 4.2 *Tissue specific expression of gmRXRα, gmRXRβ1, gmRXRβ2 and gmRXRγ*

Synthesis of cDNA from RNA was performed as described in 3.3. The RNA originated from a total 11 different tissue types derived from three juvenile female Atlantic cod individuals. The cDNA was initially used in this study as template for primer pair testing, and subsequently in qPCR analyses to measure *gmrxrα*, *gmrxrβ*, *gmrxrβ2* and *gmrxrγ* tissue expression in Atlantic cod.

### 4.2.1 *qPCR primer design and testing*

Primers used in the qPCR protocol were designed as described in 3.7.1. To ensure amplification of only targeted transcripts (i.e., *gmrxrα, gmrxrβ1, gmrxrβ2* and *gmrxrγ*) the specificity of the primer pairs was initially assessed with PCR. gmRXR isoforms were first amplified using liver cDNA as template and further separated on an agarose gel. Primer pairs yielding a singular PCR product at their calculated size were considered as well-suited candidates for qPCR. Primer pairs producing several bands would indicate multiple amplification sites as a result of unspecific template binding, yielding off-target products which would be inadequate for qPCR use.

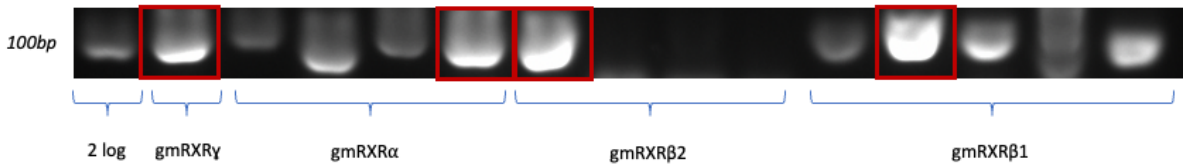


**Figure 15. PCR amplification of *gmrxr* isoforms using primers designed for qPCR.** 2µL amplified *gmrxr* PCR-product was added to each well and separated in an 2% agarose gel. GelRed was added during preparation of the agarose gel for visualizing (GelRed) DNA fragments. 2 Log molecular weight standard was used to verify expected size of the PCR product corresponding to the *gmrxr* isoforms. Red boxes indicate the corresponding primer pairs used in melt-curve analysis (Appendix Fig 28). Primers tested that was not used, are not named in this thesis. Primers tested that was not used, are not named in this thesis.

One promising primer pair for each of *gmrxrα, gmrxrβ1*, *gmrxrβ2* and *gmrxrγ* (Fig 15), was chosen for the melt-curve analysis to further confirm specific amplification of a singular desired qPCR product. The melting curves for the different primer pairs were produced using the qPCR protocol (3.7.2) and liver tissue cDNA as template (Appendix Fig 28). The four primer pairs, representing the different gmRXR isoforms, were all observed to produce a single peak in the melting curve analyses. Based on the agarose gel electrophoresis and the melting curve analyses these primers were used further for qPCR analysis of tissue specific expression of the gmRXR isoforms.

### 4.2.2 *Tissue specific expression profiles of gmrxrα, gmrxrβ1, gmrxrβ2 and gmrxrγ*

Differences in tissue expression of *gmrxrα, gmrxrβ1, gmrxrβ2 and gmrxrγ* in Atlantic cod was analyzed using the protocol for qPCR (3.7.2-3.7.4) and *actβ2* was used as a housekeeping gene for normalization of the transcript levels. The tissues analyzed included ovary, muscle, head kidney, skin, spleen, heart, stomach, liver, brain, gill and eye. The qPCR data revealed significantly different expression profiles (Fig 16). *gmrxrα* was expressed in significantly lower levels in all tissues compared to the other *gmrxr* isoforms. Although not discernible in figure 16, *gmrxrα* was expressed in all tissues apart from muscle and stomach (Appendix Fig 29). *gmrxrγ* and *gmrxrβ2* had a relatively ubiquitous expression profiles at moderate levels, while *gmrxrβ1* was expressed at highest levels in most tissues.

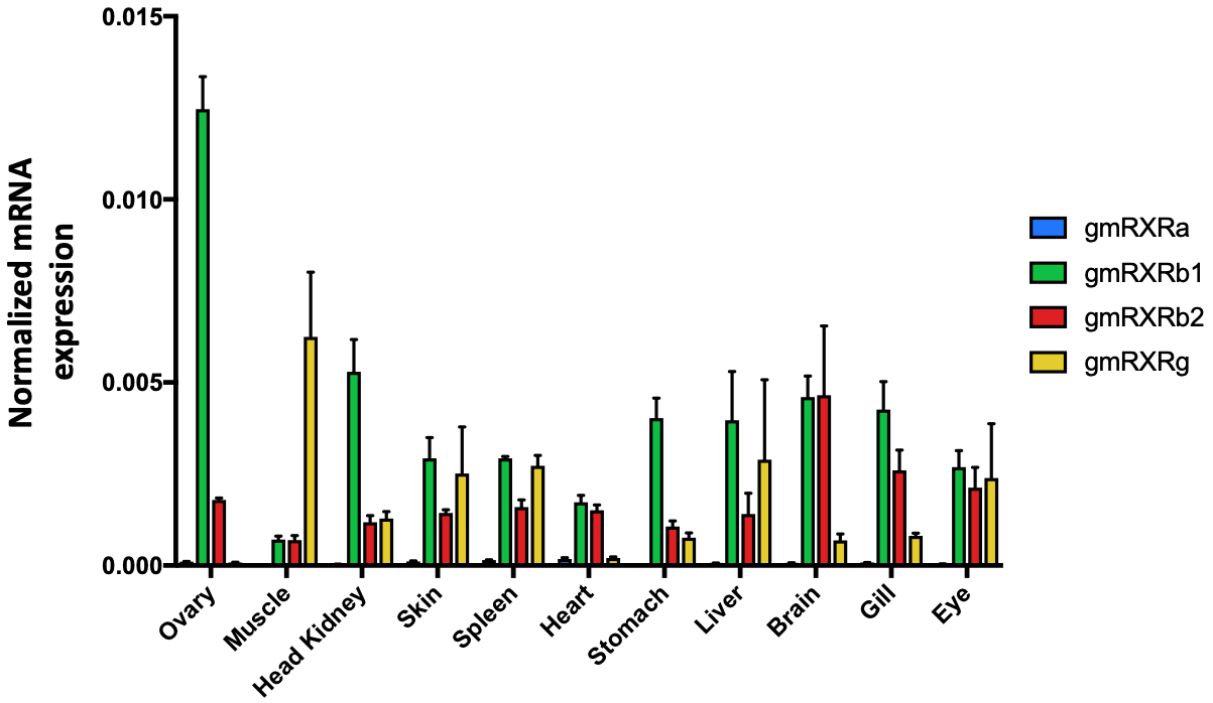


**Figure 16. Normalized mRNA expression of *gmrxr* isoforms in different tissues of Atlantic cod.** qPCR was used to quantify the levels of *gmrxr*-isoform transcripts in the following tissues: ovary, muscle, head kidney, skin, spleen, heart, stomach, liver, brain, gill and eye. *act2β* expression was used as a reference gene to normalize *gmrxr* expression.

### 4.3 *Blunt-end cloning and construction of pCMX-GAL4-RXRβ1-hinge-LBD plasmids and pCMX-GAL4-RXRγ-hinge-LBD expression plasmids*

Due to time constraints of this study, it was not feasible to produce expression plasmids and perform ligand activation analyses of all four gmRXR-isoforms. Based on the tissue specific expression profiles (Fig 16), gmRXRγ and gmRXRβ1 were the most prominent isoforms expressed in Atlantic cod liver and were thus selected for further testing throughout this study. Liver expression was the deciding factor as it is highly relevant within the field of toxicology, representing the major detoxifying organ for exogenous compounds, including OTCs.

#### 4.3.1 *Testing primers containing restriction enzyme recognition sequences*

Primers used for blunt PCR cloning and construction of pCMX-GAL4-RXRβ1/γ-hinge-LBD plasmids were designed as described in 3.8.1, by introducing the EcoRI and NheI recognition sequences. Forward primers were placed at the N-terminal end of the hinge region, while reverse primers were designed to align at the far end of the C-terminal of the LBDs. This would ensure amplification of full length gmRXR-LBDs and subsequent incorporation into pCMX-GAL4 plasmids fused to the GAL4-DBD. Using liver cDNA as template, the hinge-LBD encoding DNA fragment of gmRXRβ1 and gmRXRγ were amplified using PCR and separated on an 0.7% agarose gel (Fig 17). The PCR-products of *gmrxrγ* and *gmrxrβ* were calculated to be approximately 800bp and 830bp, respectively. The primer pairs producing a singular DNA fragment for *gmrxrγ* and *gmrxrβ1* and were thus used further and correspond to the primers given in Table 40.

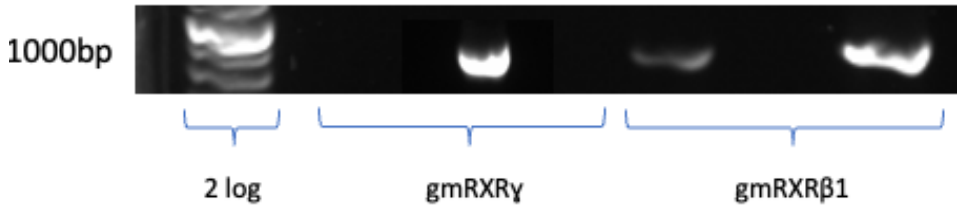


**Figure 17. Amplification of gmRXRβ1/γ-hinge-LBD used in cloning and construction of both pSC-B-RXR-hinge-LBD and pCMX-GAL4-RXR-hinge-LBD.** The hinge region and LBD of gmRXRβ1 and gmRXRγ was amplified with PCR and 5µL PCR-product was applied to a 0.7% agarose gel for separation and visualization (GelRed). Primers used for amplification of gmRXRβ1/γ-hinge-LDB are found in Table 40.

### 4.3.2 *Construction of pSC-B-RXRβ1/γ-hinge-LBD*

Amplified PCR products of the hinge-LBD of gmRXRβ1 and gmRXRγ were directly ligated into the cloning plasmid (pSC-B) using blunt-end cloning (3.8.2). pSC-B-RXRβ1/γ-hinge-LBD plasmids were then transformed into competent *E. coli* cells (3.8.8), which were cultivated o/n and screened using blue-white screening with X-gal. Six white colonies were then randomly chosen for each isoform and analyzed with colony PCR. PCR products was separated on an agarose gel to confirm positive transformants. Figure 18 show that all colonies analyzed had incorporated a fragment of approx. 800bp in size, in accordance with the predicted size of gmRXRβ1-hinge-LBD (~830bp) and gmRXRγ-hinge-LBD (~800bp). One colony for gmRXRβ1-hinge-LBD and one for gmRXRγ-hinge-LBD was selected for further plasmid purification (miniprep).

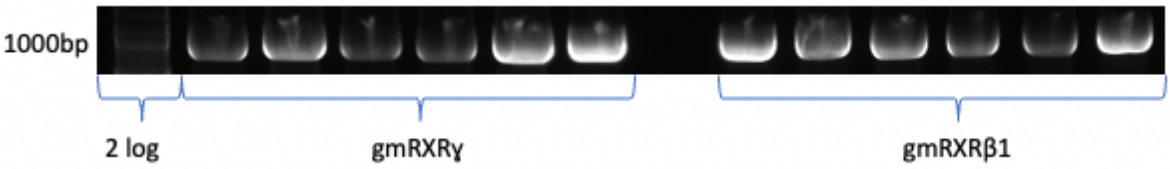


**Figure 18. PCR-screening for positive pSC-B-RXRβ1/γ-hinge-LBD transformants.** To confirm successful integration of gmRXRβ1/γ-hinge-LBD in pSC-B plasmid after blunt-end cloning, colony PCR was performed. Six colonies for both the gmRXRβ1hinge-LBD and gmRXRγ-hinge-LBD cloning were identified from blue-white screening and selected at random. gmRXR fragments was amplified using PCR, and further separated in an 0.7% agarose gel before visualization (GelRed). Expected DNA fragment size was ~850bp. 2Log molecular weight standard was used to verify expected size of the PCR product.

### 4.3.3 *Construction of the pCMX-GAL4-RXRβ1/γ-hinge-LBD plasmids*

To construct the pCMX-GAL4-RXRβ1/γ-hinge-LBD expression plasmids, double digestion reactions were performed using the restriction enzymes corresponding to the primer-introduced recognition sites from the initial blunt-end cloning step. Thus, EcoRI and NheI was used as restriction enzymes for digesting both pSC-B-RXRβ1/γ-hinge-LBD and the previously constructed plasmid pCMX-GAL4-AHR2, yielding compatible ends during ligation. SAP was added to inhibit religation of linearized DNA. The pCMX-GAL4-AHR2 plasmid was used to more efficiently locate the pCMX-GAL4 empty vector fragment after AHR2 removal, which was needed for correct gmRXRβ1/γ-hinge-LBD insertion during ligation. The digested plasmids were separated on an agarose gel for visualization. Figure 19 shows the pSC-B-RXRβ1/γ-hinge-LBD plasmids after digestion reaction where the lowest bands represent gmRXRβ1/γ-hinge-LBD fragments (~850bp). These fragments were extracted from the

agarose gel. Double digested pCMX-GAL4-AHR2 were also separated on an agarose gel, and the band marked with a red box in figure 20 represented empty pCMX-GAL4-DBD (4500bp). This vector fragment was subsequently extracted from gel.

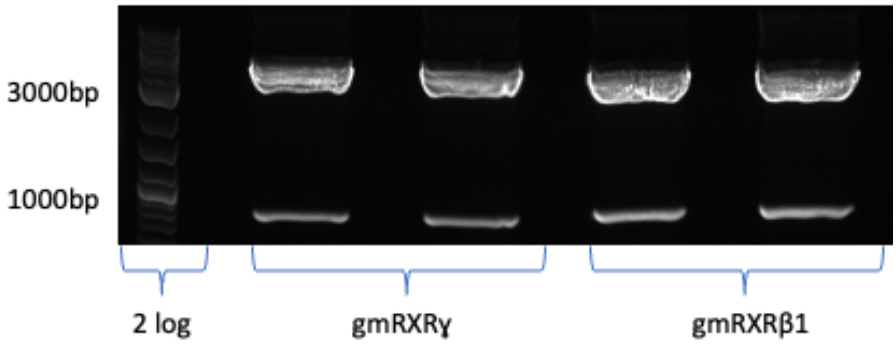


**Figure 19. Restriction enzyme digestion of pSC-B-RXRβ1/γ-hinge-LBD plasmids.** The fragments corresponding to the gmRXRβ1/γ-hinge-LBD were digested out from the pSC-B-gmRXRβ1/γ-hinge-LBD plasmids using EcoRI (3´end) and NehI (5´end) restriction enzymes. Confirmation of successful digestion reaction was done by separation of digestion products on a 0.7% agarose gel. The slowest moving band (>3000bp) represented undigested pSC-B-RXRβ1/γ-hinge-LBD and empty pSC-B (size difference too small to differentiate the two DNA fragments) and the lower band (<1000bp) represent the gmRXRβ1/γ-hinge-LBD fragment. 2 Log molecular weight standard was used to verify expected size digestion reaction products.

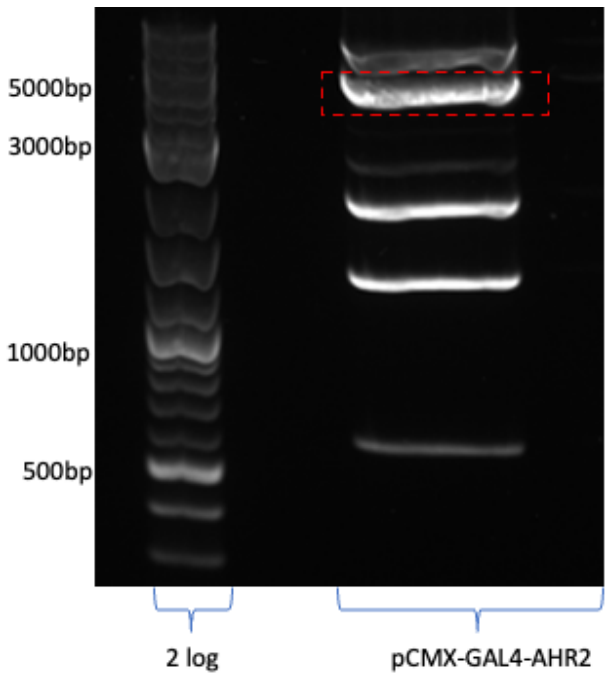


**Figure 20. Restriction enzyme digestion of the pCMX-GAL4-AHR2 plasmid.** Using EcoRI (3´end) and NehI (5´end) restriction enzymes, pCMX-GAL4-AHR2 was digested. The result of the digestion reaction was assessed using a 0.7% agarose gel. Empty pCMX-GAL4 plasmid is marked with a red box. Several fragments appear on the gel due to internal restriction enzyme sites in the AHR2 fragment. 2 Log molecular weight standard was used to verify expected size digestion reaction products.

Extracted gmRXRβ1/γ-hinge-LBD and empty pCMX-GAL4-DBD fragments were then mixed and ligated (3.8.7), and the ligation products were used to transform competent *E. coli* cells (3.8.8). The transformed *E. coli* cells was then cultivated and grown on agar plates. To increase the likelihood of selecting positive transformants, a large variety of colonies were selected. From the agar plates, 34 colonies were randomly picked for transformants containing gmRXRγ-hinge-LBD and 28 for gmRXRβ1-hinge-LBD. Cloning primers (Table 40) and PCR were used to amplify the gmRXRβ1/γ-hinge-LBD fragment for identifying successfully transformed colonies. As there was some variety among the colonies, i.e., producing PCR fragments of >1000bp and <800bp in size (Fig 21), three colonies producing the >1000bp fragments, and three colonies producing the <800bp fragments were selected at random for both gmRXR isoforms and further purified using the midiprep protocol (3.8.5).

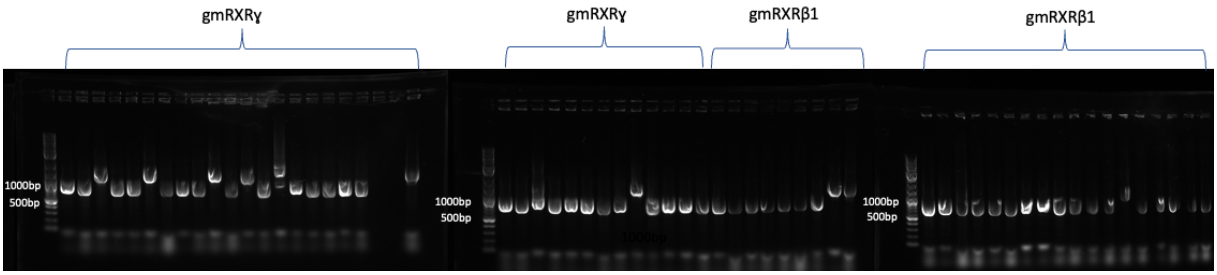


**Figure 21. Screening of pCMX-GAL4-RXRβ1/γ-hinge-LBD transformed *E. coli* using colony PCR.** pCMX-GAL4-RXRβ1/γ-hinge-LBD was transformed into *E. coli* cells and grown on agar plates o/n. Colonies grown were selected for both gmRXRβ1-hinge-LBD and gmRXRγ-hinge-LBD insertion. The RXRβ1/γ-hinge-LBD fragments were amplified using the colony PCR (3.8.4) and the PCR products were separated and visualized using a 0.7% agarose gel. 2 Log molecular weight standard was used to verify expected size of the RXRβ1/γ-hinge-LBD fragments. From the agarose gel, three colonies producing fragments >1000bp and three colonies producing fragments <800bp were chosen at random for further purification and Sanger sequencing.

### 4.3.4 *Sequencing pCMX-GAL4-RXRβ1/γ-hinge-LBD plasmids*

The six purified pCMX-GAL4-RXRβ1/γ-hinge-LBD plasmids from 4.3.3 were prepared for Sanger sequencing. Sequencing of pCMX-GAL4- RXRβ1/γ-hinge-LBD was performed at UiB in both directions, by using plasmid specific forward and reverse primers. Sequencing results from the triplicate colonies forming DNA fragments at <800bp, showed that the RXRβ1/γ-hinge-LBD sequence was fully incorporated to the pCMX-GAL4-DBD plasmid. The colonies forming fragments >1000bp were not used, as they contained additional nucleotides upstream from the hinge-region. gmRXRβ1-hinge-LBD was observed to have obtained a single point mutation of an adenine to a guanine in comparison to the genomic sequence. However, this proved to be a silent mutation and should therefore not have an impact on receptor function during the luciferase reporter gene assay.

## 4.4 *Verification of pCMX-GAL4-RXRβ1/γ-hinge-LBD fusion protein expression in COS-7 transfected cells*

COS-7 cells were transfected with the GAL4-DBD-RXRβ1/γ-hinge-LBD expression plasmids, and total protein staining along with Western blotting were performed to confirm transcription and synthesis of the fusion proteins. Lysed COS-7 cells were obtained 48-hours after seeding and 24 hours after pCMX-GAL4-RXRβ1/γ-hinge-LBD transfection. Two parallel 1 mm SDS-PA gels were used for separation of the cell lysates using electrophoresis. To verify protein content and separation of the polypeptides, total protein staining with Coomassie Brilliant Blue was performed with one of the gels. Total protein staining indicated successful protein separation and approx. equal protein content distribution in each well (Fig 22). Gel number two was used for Western blotting. Through primary and secondary antibody probing, the synthesis of GAL4-DBD-RXRβ1/γ-hinge-LBD fusion proteins and β-actin (loading control) were assessed. The fusion proteins of GAL4-RXRγ-hinge-LBD and GAL4-RXRβ1-hinge-LBD migrated according to their predicted Mw, forming immunoreactive bands at 46kDa and 48kDa respectively. Only cells transfected with either gmRXRγ-hinge-LBD or gmRXRβ1-hinge-LBD produced bands at predicted sized for the two proteins, while β-actin (positive control) were observed in both transfected and non-transfected cells at 42kDa. This demonstrates that only transfected COS-7 cells expressed the desired fusion proteins.

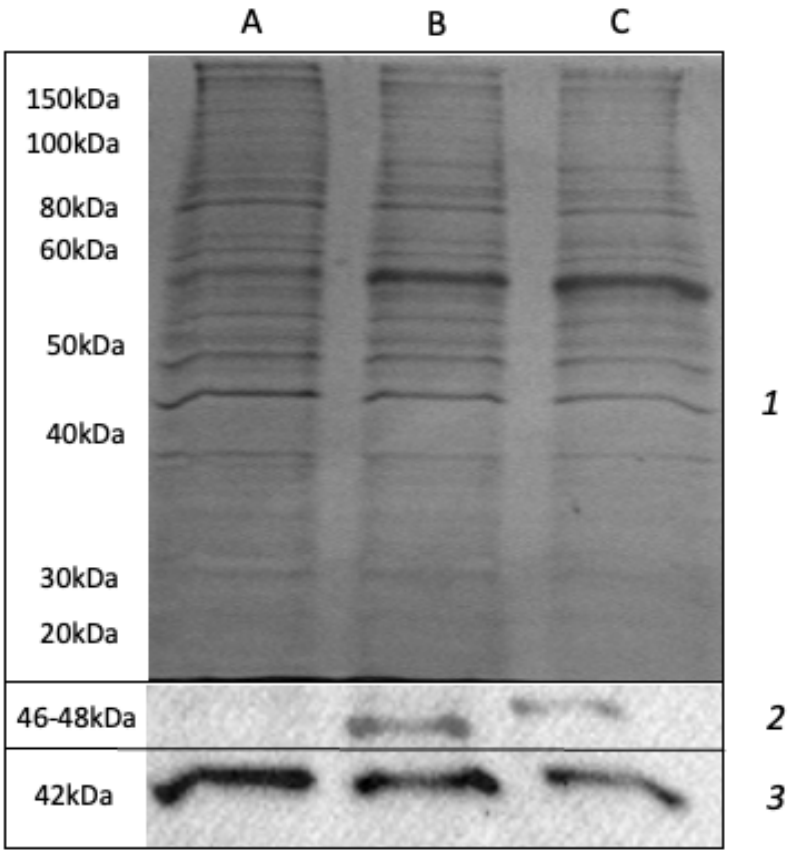


**Figure 22. Detection of expressed GAL4-RXRγ-hinge-LBD and GAL4-RXRβ1-hinge-LBD fusion proteins in transfected COS-7 cells.** Western blotting was performed to verify synthesis of fusion protein in transfected COS-7 cells. Well A) is a non-transfected control; well B) is GAL4-DBD-RXRγ-hinge-LBD transfected cells (46kDa); and well C) is GAL4-DBD-RXRβ1-hinge-LBD transfected cells (48kDa). (1) Total protein staining of parallel SDS-PAGE gel using Coomassie Brilliant Blue. (2) PVDF-membrane treated first with 1:500 diluted mouse anti-GAL4 antibodies, and secondly with 1:2000 sheep anti-mouse-IgG. (3) β-actin (42kDa) revealed with 1:1000 dilution of mouse anti-β-actin antibodies and 1:2000 sheep anti-mouse-IgG. SuperSignal ™ West Femto Maximum Sensitivity Substrate kit was used to visualize the immunoreactive bands.

### 4.5 *Luciferase reporter gene assay*

Seeded COS-7 cells were then transfected with a plasmid mix consisting of either pCMX-GAL4-RXRβ1-hinge-LBD or pCMX-GAL4-RXRγ-hinge-LBD, together with (mh100)x4tk luc (reporter plasmid) and pCMV-β-gal (normalization plasmid). The plasmid mix was prepared with a 1:10 plasmid mass ratio between pCMX-GAL4-RXRβ1/γ-hinge-LBD plasmids and the mh100)x4tk luc/pCMV-β-gal plasmids. After transfection, cells were exposed to serial diluted concentrations of 9-cis-RA, and the following OTCs: tributyltin chloride (TBT), tripropyltin chloride (TPT), fentin chloride (FC), fentin hydroxide (FH) and trimethyltin chloride (TMTC) (exposure concentrations: Table 53). After a 24-hour exposure period, the enzymatic activity of luciferase and β-galactosidase in COS-7 cell lysates were measured through luminescence and absorbance readings, respectively. β-galactosidase activity was used to normalize transfection efficiency between wells. The normalized luciferase activity was calculated as fold change in gmRXRβ1/γ activation compared to a baseline DMSO control. The assay was performed in triplicates three separate times, to produce an average fold activation.

#### 4.5.1 *Ligand activation of gmRXRγ-hinge-LBD and gmRXRβ1-hinge-LBD*

9-cis-RA was used as a positive control for ligand activation of GAL4-RXRβ1/γ-hinge-LBD (from now on gmRXRβ1/γ), due to its presumed role as an endogenous natural ligand for the receptor. Accordingly, 9-cis-RA induced activation of gmRXRγ and produced a maximum fold change in activation ($E_{max}$) of 58 at 20 μM (Fig 23). As no activation plateau was measured during 9-cis-RA exposure, no $EC_{50}$ values were calculated. Notably, gmRXRβ1 did not respond to the presence of 9-cis-RA and thus produced no significant increase ($p<0.05$) in fold change in a dose-response dependent manner (Fig 24).

However, as the Western blot analyses (4.4) verified the synthesis of GAL4-DBD-RXRβ1/γ-hinge-LBD fusion proteins in transfected CO7- cells, both proteins were further included in the assessment of the OTCs. The OTCs used were TBT, TPT, FC, FH and TMTC, representing a selection of OTCs that has been present in marine environments. COS-7 cells transfected with the gmRXRβ1/γ fusion proteins were exposed for 24 hours using the same dilution series for all the OTCs.

For gmRXRγ, all OTC ligands produced significant ($p<0.05$) activation of the receptors apart from TMTC, where no significant activation occurred (Fig 23). TBT and TPT produced the maximum fold activation in luciferase activity of approx. 55 and 65 respectively at 0.1 μM. FC and FH had similar activation profiles with measured $E_{max}$ of 33 and 31 at 0.1 μM respectively. The calculated $EC_{50}$ and LOEC values further demonstrated a high potency of all OTCs in inducing transactivation of gmRXRγ. TBT, FC and FH all indicated similar levels of potencies, however, TBT had slightly higher $EC_{50}$ compared to FC and FH, at 0.006 μM, 0.0045 μM and 0.0041 μM, respectively (Table 55). In contrast, the LOEC values for TBT were slightly higher than that of FC and FH, at 0.008 μM (0.004 μM for FC and FH). TPT was the least potent of the compounds tested with $EC_{50}$ at 0.14 μM and LOEC at 0.02 μM. No $EC_{50}$ values were calculated for TMTC as it did not induce transactivation of gmRXRγ. In figure 23, the top concentration (0.5 μM) for all but TMTC, was removed due to cytotoxicity (see below). For gmRXRβ1 (Fig 24), no activation was observed for any of the OTCs assessed. For TPT, FC and FH a slight decline in activation was observed. However, this is most likely due to cytotoxic effects observed in 4.5.3 and not an antagonistic effect on the receptor.

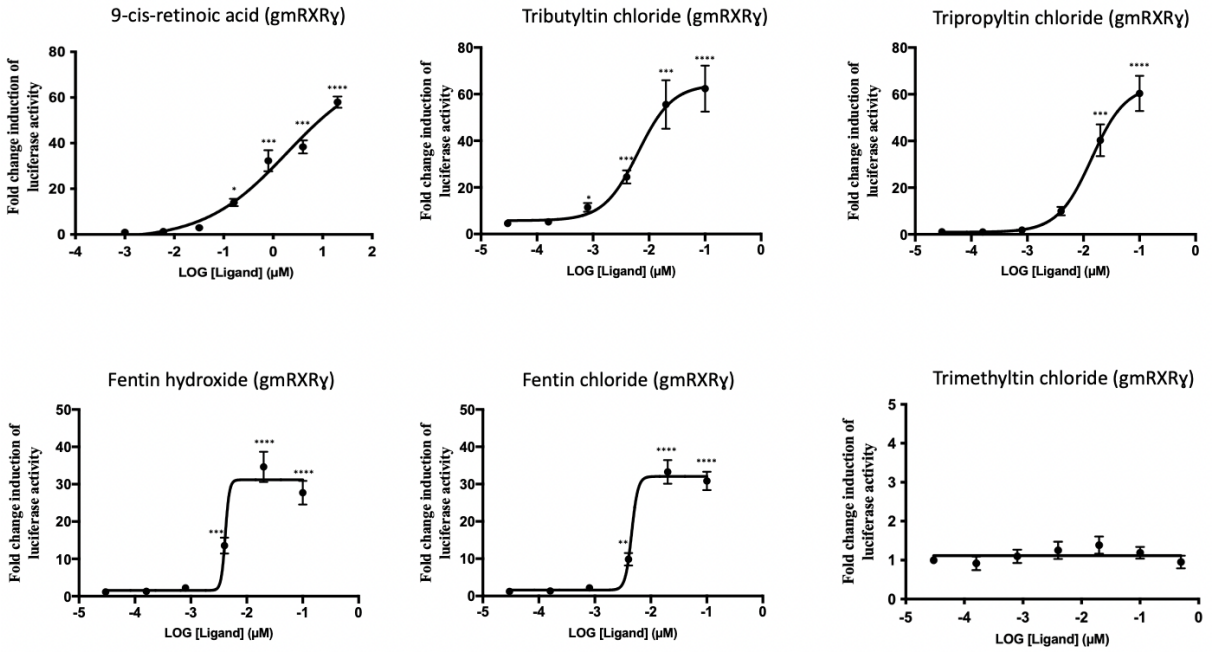


**Figure 23. Ligand activation of gmRXRγ by 9-cis-RA, TBT, TPT, FH, FC, TMTC.** Transfected COS-7 cells were exposed to the OTCs at identical concentrations. Each point represents gmRXRγ activation through relative fold change in luciferase activity compared to DMSO (0.2-0.4%) exposed cells. The points are average activation of triplicate concentrations obtained from three separate and identical experiments, with standard error of mean (SEM). Points representing the highest concentration (0.5 μM) are removed from the graphs of TBT, TPT, FC and FH due to cytotoxicity. The dose-response curves were produced in GraphPad Prism 9. Statistical significance was calculated using Kruskal-Wallis test with Dunn´s multiple comparisons test and indicated with "*": *=p≤0,05, **=p≤0,01, ***=p≤0,001 and ****=p≤0,0001.

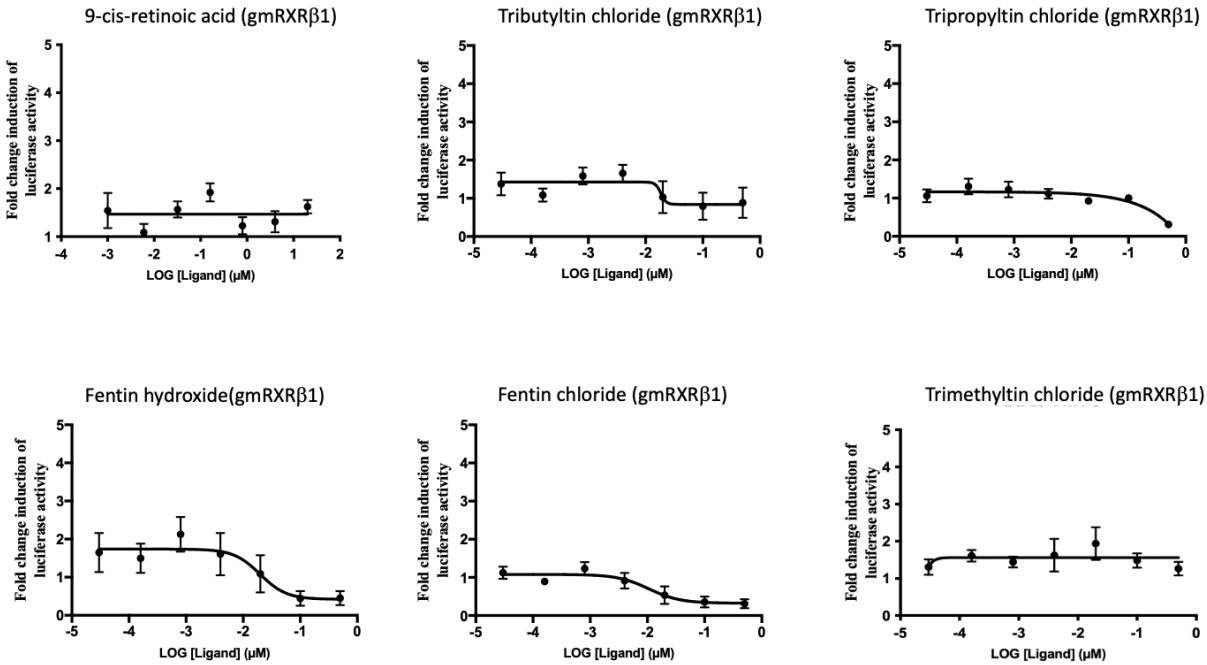


**Figure 24. Ligand activation of gmRXRβ1 by 9-cis-RA, TBT, TPT, FH, FC, TMTC.** Transfected COS-7 cells were exposed to the OTCs at identical concentrations. Each point represents gmRXRβ1 activation through relative fold change in luciferase activity compared to DMSO (0.2-0.4%) exposed cells. The points are average activation of triplicate concentrations obtained from three separate and identical experiments, with standard error of mean (SEM). The dose-response curves were produced in GraphPad Prism 9.

**Table 55. LOEC, $EC_{50}$, and $E_{max}$ for gmRXRγ activated by 9-cis-RA and OTCs.** Values for LOEC (μM), $EC_{50}$ (μM) and $E_{max}$ were calculated in GraphPad Prism 9. Statistical significance (p-value) of $E_{max}$ was calculated using Kruskal-Wallis test with Dunn´s multiple comparisons test.

| Receptor | Agonist | Lowest observed effective concentration (LOEC) (μM) | Half maximal effective concentration 50 ($EC_{50}$) (μM) | Maximum fold activation ($E_{max}$) | p-value ($E_{max}$) |
|---|---|---|---|---|---|
| gmRXRγ | 9-cis-RA | 0.16 | * | 58 | <0.001 |
| gmRXRγ | TBT | 0.008 | 0.006 | 55 | 0.0081 |
| gmRXRγ | TPT | 0.02 | 0.014 | 65 | 0.00275 |
| gmRXRγ | FC | 0.004 | 0.0045 | 33 | <0.001 |
| gmRXRγ | FH | 0.004 | 0.0041 | 31 | <0.001 |
| gmRXRγ | TMTC | | - | - | - |

* $EC_{50}$ values for 9-cis-RA was not calculated as an activation plateau was not reached.

### 4.5.2 *Assessing differences in RXR-LBD sequences*

To investigate possible reasons why the ligand activation profile of gmRXRγ and gmRXRβ1 differed dramatically, the sequence similarity of their respective LBDs was examined in more detail. Amino acids constituting the LBD was selected and aligned for gmRXRα, gmRXRβ1, gmRXRβ2 and gmRXRγ. Tsuji *et al.,* (2015) and Billas *et al.,* (2001) have previously reported 13 amino acids involved in 9-cis-RA binding for RXR. In Figure 25, these 13 conserved amino acids were identified in the LBD sequences. Notably, a single difference in H3 was found between the gmRXR-LBDs. Here, an alanine (Ala236, gmRXRγ) is exchanged for a threonine (Thr237) residue in gmRXRβ1-LBD. A subsequent MSA was produced for the gmRXR-LBD isoforms along with obtained LBD sequences of RXR isoforms from *D. rerio* and *H. sapiens* (Fig 25). The same conserved alanine (Ala236, gmRXRγ) residue was again observed to be conserved in all aligned sequences apart from gmRXRβ1-LBD. Further, a cysteine group (Cys41) on the very C-terminal end of H10, reported to be involved in covalent binding and anchoring of the tin atom of OTCs to RXR-LBD, was conserved across all aligned sequences assessed (le Maire et al., 2009). In H7 of gmRXRβ1 and gmRXRβ2, a 14-residue insertion was observed. This insertion was in a region of high conservation across teleost and mammalian RXR isoforms. Notably, a subsequent MSA including the RXR isoforms δ and ε found in *D. rerio*, revealed that this insertion was shared by gmRXRβ1, gmRXRβ2, *D. rerio* RXRδ, and RXRε (Fig 26). All 13 residues involved in 9-cis-RA binding, including the alanine residue (Ala236, gmRXRγ), is also observed conserved in *D. rerio* RXRδ and RXRε.

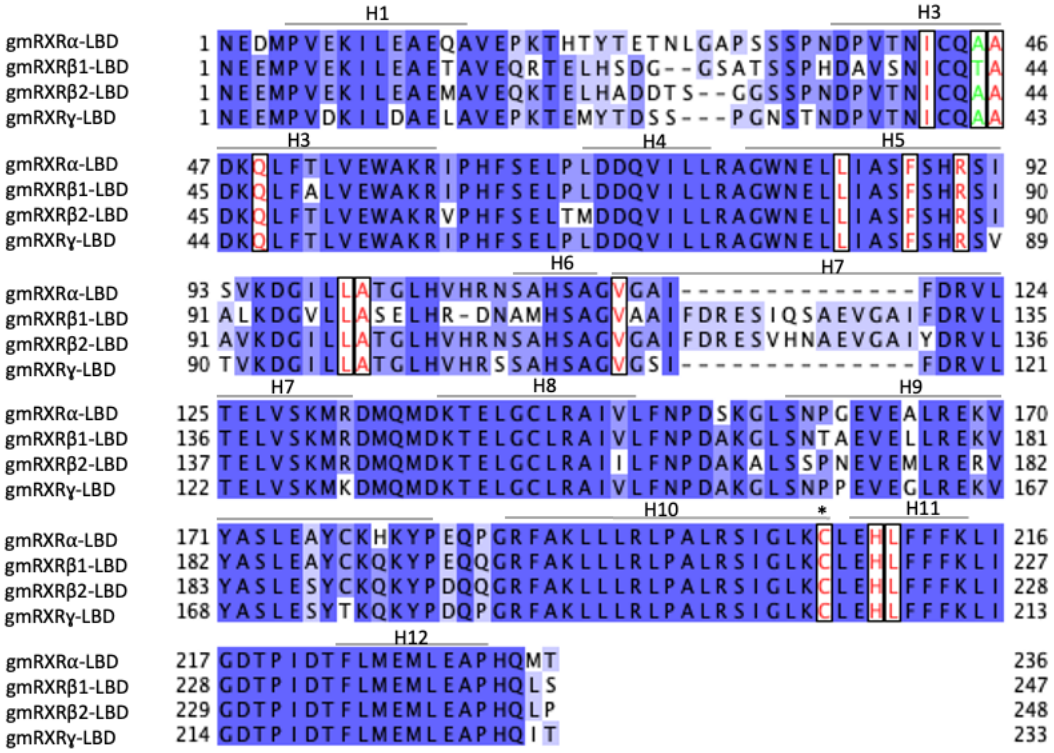


**Figure 25. Multiple sequence alignment of gmRXRα, gmRXRβ1, gmRXRβ2 and gmRXRγ LBDs.** The MSA shows aligned LBD sequences from the different gmRXR isoforms. Conserved amino acids involved in 9-cis-RA binding are indicated as red residues. None-conserved amino acids involved in 9-cis-RA binding are indicated with green residues. The "*" over Cys217 (gmRXRβ1) represents a residue involved in anchoring OTCs during RXR binding. Helices 1, 3-12 are represented with grey lines and are numbered H1, H3, H4, etc. MSA produced in Clustal Omega and visualized in JalView. The percentage amino acid identity is colored in blue.

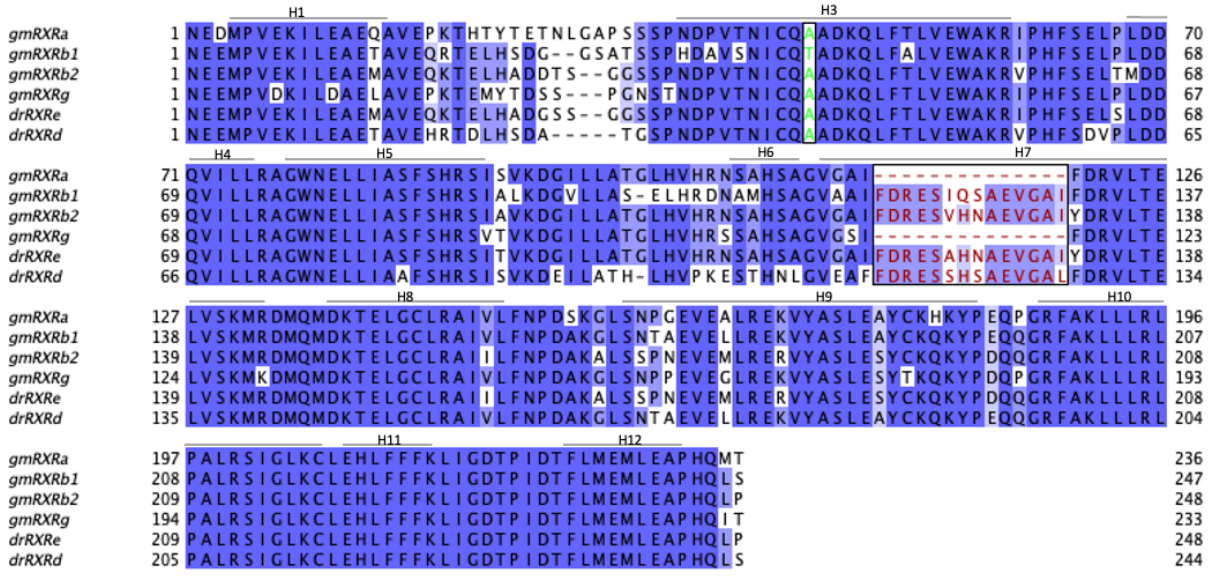


**Figure 26. Multiple sequence alignment of LBD sequences from gmRXRα, gmRXRβ1, gmRXRβ2, gmRXRγ, drRXRε and drRXRδ.** The MSA of the LBDs of gmRXR isoforms and *D. rerio* RXRε and RXRδ (drRXRε and drRXRδ). A 14-residue insert located on gmRXR in H7, marked in red, is conserved between gmRXRβ1, gmRXRβ2, drRXRε and drRXRδ. Further, the alanine residue (Ala236, gmRXRγ) is still conserved for all but gmRXRβ1 (green). Alignment produced in Clustal Omega and visualized in JalView. The percentage amino acid identity is colored in blue.

### 4.5.3 *Cytotoxicity and cell viability*

To investigate the possible cytotoxic effects of 9-cis-RA and the OTCs used in the luciferase reporter gene assay, a COS-7 cell viability assay was done parallel to the Luciferase reporter gene assay. gmRXRβ1/γ transfected COS-7 cells were exposed to 9-cis-RA at concentrations of 20 μM, 4 μM and 0.8 μM, while the OTCs were exposed at 0.5 μM, 0.1 μM and 0,02 μM, thus representing the three highest concentrations used in the luciferase reporter gene assay. Triton X-100 (0.5 μM) was used as positive control for cytotoxicity. Exposures for all compounds were over a 24-hour period, identical to exposure regime used in the luciferase reporter gene assay. A significant decrease ($p<0.05$) in membrane permeability (CFDA-AM) was observed at 0.5 μM for FC and FH, while a significant decrease ($p<0.05$) in metabolic activity (rezasurin) was observed for TBT, FC, FH and TPT at 0.5μM (Fig 27).

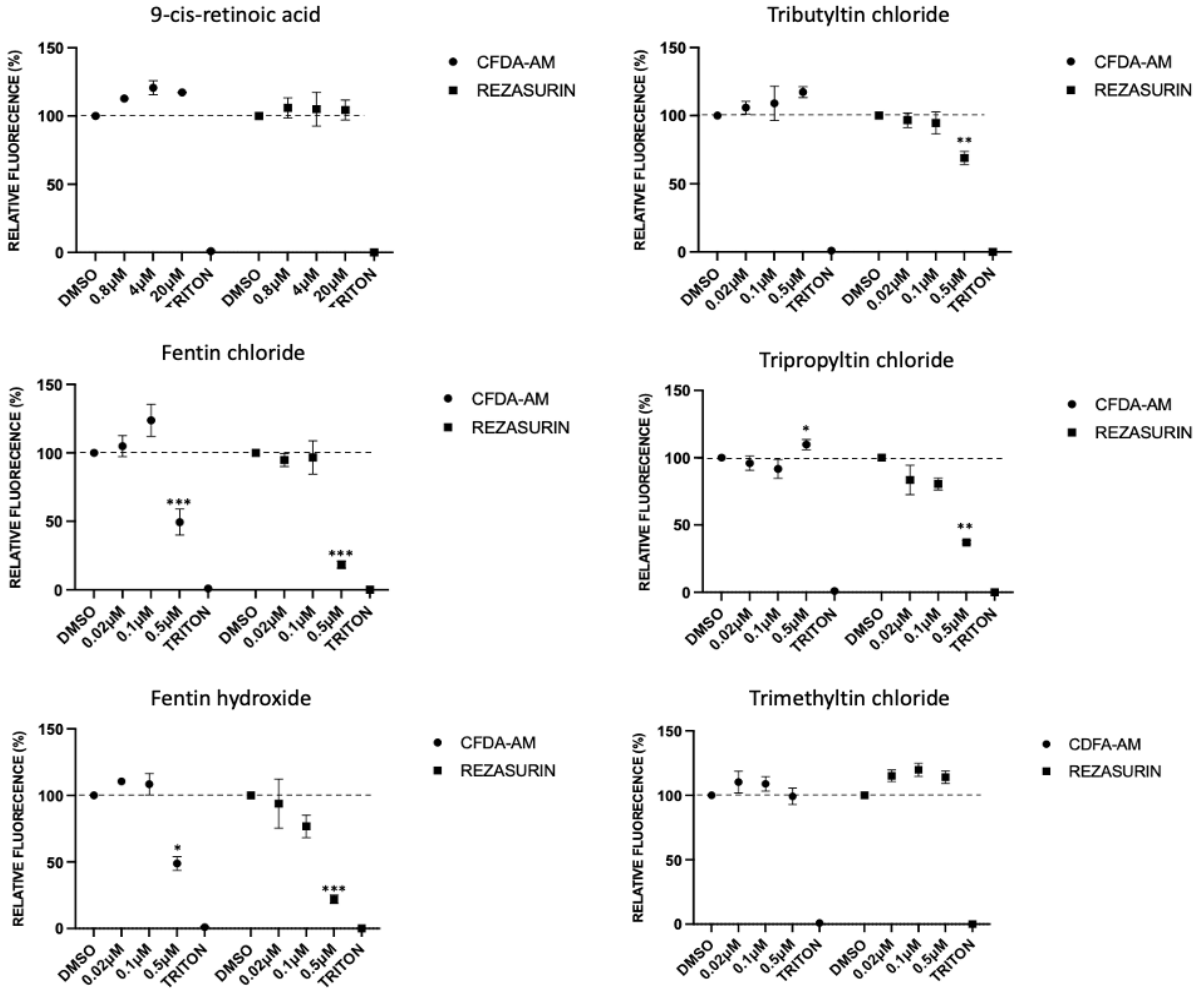


**Figure 27. Changes in COS-7 cell viability after ligand exposure.** Transfected COS-7 cells were exposed to the three highest concentrations of 9-cis-RA, TBT, TPT, FC, FH and TMTC, used in luciferase reporter gene assay. Triton X-100 was used as positive control of cytotoxicity. Exposure to DMEM with 0.5% DMSO was used as solvent control and is illustrated as stippled line. Rounded dots represent change in membrane permeability (CFDA-AM) and squares represent change in metabolic activity (rezasurin). Statistical significance was calculated using Kruskal-Wallis test with Dunn´s multiple comparisons test in GraphPad Prism 9 and indicated with "*": *=p≤0,05, **=p≤0,01 and ***=p≤0,001.

# 5. Discussion

This thesis has focused on identifying and characterizing the different isoforms of RXR in Atlantic cod (gmRXR) regarding their primary structure, phylogeny, tissue-specific expression, and interactions with endogenous and exogenous ligands. RXR in other species have been observed to be activated by 9-cis-RA, the proposed natural endogenous ligand of RXR. OTCs represent a highly toxic group of environmental pollutants capable of causing endocrine disruption through RXR-biding in both terrestrial and marine environments. OTCs have previously been observed to have particularly detrimental effects on marine environments, as their half-life is significantly prolonged here compared to terrestrial environments. Thus, assessing the potential of OTCs to bind and transactivate gmRXR isoforms, may provide further insights into the adverse effects these compounds may have on Atlantic cod and marine teleosts in general.

## 5.1 *Evolution, localization and characterization of gmRXR isoforms*

RXR isoforms and their abilities to associate to and regulate the function of several different NRs across phyla, have made them key figures within the fields of molecular endocrinology and toxicology. RXR-encoding genes have been revealed in all vertebrates, including identification of RXR homologues in some of the oldest metazoan lifeforms, such as *Porifera* (Wiens et al., 2003). In this study, four paralogous RXR genes were identified in the Atlantic cod genome and shown to group phylogenetically with RXR homologs from other *Gadiformes* species. The gmRXRs were further phylogenetically clustered together with other teleost RXR isoforms (i.e., RXRα1, RXRβ1, RXRβ2 and RXRγ1), allowing the four Atlantic cod RXR proteins to be classified as gmRXRα, gmRXRβ1, gmRXRβ2 and gmRXRγ. Of these gmRXR isoforms, gmRXRβ2 homologs were only identified in other teleosts. In fact, genes encoding NRs have in general been identified in larger numbers in teleosts compared to mammalian species. In Atlantic cod, 72 NR-encoding genes have been identified, while only 48 NR genes are found in humans (Eide et al., 2018). However, the diversity in presence and numbers of NR isoforms in teleost species seem to vary substantially throughout evolution. In fact, genome mining performed of RXR in *D. rerio*, *S. salar* and Atlantic cod, was in this study found to possess genes encoding six, five and four RXR proteins, respectively. Two initial whole genome duplication (WGD) events in early vertebrate evolution, followed by a third teleost specific WGD event (Meyer & Van de Peer, 2005), along with other evolutionary events, including neo- and subfunctionalization, gene loss, and chromosomal inversions, are suggested

to explain how both number and presence of NR isoforms are substantially different between teleost species (Sandve et al., 2018). Through WGD events, a single RXR gene might evolve to encode functionally diverse proteins (i.e., RXRα, RXRβ and RXRγ) through deletion, insertion or substitution of nucleotides. With additional teleost specific WGD events giving rise to new isoforms, such as RXRα1, RXRβ1, RXRβ2, RXRγ1, RXRδ and RXRε. Further, observed 9-cis-RA binding in some of the most primitive Cnidarian species, such as *Tripedalia cystophora,* indicates an early gain of function in ligand-binding from an evolutionary perspective (Groot et al., 2006). Interestingly, reports of RXR homologues in arthropods unable to bind 9-cis-RA may suggest a secondary loss of ligand binding capacity during metazoan evolution (Fonseca et al., 2020). However, some arthropod orthologues of RXR, called ultraspiracle protein (USP), in species such as *Locusta migratoria* have proven to bind 9-cis-RA at high affinities (Fonseca et al., 2020). Thus, a more comprehensive and detailed phylogenetic study is needed to produce a map covering episodes of gain and loss in function when regarding 9-cis-RA binding to RXR.

The gmRXRα, gmRXRβ1, gmRXRβ2 and gmRXRγ isoforms identified in the Atlantic cod genome in this study were encoded from separate genes located on chromosome 19, 6, 22 and 12, respectively. Complete DNA-sequences of these genes were obtained, and the amino acid sequences were deduced. This allowed the annotation of exonic and intronic sequences, and further the annotation of the DBDs, the hinge-regions, the LBDs, and identification of residues previously shown to be involved in 9-cis-RA ligand biding in other species. The gmRXR encoding genes translate into proteins that slightly vary in size, gmRXRβ1 being the smallest at 50kDa, and gmRXRα the largest at 63kDa. gmRXRβ1, gmRXRβ2 and gmRXRγ share similar sizes as RXR proteins in other species, which typically range between 50-55kDa (Feldman et al., 2008). In contrast, the gmRXRα is relatively large when compared to *H. sapiens* RXRα and the two RXRα isoforms (RXRα1 and RXRα2) in *D. rerio´s*, which are 50kDa, 46kDa and 47kDa, respectively. This is due to an observed extended N-terminal of gmRXRα. This extension is reoccurring and seemingly unique to RXRα of some other examined teleost species, including *E. lucius, S. salar* and *Cyprinus carpio*. To which extent this elongation of the N-terminal might affect receptor function is however not known. Protein sequence alignment of the different functional domains of gmRXR isoforms, indicated extensive conservation of the DBD. Comparison of the DBDs in the gmRXR isoforms compared with corresponding isoforms from *H. sapiens* and *D. rerio* demonstrated sequence

similarities exceeding 80%, while the LBD was moderately conserved comparatively at 56% sequence similarity. These functional domains are generally well conserved in NRs as they determine the NRs ability to bind DNA and ligands as well as their ability to associate with partner NRs or other proteins (heat-shock proteins, p-proteins, co-activators, etc.). Interestingly, the area of the DBD sequence that demonstrated the highest level of variability among both the gmRXR isoforms and other species was the T-box. Both hetero- and homodimeric complexes of RXR extensively use the T-box when mediating protein-protein interactions with the upstream zinc-finger (II) modular region (Dawson & Xia, 2012). This region of RXR has been observed in other species to be able to undergo conformational changes to accommodate binding of both RXR homo- and heterodimers (Rastinejad et al., 2000). This degree of structural freedom in the gmRXR-T-box may suggest a similar ability of Atlantic cod isoforms to form functional complexes with a variety of different partner NRs and other proteins. Further, there were some key differences in the LBD structures related to ligand binding properties that will be discussed later (5.3.2).

## 5.2 *Tissue specific expression of gmRXR isoforms*

The eleven tissues obtained from juvenile female Atlantic cod (i.e., ovary, muscle, head-kidney, skin, spleen, heart, stomach, liver, brain, gill and eye), were used to produce comprehensive tissue specific expression profiles for *gmrxrα, gmrxrβ1, gmrxrβ2* and *gmrxrγ*. From these analyses, *gmrxrβ1* was observed to be the most abundant and widely expressed isoform in all tissues. Particularly high levels of *gmrxrβ1* transcripts were measured in ovary and head-kidney, with lowest levels measured in muscle tissues. *gmrxrβ2* and *gmrxrγ* were relatively ubiquitously expressed with high levels of *gmrxrβ2* transcripts measured in brain and stomach, and *gmrxrγ* transcripts measured at high levels in liver and muscle. *gmrxrα* was by far the least expressed of the gmRXR isoforms in all tissues examined. Interestingly, tissue specific profiles of *H. sapiens* RXR isoforms have provided evidence that *rxrα* is particularly abundant in testis/ovaries, liver and kidney (Uhlén et al., 2015). However, when comparing expression profiles of *gmrxrα* and *gmrxrβ1* in ovary tissue, *gmrxrβ1* transcript was measured at levels 118 times higher than that of *gmrxrα*. Further, when comparing of the most abundant gmRXR isoforms in liver tissue (i.e., *gmrxrβ1* and *gmrxrγ*) to *gmrxrα*, the transcripts for *gmrxrβ1* and *gmrxrγ* were measured to be ~76 and ~56 times higher than that of *gmrxrα*. Interestingly, He et al (2009) reported the tissue specific profiles of RXR isoforms (smRXRα, smRXRβ and smRXRγ) in the marine teleost *Sebastiscus marmiratus*. When comparing gmRXR tissue

specific expression to RXR expression in *S. marmiratus*, several similarities were observed. Here, *smrxrβ* was, like *gmrxrβ1*, most widely abundant isoform in overall tissue expression, followed by *smrxrγ*, with *smrxrα* measured to be the least abundant. Further, *smrxrβ* and *smrxrγ* expression levels in ovary and liver tissues in *S.marmiratus*, were observed to be similar to that of *gmrxrβ1* and *smrxrγ* in corresponding tissues in Atlantic cod. Unfortunately, further comparisons of tissue specific expression in other fish are difficult as data of other teleost species is scarce, with studies performed mostly with regards to tissue expression of RXR in embryonal or larval stages. However, with the apparent similarities in RXR expression profiles between Atlantic cod and *S. marmiratus*, and the disagreement in RXR expression profiles when comparing Atlantic cod and *H. sapiens*, it may suggest that Atlantic cod, and teleost species alike, have different functional roles compared to that of mammalian RXR. Thus, it can be suggested that a neofunctionalization of gmRXRβ1 and a subfunctionalization of gmRXRα, have occurred during Atlantic cod evolution, although more studies are needed to confirm this hypothesis. Further, the high expression levels of *gmrxrβ1* and *smrxrβ* in Atlantic cod and *S. marmiratus* ovary, respectively, suggest an active role in sexual maturation, development, and/or fertility. In fact, based on embryonic expression patterns of RXRβ in *D. rerio*, Waxman & Yelon (2007) suggested that RXRβ isotypes and isoforms are the only RXRs mediating heterodimeric interactions with hormone receptors during development in both teleost fishes and mammals (Waxman & Yelon, 2007). This is supported by observations where only RXRβ null mice resulted in approx. 50% death before or at birth, with the remaining mutants alive being sterile (Krezel et al., 1996). However, to my knowledge, no knockout studies of RXR isoforms in teleost species have been performed, but it should be done to assess the importance and involvement of specific teleost RXR isoforms during fish development. Further, Atlantic cod *gmrxrβ1* and *gmrxrγ,* as well as *S. marmiratus smrxrβ* and *smrxrγ*, were measured to be abundant in liver-tissue, indicating an involvement of these RXR isoforms in recognizing xenobiotics and mediating a response as a dimeric partner. However, with the reported the loss of PXR in Atlantic cod (Eide et al., 2018), it may suggest that gmRXRβ1/γ have a different mechanism of action when mediating a responses to xenobiotic exposure. In mammals the RXR:PXR heterodimer is suggested to promote *cyp3a4* expression as a response to numerous different xenobiotic exposures (Yuan et al., 2020). Thus, identifying the response mechanism and possible alternative heterodimeric partners of gmRXRβ1/γ during xenobiotic exposure, would be useful in expanding our understanding of how Atlantic cod, and related teleost species, are affected by and respond to environmental pollutants.

## 5.3 *Ligand induced activation of gmRXRβ1 and gmRXRγ*

Due to time constraints, ligand induced activation assessment of gmRXRs isoforms was performed solely using gmRXRβ1 and gmRXRγ. gmRXRβ1 and gmRXRγ was chosen based on their high levels of expression in liver tissue, as the liver is prone to interact with most xenobiotics that enter the organism and has a major role in handling such compounds. In this thesis, a GAL4-UAS based luciferase reporter gene assay was established and used for obtaining ligand-activation profiles for gmRXRβ1 and gmRXRγ. Some advantages using the GAL4-UAS based system include: (1) The UAS results in downstream gene expression at higher levels than that of endogenous tissue-specific promoters, and thus increase sensitivities (Yamada et al., 2020). (2) The use of an exogenous promoter from yeast (UAS) will minimize the potential interference of endogenous components present in the cell line used for the assay (Yamada et al., 2020). (3) With GAL4-UAS, transactivation of NR is un-affected by the absence of dimerization partners (Zarifi et al., 2012). In this assay, the expression of the reporter genes is directly correlated to transactivation of the NR in question and can be measured through luminescence (produced by luciferase). This allows comparisons of activation profiles induced by ligand exposure, as well as analyzing ligand potency and efficacy over varying concentrations.

### 5.3.1 *Assessing ligand activation profiles of gmRXRβ1 and gmRXRγ*

COS-7 cells were transfected with the plasmids pCMX-GAL4-gmRXRβ1-hinge-LBD and pCMX-GAL4-gmRXRγ-hinge-LBD, and subsequently exposed to 9-cis-RA. 9-cis-RA was used as a control ligand (agonist) due to this compound being the most widely used endogenous ligand within RXR research. Although not regarded as a bona fide natural endogenous ligand, high affinity binding of 9-cis-RA to RXR has been reported in a plethora of evolutionary linages, such as vertebrates, annelids and mollusks. Based on these factors, transactivation of both gmRXRβ1 and gmRXRγ induced by 9-cis-RA exposure was expected. Accordingly, 9-cis-RA exposure of gmRXRγ produced a clear dose-response. Initial testing started with a maximum concentration of 1 μM 9-cis-RA and subsequently increased in new experiments as no clear plateau of activation was observed. However, increasing maximum concentrations from 1 μM to 20 μM, still did not to produce a plateau. In previous studies using different cell lines such as JEG-3 cells, COS-1 cells, HepG2 cells and Caco-2 cells, it was reported a maximum 9-cis-RA-mediated activation of RXR at 1μM (JEG-3 and COS-1) and 10μM (HepG2 and Caco-2) (Nakanishi et al., 2005; Fonseca et al., 2020; Wang et al., 2008). Backlund

& Ingelman-Sundberg (2005) observed that ligand activation of another transcription factor, the aryl hydrocarbon receptor (AHR), fluctuated between cell lines when a GAL4-DBD-AHR system was used. Thus, in future studies it might be worth investigating different cell lines when assessing 9-cis-RA-induced RXR transactivation. Surprisingly, no dose-response was measured during 9-cis-RA exposure of COS-7 cells transfected with gmRXRβ1, at any concentrations tested. As a result of this, possibilities that transfected COS-7 cells did not transcribe, nor synthesize the functional GAL4-RXRβ1-hinge-LBD fusion proteins were considered. However, western blotting confirmed synthesis of the fusion proteins in transfected COS-7 cells, with immunoreactive bands forming at expected Mw for both GAL4-RXRβ1-hinge-LBD and GAL4-RXRγ-hinge-LBD. Thus, the possibility of gmRXRβ1 being unresponsive to 9-cis-RA was accepted, and subsequent assessment of gmRXRγ and gmRXRβ1 activation after exposure to OTCs was performed.

OTCs have long been associated with RXR as an agonistic xenobiotic ligand, with compounds such as TBT observed to induce imposex in marine gastropods and masculinization of *D. rerio* as a result of disruption of the RXR signaling pathway (Gooding Lassiter et al., 2003). TBT along with TPT, FC and FH are potent active agents found in pesticides (i.e., fungicides, molluscicides, insecticides, etc.) that previously were used in marine antifoulants and observed to bioaccumulate in marine species (Demehin et al., 2017). Over the past two decades, these compounds have globally been banned from commercial use and environmental concentrations are slowly decreasing (Schøyen et al., 2019), although illegal production and use is still found around some parts of Africa and east-Asia. TMTC is one of the few chemicals in the OTC family that does not originate exclusively from an anthropogenic origin. Although not previously observed as an RXR agonist, TMTCs unique ability to form naturally in the environment made it interesting to include in the present study. Although the agonistic relationship between OTCs and RXR have been reported previously, no information is available considering their effect on RXR from Atlantic cod. Thus, the chemicals mentioned above were chosen when assessing the potential ability of OTCs to transactivate gmRXRγ and gmRXRβ1. gmRXRγ was activated by TBT, TPT, FC and FH. Both TBT and TPT produced the highest fold change in activation profile, with $E_{max}$ of 55 and 65 respectively. Consistent with previous observations, TMTC did not act in an agonistic manner (Nakanishi et al., 2005). Notably, TBT, TPT, FC and FH all achieved relatively high efficacies ($E_{max}$) at low concentrations (0.1 μM) compared to 9-cis-RA, where far higher concentrations where needed to produce a similar

response. Even in studies utilizing other cell lines, considerably higher concentrations of 9-cis-RA is still needed to induce transactivation of the receptors, compared to the concentrations used for OTCs in the present study. This suggests that gmRXRγ has a higher activation potential when binding OTCs compared to the proposed endogenous ligand. Further, the high $E_{max}$ values, paired with the low $EC_{50}$ -and LOEC values produced by these OTCs at low concentrations, indicates high potency and efficacy in inducing transactivation of RXR in Atlantic cod. Similarly, TBT exposure studies on gastropods indicates the ability of these compounds to produce adverse health effects at low concentrations. Gooding et al (2003) observed TBT induced imposex of *Ilyanassa obsoleta* at concentrations as low as 1ng/L, with Abidli et al (2009) observing TBT-induced imposex of *Gastropoda muricidae* at 5ng/L. Moreover, recent studies reported high concentrations of accumulated fentin in teleost liver tissue (1000-3500 ng/g ww), suggesting that teleosts may not be able to effectively metabolize these compounds (Sham et al., 2021). Thus, considering the observed potency of OTCs to transactivate gmRXRγ in Atlantic cod, and previous studies indicating low rates of OTC degradation in teleost liver, as well as OTC-induced imposex at low concentrations in gastropods, it is reason to suggest that OTCs are still an imminent threat to marine species, even though environmental concentrations are decreasing. However, more data from long term exposures of OTCs on teleost species is needed to further investigate the potential adverse effects such compounds produce at low (ng) concentrations. Notably, and as observed with 9-cis-RA exposure analysis, gmRXRβ1 was not activated by any of the OTCs assessed.

### 5.3.2 *Differences in gmRXRγ-LBD and gmRXRβ1-LBD that may affect ligand binding*

The dramatic differences in activation profiles for gmRXRγ and gmRXRβ1 after exposure to both 9-cis-RA and OTCs, prompted a more thorough assessment of their LBDs. This was done to assess for differences in the amino acid sequence, which in turn might manifest as the inability of gmRXRβ1 to bind and be activated by 9-cis-RA and OTCs. When inspecting the LBD alignments for gmRXRα1, gmRXRβ1, gmRXRβ2 and gmRXRγ, a conserved region of 14 residues in H7 for both gmRXRβ1 and gmRXRβ2 was observed. Interestingly, a similar insertion is found in RXRδ-LBD and RXRε-LBD of *D. rerio* (B. Jones et al., 1995). *D. rerio* RXRδ and RXRε are believed to have evolved separately after a common ancestor branched off the RXR family, and 9-cis-RA was observed to not induce transactivation of these two isoforms (B. Jones et al., 1995; Philip et al., 2012). These RXR isoforms have further been observed unaffected by ATRA, 11-cis-RA, 13-cis-RA and retinol exposure (Seo et al., 2002). Moreover, these RXR isoforms are therefore believed to be activated through other interactions than ligand binding. For both gmRXRβ1 and gmRXRβ2, as well as *D. rerio* RXRδ and RXRε, the additional stretch of amino acids is located at regions with relatively well conserved amino acid sequences on both sides of this insertion. X-ray crystallography studies of this conserved region in *D. rerio* suggested that this region constitute important parts of the ligand binding pocket (LBP)(B. Jones et al., 1995). Thus, it is hypothesized that the insert in *D. rerio* RXRδ-LBD and RXRε-LBD causes structural differences to the LBP and inhibit 9-cis-RA binding along with other ligands, both endogenous and exogenous. Although gmRXR crystallography data is not available, given the close sequence similarity between gmRXRs and *D. rerio* RXRs, it is not unlikely that the 14 amino acid extension in the gmRXRβ1 LBD produces similar changes to the LBP structure and subsequent function. With X-ray crystallography and/or docking simulations, such data can be derived. If in fact this insertion proves to alter the LBP structure in gmRXRβ1, it may suggest that this gmRXR isoform has different properties than that of *H. sapiens* RXRβ and *D. rerio* RXRβ, as these are able to bind both 9-cis-RA and OTCs. One possibility is that gmRXRβ1 strictly functions as a non-permissive heterodimer with no synergistic activation mediated by ligand binding to both dimeric partners. Here, gmRXRβ1 would only be transactivated through interacting with a ligand-bound partner NR (i.e., PXR, RAR, VDR, etc.). This may further suggest that gmRXRβ1 regulates transcription in a strictly heterodimeric fashion, unable to form functional homodimeric configurations. However, with the high gmRXRβ1 abundance in most juvenile Atlantic cod tissues, it is likely that this isoform

is involved in regulation of a vast array of physiological processes in numerous cell types, possibly through interactions with several NRs. Thus, even if gmRXRβ1 is structurally inhibited from being activated by the tested compounds, it may still play an important role as a transcriptional regulator in multiple tissues of, as an obligate non-permissive heterodimer.

Further, 13 amino acid residues were identified in the LBD, representing key residues in binding to 9-cis-RA in other species (Billas et al., 2001). These residues were conserved in the gmRXR isoforms, as well as in *H. sapiens* RXRα, RXRβ, and RXRγ, and in *D. rerio* RXRα1, RXRβ1, RXRβ2 and RXRγ. However, of these 13 residues, a single amino acid difference was found in gmRXRβ1. Here, the conserved alanine (e.g., Ala236, gmRXRγ) residue was exchanged for a threonine (Thr237, gmRXRβ1). These residues are apparently located on H3, which has been observed to undergo conformational changes to accommodate and stabilize co-activator binding. Upon ligand biding to *H. sapiens* RXRα, H3 undergoes a 13Å tilt allowing it to interact with H4 and H12. In this configuration, a surface structure is created between H3, H4 and H12, uncovering NR-box motifs and enabling co-activator and co-repressor binding (Dawson & Xia, 2012). The binding of co-activators further facilitates recruitment of other regulatory proteins. One set of these regulatory proteins may consist of transcriptional protein complexes which recognize and place the RXR-complex at the transcriptional start site. Apart from co-activator binding, the interaction between H3 and H12 is especially important as H12 contains the AF-2 domain, involved in transcriptional regulation. Through H3 interactions with AF-2, H3 is suggested to act as a conduit in stabilizing homo-and heterodimeric interactions, along with being a binding site for regulatory proteins (Kojetin et al., 2015). Thus, it is suggested that the residue substitution of Ala236 (gmRXRγ) to Thr237 (gmRXRβ1) might affect co-activator and regulatory protein binding to gmRXRβ1. To what extent this may result in an altered ligand binding profile remains to be elucidated. To assess the possibility that the residue substitution observed in gmRXRβ1-H3 may affect ligand binding, in vitro mutagenesis studies should be performed in the future where Thr237 (gmRXRβ1) is mutated to Ala.

## 5.4 *Conclusion*

In this study four isoforms of the homo- and heterodimeric NR partner, RXR, involved in major cellular pathways such as development, metabolism and homeostasis, were identified in the Atlantic cod genome. These RXR isoforms were further characterized regarding their primary structure, tissue specific expression, and phylogeny. The four gmRXR isoforms included gmRXRα, gmRXRβ1, gmRXRβ2 and gmRXRγ. Based on tissue specific expression profiles, gmRXRβ1 and gmRXRγ were cloned from Atlantic cod liver, and the effects of 9-cis-RA and OTCs on receptor activation was assessed by establishing a luciferase-based reporter gene assay. gmRXRβ1 and gmRXRγ demonstrated significant deviations in activation profiles. Here, gmRXRγ was potently activated by both the presumed natural endogenous ligand (9-cis-RA) and all OTCs (TBT, TPT, FC, FH) assessed, apart from TMTC. On the other hand, gmRXRβ1 showed no response to any of the ligands after exposure. Subsequent findings of a 14 amino acid insert in gmRXRβ1-LBD, along with a single substitution in conserved amino acids involved in 9-cis-RA binding (Ala237 to a Thr237), were suggested as possible reasons for the lack of gmRXRβ1 activation. As a result of this, along with the tissue specific expression profiles, it is suggested that gmRXRβ1 may have undergone neofunctionalization during Atlantic cod evolution, manifesting as transcriptional regulation in different cells and tissues through obligate non-permissive heterodimeric interactions with other NRs. In contrast, gmRXRγ is believed to maintain similar functional roles as observed in previous studies from e.g., *H. sapiens* RXR and *D. rerio* RXR, being a NR capable of inducing transcriptional regulation when bound by a ligand, likely through both homo- and heterodimeric interactions. Nevertheless, the high potency and efficacy of OTCs in inducing gmRXRγ transactivation, along with previous published studies, indicate the ability of OTCs to produce adverse health effects through disruption of RXR signaling at low concentrations in Atlantic cod. It is therefore suggested that these compounds are still a major threat to the wellbeing of marine wildlife, even though OTC pollution in marine environments is decreasing.

## 5.5 *Future perspectives*

In this study a lot of new information regarding gmRXR isoforms was produced. However, the limited numbers of previous studies involving RXR isoforms in Atlantic cod, or teleosts in general, left a desire for more. Firstly, a more thorough and comprehensive phylogenetic mapping of gmRXR, and other cold-water teleost RXRs, should be performed. This could be used as a tool to uncover potential episodes of primary and secondary loss and gain in ligand binding function, throughout RXR evolution. Further, continuing the functional characterization of Atlantic cod gmRXR, and other NRs, is important to continue to observe the effects environmental pollutants may have on Atlantic cod.

In this study, a UAS/GAL4 based reporter gene assay was established with gmRXRβ1 and gmRXRγ. This could be used for further assessments of other potential exogenous compounds ability to transactivate the gmRXRs. With the characterization of gmRXRα and gmRXRβ2 in this study, these isoforms could also be cloned and included into a reporter gene assay, to further assess possible similarities and differences in ligand binding profiles for all the gmRXR isoforms. However, as the GAL4-UAS system used in this study is cell-dependent, it would be interesting to see if a cell-independent assay would produce more representative studies. The AlphaLisa assay is one potential way to assess cell-independent ligand activation of gmRXR isoforms, and other NRs in general. Recombinant expression, protein purification, and X-ray crystallography, along with 9-cis-RA docking simulations, could further provide important insight in how the isoforms might differ structurally and how this may affect ligand binding of different environmental pollutants.

Continuing, a mutagenesis assay of gmRXRβ1 where the inserted Thr237 is mutated to the conserved Ala-residue, found in all other examined RXR isoforms, would also be interesting. This would provide insight in whether this alteration in sequence is manifested as an inability to bind ligand(s). A mutagenesis study should also be performed to remove the 14 amino acids insert in gmRXRβ1 and gmRXRβ2, to assess its potential role in inhibiting ligand binding. Chromatin immunoprecipitation (ChIP) assays could also be utilized to assess the hypothesis proposed of gmRXRβ1 as an obligate non-permissive heterodimer through examining target genes for the isoform. However, for ChIP, development and production of gmRXR specific antibodies are required.

Furthermore, to assess the involvement of the gmRXR isoforms involvement in development and xenobiotic response, a larger tissues sample pool from different Atlantic cod individuals at different developmental stages would be useful. By utilizing tissue samples from a larger number of individuals, both juveniles and adults, and of both sexes, a more complete and reliable profile of tissue specific *gmrxr* expression could be produced. Using *in situ* hybridization, the expression of the isoforms during embryonic and larval stages could be performed, while tissue or cell-culture exposure would allow investigating of adult individuals as an alternative to *in vivo* experiments.

# 6 References


Ahuja, H. S., Szanto, A., Nagy, L., & Davies, P. (2003). The retinoid X receptor and its ligands: Versatile regulators of metabolic function, cell differentiation and cell death. *Journal of biological regulators and homeostatic agents*, *17*, 29–45.

Aranda, A., & Pascual, A. (2001). Nuclear hormone receptors and gene expression. *Physiological Reviews*, *81*(3), 1269–1304. https://doi.org/10.1152/physrev.2001.81.3.1269

Ashraf, M. A. (2017). Persistent organic pollutants (POPs): A global issue, a global challenge. *Environmental Science and Pollution Research*, *24*(5), 4223–4227. https://doi.org/10.1007/s11356-015-5225-9

Berg, P. R., Star, B., Pampoulie, C., Sodeland, M., Barth, J. M. I., Knutsen, H., Jakobsen, K. S., & Jentoft, S. (2016). Three chromosomal rearrangements promote genomic divergence between migratory and stationary ecotypes of Atlantic cod. *Scientific Reports*, *6*(1), 23246. https://doi.org/10.1038/srep23246

Billas, IsabelleM. L., Moulinier, L., Rochel, N., & Moras, D. (2001). Crystal Structure of the Ligand-binding Domain of the Ultraspiracle Protein USP, the Ortholog of Retinoid X Receptors in Insects. *Journal of Biological Chemistry*, *276*(10), 7465–7474. https://doi.org/10.1074/jbc.M008926200

Castillo, A. I., Sánchez-Martínez, R., Moreno, J. L., Martínez-Iglesias, O. A., Palacios, D., & Aranda, A. (2004). A Permissive Retinoid X Receptor/Thyroid Hormone Receptor Heterodimer Allows Stimulation of Prolactin Gene Transcription by Thyroid Hormone and 9-cis-Retinoic Acid. *Molecular and Cellular Biology*, *24*(2), 502–513. https://doi.org/10.1128/MCB.24.2.502-513.2004

Cheshenko, K., Pakdel, F., Segner, H., Kah, O., & Eggen, R. I. L. (2008). Interference of endocrine disrupting chemicals with aromatase CYP19 expression or activity, and consequences for reproduction of teleost fish. *General and Comparative Endocrinology*, *155*(1), 31–62. https://doi.org/10.1016/j.ygcen.2007.03.005

Cruz, A., Anselmo, A. M., Suzuki, S., & Mendo, S. (2015). Tributyltin (TBT): A Review on Microbial Resistance and Degradation. *Critical Reviews in Environmental Science and Technology*, *45*(9), 970–1006. https://doi.org/10.1080/10643389.2014.924181

Dawson, M. I., & Xia, Z. (2012). The Retinoid X Receptors and Their Ligands. *Biochimica et biophysica acta*, *1821*(1), 21–56. https://doi.org/10.1016/j.bbalip.2011.09.014

Delfosse, V., Huet, T., Harrus, D., Granell, M., Bourguet, M., Gardia-Parège, C., Chiavarina, B., Grimaldi, M., Mével, S. L., Blanc, P., Huang, D., Gruszczyk, J., Demeneix, B., Cianférani, S., Fini, J.-B., Balaguer, P., & Bourguet, W. (2021). Mechanistic insights into the synergistic activation of the RXR–PXR heterodimer by endocrine disruptor mixtures. *Proceedings of the National Academy of Sciences*, *118*(1). https://doi.org/10.1073/pnas.2020551118

Demehin, A. I., Babajide, J. O., & Salihu, S. O. (2017). *The Environmental Persistence of Organotin Compounds*. 10.

Doherty, J. D., & Irwin, W. A. (2011). Chapter 49—Organotins (tributyltin and triphenyltin). I R. C. Gupta (Red.), *Reproductive and Developmental Toxicology* (s. 657–672). Academic Press. https://doi.org/10.1016/B978-0-12-382032-7.10049-9

Dowhan, D. H., & Muscat, G. E. (1996). Characterization of the AB (AF-1) region in the muscle-specific retinoid X receptor-gamma: Evidence that the AF-1 region functions in a cell-specific manner. *Nucleic Acids Research*, *24*(2), 264–271.

Egea, P. F., Mitschler, A., Rochel, N., Ruff, M., Chambon, P., & Moras, D. (2000). Crystal structure of the human RXRα ligand-binding domain bound to its natural ligand: 9-cis retinoic acid. *The EMBO Journal*, *19*(11), 2592–2601. https://doi.org/10.1093/emboj/19.11.2592

Eide, M., Rydbeck, H., Tørresen, O. K., Lille-Langøy, R., Puntervoll, P., Goldstone, J. V., Jakobsen, K. S., Stegeman, J., Goksøyr, A., & Karlsen, O. A. (2018). Independent losses of a xenobiotic receptor across teleost evolution. *Scientific Reports*, *8*(1), 10404. https://doi.org/10.1038/s41598-018-28498-4

Evans, R. M., & Mangelsdorf, D. J. (2014). Nuclear Receptors, RXR & the Big Bang. *Cell*, *157*(1), 255–266. https://doi.org/10.1016/j.cell.2014.03.012

Feldman, D., Malloy, P. J., Krishnan, A. V., & Balint, E. (2008). CHAPTER 13 - Vitamin D: Biology, Action, and Clinical Implications. I R. Marcus, D. Feldman, D. A. Nelson, & C. J. Rosen (Red.), *Osteoporosis (Third Edition)* (s. 317–382). Academic Press. https://doi.org/10.1016/B978-012370544-0.50015-X

Fonseca, E., Ruivo, R., Borges, D., Franco, J., Santos, M., & Castro, L. (2020). Of Retinoids and Organotins: The Evolution of the Retinoid X Receptor in Metazoa. *Biomolecules*, *10*, 594. https://doi.org/10.3390/biom10040594

Fodor, I., Urbán, P., Scott, A. P., & Pirger, Z. (2020). A critical evaluation of some of the recent so-called 'evidence' for the involvement of vertebrate-type sex steroids in the reproduction of mollusks. *Molecular and Cellular Endocrinology*, *516*, 110949. https://doi.org/10.1016/j.mce.2020.110949

Gampe, R. T., Montana, V. G., Lambert, M. H., Wisely, G. B., Milburn, M. V., & Xu, H. E. (2000). Structural basis for autorepression of retinoid X receptor by tetramer formation and the AF-2 helix. *Genes & Development*, *14*(17), 2229–2241.

Garrod, D. (2011). Population Dynamics of the Arcto-Norwegian Cod. *Journal of the Fisheries Research Board of Canada*, *24*, 145–190. https://doi.org/10.1139/f67-012

Gooding Lassiter, M., Wilson, V., Folmar, L., Marcovich, D., & Leblanc, G. (2003). The Biocide Tributyltin Reduces the Accumulation of Testosterone as Fatty Acid Esters in the Mud Snail (Ilyanassa obsoleta). *Environmental health perspectives*, *111*, 426–430. https://doi.org/10.1289/ehp.5779

Griffith, C. M., Baig, N., & Seiber, J. N. (2015). Contamination from Industrial Toxicants. I P. C. K. Cheung (Red.), *Handbook of Food Chemistry* (s. 1–27). Springer. https://doi.org/10.1007/978-3-642-41609-5_11-1

Groot, A., Rosny, E., Juillan-Binard, C., Ferrer, J.-L., Laudet, V., Pierce, R., Pebay-Peyroula, E., Fontecilla-Camps, J., & Borel, F. (2006). Crystal Structure of a Novel Tetrameric Complex of Agonist-bound Ligand-binding Domain of Biomphalaria glabrata Retinoid X Receptor. *Journal of molecular biology*, *354*, 841–853. https://doi.org/10.1016/j.jmb.2005.09.090

Giulianelli, S., Primost, M. A., Lanari, C., & Bigatti, G. (2020). RXR Expression in Marine Gastropods with Different Sensitivity to Imposex Development. *Scientific Reports*, *10*(1), 9507. https://doi.org/10.1038/s41598-020-66402-1

Hagger, J. A., Depledge, M. H., & Galloway, T. S. (2005). Toxicity of tributyltin in the marine mollusc Mytilus edulis. *Marine Pollution Bulletin*, *51*(8–12), 811–816. https://doi.org/10.1016/j.marpolbul.2005.06.044

Haschek, W. M., Rousseaux, C. G., & Wallig, M. A. (2010). Chapter 15—Immune System. I W. M. Haschek, C. G. Rousseaux, & M. A. Wallig (Red.), *Fundamentals of Toxicologic Pathology (Second Edition)* (s. 451–489). Academic Press. https://doi.org/10.1016/B978-0-12-370469-6.00015-5

Haug, T., Falk-Petersen, S., Greenacre, M., Hop, H., Lindstrøm, U., Meier, S., Nilssen, K. T., & Wold, A. (2017). Trophic level and fatty acids in harp seals compared with common minke whales in the Barents Sea. *Marine Biology Research*, *13*(9), 919–932. https://doi.org/10.1080/17451000.2017.1313988

He, S., Li, P., & Li, Z.-H. (2021). Review on endocrine disrupting toxicity of triphenyltin from the perspective of species evolution: Aquatic, amphibious and mammalian. *Chemosphere*, *269*, 128711. https://doi.org/10.1016/j.chemosphere.2020.128711

Hiromori, Y., Aoki, A., Nishikawa, J., Nagase, H., & Nakanishi, T. (2015). Transactivation of the human retinoid X receptor by organotins: Use of site-directed mutagenesis to identify critical amino acid residues for organotin-induced transactivation. *Metallomics: Integrated Biometal Science*, *7*(7), 1180–1188. https://doi.org/10.1039/c5mt00086f

Ho, K. K. Y., Zhou, G.-J., Xu, E. G. B., Wang, X., & Leung, K. M. Y. (2016). Long-Term Spatio-Temporal Trends of Organotin Contaminations in the Marine Environment of Hong Kong. *PLOS ONE*, *11*(5), e0155632. https://doi.org/10.1371/journal.pone.0155632

Hoch, M. (2001). Organotin compounds in the environment—An overview. *Applied Geochemistry*, *16*(7), 719–743. https://doi.org/10.1016/S0883-2927(00)00067-6

Huang, W., Wu, Q., Xu, F., Li, L., Li, J., Que, H., & Zhang, G. (2020). Functional characterization of retinoid X receptor with an emphasis on the mediation of organotin poisoning in the Pacific oyster (Crassostrea gigas). *Gene*, *753*, 144780. https://doi.org/10.1016/j.gene.2020.144780

IJpenberg, A., Tan, N. S., Gelman, L., Kersten, S., Seydoux, J., Xu, J., Metzger, D., Canaple, L., Chambon, P., Wahli, W., & Desvergne, B. (2004). In vivo activation of PPAR target genes by RXR homodimers. *The EMBO Journal*, *23*(10), 2083–2091. https://doi.org/10.1038/sj.emboj.7600209

Jin, L., & Li, Y. (2010). Structural and functional insights into nuclear receptor signaling. *Advanced drug delivery reviews*, *62*(13), 1218–1226. https://doi.org/10.1016/j.addr.2010.08.007

Jones, B., Ohno, C., Allenby, G., Boffa, M., Levin, A., Grippo, J., & Petkovich, M. (1995). New retinoid-X-receptor subtypes in Zebra fish (Danio rerio) differentially modulate transcription and do not bind 9-cis retinoic acid. *Molecular and cellular biology*, *15*, 5226–5234. https://doi.org/10.1128/MCB.15.10.5226

Jones, K. C., & de Voogt, P. (1999). Persistent organic pollutants (POPs): State of the science. *Environmental Pollution*, *100*(1), 209–221. https://doi.org/10.1016/S0269-7491(99)00098-6

Kane, M. A. (2012). Analysis, occurrence, and function of 9-cis-retinoic acid. *Biochimica et Biophysica Acta (BBA) - Molecular and Cell Biology of Lipids*, *1821*(1), 10–20. https://doi.org/10.1016/j.bbalip.2011.09.012

Kojetin, D., Matta-Camacho, E., Hughes, T., Srinivasan, S., Nwachukwu, J., Cavett, V., Nowak, J., Chalmers, M., Marciano, D. P., Kamenecka, T., Shulman, A., Rance, M., Griffin, P., & Nettles, K. (2015). Structural mechanism for signal transduction in RXR nuclear receptor heterodimers. *Nature communications*, *6*, 8013. https://doi.org/10.1038/ncomms9013

Krezel, W., Dupé, V., Mark, M., Dierich, A., Kastner, P., & Chambon, P. (1996). RXR gamma null mice are apparently normal and compound RXR alpha +/-/RXR beta -/-/RXR gamma -/- mutant mice are viable. *Proceedings of the National Academy of Sciences of the United States of America*, *93*(17), 9010–9014. https://doi.org/10.1073/pnas.93.17.9010

Lagarde, N., Delahaye, S., Zagury, J.-F., & Montes, M. (2016). Discriminating agonist and antagonist ligands of the nuclear receptors using 3D-pharmacophores. *Journal of Cheminformatics*, *8*(1), 43. https://doi.org/10.1186/s13321-016-0154-2

Lauretta, R., Sansone, A., Sansone, M., Romanelli, F., & Appetecchia, M. (2019). Endocrine Disrupting Chemicals: Effects on Endocrine Glands. *Frontiers in Endocrinology*, *10*, 178. https://doi.org/10.3389/fendo.2019.00178

le Maire, A., Grimaldi, M., Roecklin, D., Dagnino, S., Vivat-Hannah, V., Balaguer, P., & Bourguet, W. (2009). Activation of RXR-PPAR heterodimers by organotin environmental endocrine disruptors. *EMBO Reports*, *10*(4), 367–373. https://doi.org/10.1038/embor.2009.8

Levin, A. A., Sturzenbecker, L. J., Kazmer, S., Bosakowski, T., Huselton, C., Allenby, G., Speck, J., Kratzeisen, C., Rosenberger, M., & Lovey, A. (1992). 9-cis retinoic acid stereoisomer binds and activates the nuclear receptor RXR alpha. *Nature*, *355*(6358), 359–361. https://doi.org/10.1038/355359a0

Link, J. S., Bogstad, B., Sparholt, H., & Lilly, G. R. (2009). Trophic role of Atlantic cod in the ecosystem. *Fish and Fisheries*, *10*(1), 58–87. https://doi.org/10.1111/j.1467-2979.2008.00295.x

Madsen, A. K. (2016). *Kloning, karakterisering og ligandaktivering av aryl hydrokarbonreseptor 2 (AHR2) fra Atlanterhavstorsk (Gadus morhua)*. https://bora.uib.no/bora-xmlui/handle/1956/11985

Meyer, A., & Van de Peer, Y. (2005). From 2R to 3R: Evidence for a fish-specific genome duplication (FSGD). *BioEssays: News and Reviews in Molecular, Cellular and Developmental Biology*, *27*(9), 937–945. https://doi.org/10.1002/bies.20293

Miller, E. J., & Lappin, S. L. (2021). Physiology, Cellular Receptor. I *StatPearls*. StatPearls Publishing. http://www.ncbi.nlm.nih.gov/books/NBK554403/

Moraes, L. A., Swales, K. E., Wray, J. A., Damazo, A., Gibbins, J. M., Warner, T. D., & Bishop-Bailey, D. (2007). Nongenomic signaling of the retinoid X receptor through

binding and inhibiting Gq in human platelets. *Blood*, *109*(9), 3741–3744. https://doi.org/10.1182/blood-2006-05-022566

Mortimer, D. N. (2013). 1 - Persistent organic pollutants in foods: Science, policy and regulation. I M. Rose & A. Fernandes (Red.), *Persistent Organic Pollutants and Toxic Metals in Foods* (s. 3–19). Woodhead Publishing. https://doi.org/10.1533/9780857098917.1.3

Mukha, A., Kalkhoven, E., & van Mil, S. W. C. (2021). Splice variants of metabolic nuclear receptors: Relevance for metabolic disease and therapeutic targeting. *Biochimica et Biophysica Acta (BBA) - Molecular Basis of Disease*, *1867*(10), 166183. https://doi.org/10.1016/j.bbadis.2021.166183

Nakanishi, T., Nishikawa, J., Hiromori, Y., Yokoyama, H., Koyanagi, M., Takasuga, S., Ishizaki, J., Watanabe, M., Isa, S., Utoguchi, N., Itoh, N., Kohno, Y., Nishihara, T., & Tanaka, K. (2005). Trialkyltin Compounds Bind Retinoid X Receptor to Alter Human Placental Endocrine Functions. *Molecular Endocrinology*, *19*(10), 2502–2516. https://doi.org/10.1210/me.2004-0397

Palanisami, T., & Naidu, R. (2010). The Dirty Dozen Become the Dirty 21:the new list of stockholm priority contaminants(POPs). *Remediation Australasia*, *4*, 2010.

Pellizzato, F., Centanni, E., Marin, M. G., Moschino, V., & Pavoni, B. (2004). Concentrations of organotin compounds and imposex in the gastropod Hexaplex trunculus from the Lagoon of Venice. *The Science of the Total Environment*, *332*(1–3), 89–100. https://doi.org/10.1016/j.scitotenv.2004.03.036

Penvose, A., Keenan, J. L., Bray, D., Ramlall, V., & Siggers, T. (2019). Comprehensive study of nuclear receptor DNA binding provides a revised framework for understanding receptor specificity. *Nature Communications*, *10*(1), 2514. https://doi.org/10.1038/s41467-019-10264-3

Philip, S., Castro, L. F. C., da Fonseca, R. R., Reis-Henriques, M. A., Vasconcelos, V., Santos, M. M., & Antunes, A. (2012). Adaptive evolution of the Retinoid X receptor in vertebrates. *Genomics*, *99*(2), 81–89. https://doi.org/10.1016/j.ygeno.2011.12.001

Porter, B. A., Ortiz, M. A., Bratslavsky, G., & Kotula, L. (2019). Structure and Function of the Nuclear Receptor Superfamily and Current Targeted Therapies of Prostate Cancer. *Cancers*, *11*(12), 1852. https://doi.org/10.3390/cancers11121852

Rastinejad, F., Wagner, T., Zhao, Q., & Khorasanizadeh, S. (2000). Structure of the RXR–RAR DNA-binding complex on the retinoic acid response element DR1. *The EMBO Journal*, *19*(5), 1045–1054. https://doi.org/10.1093/emboj/19.5.1045

Sandve, S. R., Rohlfs, R. V., & Hvidsten, T. R. (2018). Subfunctionalization versus neofunctionalization after whole-genome duplication. *Nature Genetics*, *50*(7), 908–909. https://doi.org/10.1038/s41588-018-0162-4

Schøyen, M., Green, N. W., Hjermann, D. Ø., Tveiten, L., Beylich, B., Øxnevad, S., & Beyer, J. (2019). Levels and trends of tributyltin (TBT) and imposex in dogwhelk (Nucella lapillus) along the Norwegian coastline from 1991 to 2017. *Marine Environmental Research*, *144*, 1–8. https://doi.org/10.1016/j.marenvres.2018.11.011

Scott, G. R., & Sloman, K. A. (2004). The effects of environmental pollutants on complex fish behaviour: Integrating behavioural and physiological indicators of toxicity. *Aquatic Toxicology*, *68*(4), 369–392. https://doi.org/10.1016/j.aquatox.2004.03.016

Seo, Y.-W., Sanyal, S., Kim, H.-J., Won, D. H., An, J.-Y., Amano, T., Zavacki, A. M., Kwon, H.-B., Shi, Y.-B., Kim, W.-S., Kang, H., Moore, D. D., & Choi, H.-S. (2002). FOR, a Novel Orphan Nuclear Receptor Related to Farnesoid X Receptor*. *Journal of Biological Chemistry*, *277*(20), 17836–17844. https://doi.org/10.1074/jbc.M111795200

Sham, R. C., Ho, K. K. Y., Hui, T. T. Y., Zhou, G.-J., Chan, J. K. Y., & Leung, K. M. Y. (2021). Tissue distribution of triphenyltin compounds in marine teleost fishes. *Journal of Hazardous Materials*, *401*, 123426. https://doi.org/10.1016/j.jhazmat.2020.123426

Sladek, F. M. (2003). Nuclear receptors as drug targets: New developments in coregulators, orphan receptors and major therapeutic areas. *Expert Opinion on Therapeutic Targets*, *7*(5), 679–684. https://doi.org/10.1517/14728222.7.5.679

Stokstad, E. (2021, april 7). *Massive collapse of Atlantic cod didn't leave evolutionary scars*. Science | AAAS. https://www.sciencemag.org/news/2021/04/massive-collapse-atlantic-cod-didn-t-leave-evolutionary-scars

Szanto, A., Narkar, V., Shen, Q., Uray, I. P., Davies, P. J. A., & Nagy, L. (2004). Retinoid X receptors: X-ploring their (patho)physiological functions. *Cell Death & Differentiation*, *11*(2), S126–S143. https://doi.org/10.1038/sj.cdd.4401533

Søfteland, L., Holen, E., & Olsvik, P. A. (2010). Toxicological application of primary hepatocyte cell cultures of Atlantic cod (Gadus morhua)—Effects of BNF, PCDD and Cd. *Comparative Biochemistry and Physiology Part C: Toxicology & Pharmacology*, *151*(4), 401–411. https://doi.org/10.1016/j.cbpc.2010.01.003

Tate, B. F., Allenby, G., Janocha, R., Kazmer, S., Speck, J., Sturzenbecker, L. J., Abarzúa, P., Levin, A. A., & Grippo, J. F. (1994). Distinct binding determinants for 9-cis retinoic acid are located within AF-2 of retinoic acid receptor alpha. *Molecular and Cellular Biology*, *14*(4), 2323–2330.

Tokuç, A. (2013). Stockholm Convention (2001). I S. O. Idowu, N. Capaldi, L. Zu, & A. D. Gupta (Red.), *Encyclopedia of Corporate Social Responsibility* (s. 2329–2336). Springer. https://doi.org/10.1007/978-3-642-28036-8_15

Tsuji, M., Shudo, K., & Kagechika, H. (2015). Docking simulations suggest that all-trans retinoic acid could bind to retinoid X receptors. *Journal of Computer-Aided Molecular Design*, *29*(10), 975–988. https://doi.org/10.1007/s10822-015-9869-9

Uhlén, M., Fagerberg, L., Hallström, B. M., Lindskog, C., Oksvold, P., Mardinoglu, A., Sivertsson, Å., Kampf, C., Sjöstedt, E., Asplund, A., Olsson, I., Edlund, K., Lundberg, E., Navani, S., Szigyarto, C. A.-K., Odeberg, J., Djureinovic, D., Takanen, J. O., Hober, S., … Pontén, F. (2015). Proteomics. Tissue-based map of the human proteome. *Science (New York, N.Y.)*, *347*(6220), 1260419. https://doi.org/10.1126/science.1260419

Ukaogo, P. O., Ewuzie, U., & Onwuka, C. V. (2020). 21 - Environmental pollution: Causes, effects, and the remedies. I P. Chowdhary, A. Raj, D. Verma, & Y. Akhter (Red.), *Microorganisms for Sustainable Environment and Health* (s. 419–429). Elsevier. https://doi.org/10.1016/B978-0-12-819001-2.00021-8

Wang, K., Chen, S., Xie, W., & Wan, Y.-J. Y. (2008). Retinoids Induce Cytochrome P450 3A4 through RXR/VDR-mediated Pathway. *Biochemical pharmacology*, *75*(11), 2204–2213. https://doi.org/10.1016/j.bcp.2008.02.030

Waxman, J. S., & Yelon, D. (2007). Comparison of the expression patterns of newly identified zebrafish retinoic acid and retinoid X receptors. *Developmental Dynamics*, *236*(2), 587–595. https://doi.org/10.1002/dvdy.21049

Weikum, E. R., Liu, X., & Ortlund, E. A. (2018). The nuclear receptor superfamily: A structural perspective. *Protein Science*, *27*(11), 1876–1892. https://doi.org/10.1002/pro.3496

Wennevik, V., Jørstad, K. E., Dahle, G., & Fevolden, S.-E. (2008). Mixed stock analysis and the power of different classes of molecular markers in discriminating coastal and oceanic Atlantic cod (Gadus morhua L.) on the Lofoten spawning grounds, Northern Norway. I J. Davenport, G. M. Burnell, T. Cross, M. Emmerson, R. McAllen, R. Ramsay, & E. Rogan (Red.), *Challenges to Marine Ecosystems* (s. 7–25). Springer Netherlands. https://doi.org/10.1007/978-1-4020-8808-7_1

Wiens, M., Batel, R., Korzhev, M., & Müller, W. E. G. (2003). Retinoid X receptor and retinoic acid response in the marine sponge Suberites domuncula. *The Journal of Experimental Biology*, *206*(Pt 18), 3261–3271. https://doi.org/10.1242/jeb.00541

Windsor, F. M., Pereira, M. G., Morrissey, C. A., Tyler, C. R., & Ormerod, S. J. (2020). Environment and food web structure interact to alter the trophic magnification of persistent chemicals across river ecosystems. *Science of The Total Environment*, *717*, 137271. https://doi.org/10.1016/j.scitotenv.2020.137271

Wolf, G. (2006). Is 9-Cis-Retinoic Acid the Endogenous Ligand for the Retinoic Acid-X Receptor? *Nutrition Reviews*, *64*(12), 532–538. https://doi.org/10.1111/j.1753-4887.2006.tb00186.x

Yamada, M., Nagasaki, S. C., Suzuki, Y., Hirano, Y., & Imayoshi, I. (2020). Optimization of Light-Inducible Gal4/UAS Gene Expression System in Mammalian Cells. *iScience*, *23*(9), 101506. https://doi.org/10.1016/j.isci.2020.101506

Yarsan, E., & Yipel, M. (2013). The Important Terms of Marine Pollution «Biomarkers and Biomonitoring,Bioaccumulation, Bioconcentration, Biomagnification». *Journal of Molecular Biomarkers & Diagnosis*, *s1*. https://doi.org/10.4172/2155-9929.S1-003

Yuan, X., Lu, H., Zhao, A., Ding, Y., Min, Q., & Wang, R. (2020). Transcriptional regulation of CYP3A4 by nuclear receptors in human hepatocytes under hypoxia. *Drug Metabolism Reviews*, *52*(2), 225–234. https://doi.org/10.1080/03602532.2020.1733004

Zarifi, I., Kiparaki, M., Koumbanakis, K. A., Giagtzoglou, N., Zacharioudaki, E., Alexiadis, A., Livadaras, I., & Delidakis, C. (2012). Essential Roles of Da Transactivation Domains in Neurogenesis and in E(spl)-Mediated Repression. *Molecular and Cellular Biology*, *32*(22), 4534–4548. https://doi.org/10.1128/MCB.00827-12

# Appendix

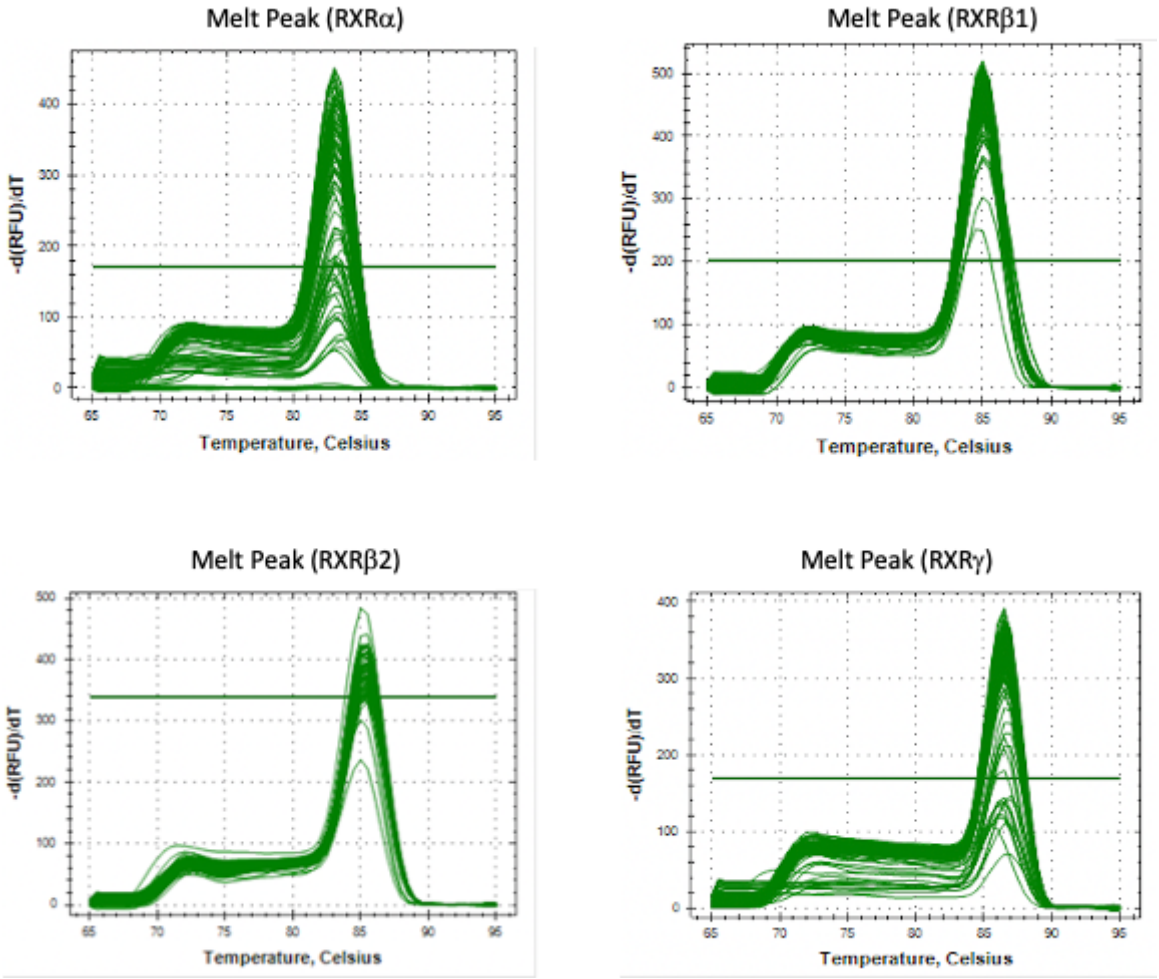


**Figure 28. Melting curve analysis.** Melting curve produced by primer pairs for gmRXRα, gmRXRβ1, gmRXRβ2 and gmRXRγ. Relative fluorescence units (RFU) with respect to temperature us indicated as X-axis, and y-axis indicates temperature in Celsius.

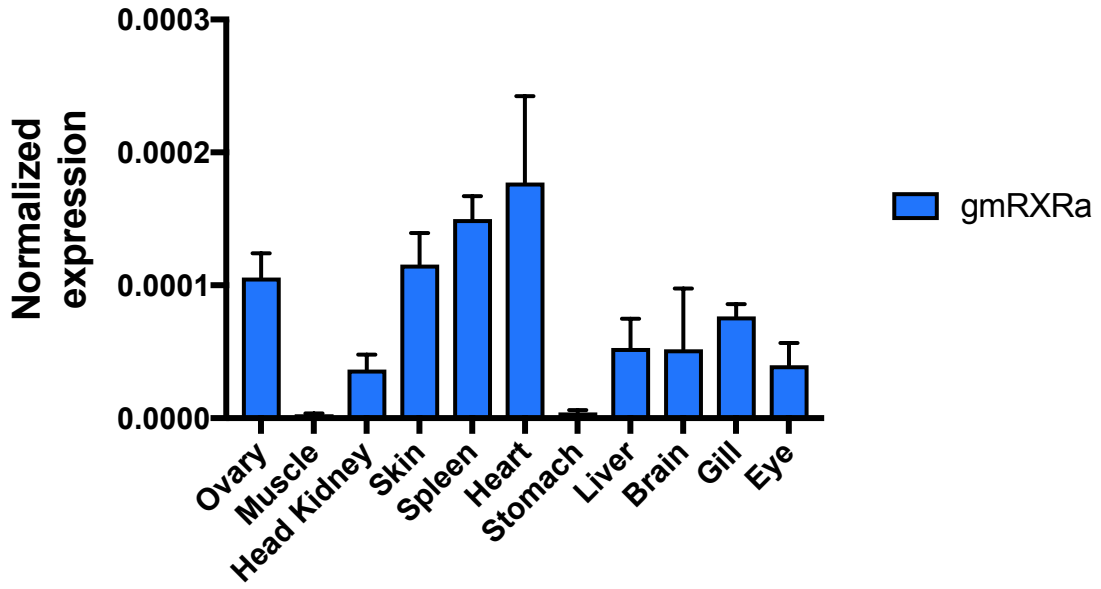


**Figure 29. Tissue specific expression of gmRXRα.** Figure shows the levels of detected gmRXRα transcripts correlating to tissue specific expression in Atlantic cod.